

THE INFLUENCE OF DIFFERENT MIXTURE DESIGN VARIABLES ON
THERMAL FATIGUE CRACKING OF ASPHALT CONCRETE PAVEMENTS

A THESIS SUBMITTED TO
THE GRADUATE SCHOOL OF NATURAL AND APPLIED SCIENCES
OF
MIDDLE EAST TECHNICAL UNIVERSITY

BY

ALI ARABZADEH

IN PARTIAL FULFILLMENT OF THE REQUIREMENTS
FOR
THE DEGREE OF MASTER OF SCIENCE
IN
CIVIL ENGINEERING

AUGUST 2015

Approval of the Thesis:

**INFLUENCE OF MIXTURE DESIGN VARIABLES ON THERMAL
FATIGUE BEHAVIOR OF ASPHALT CONCRETE**

Submitted by **ALI ARABZADEH** in partial fulfillment of the requirements for
the degree of **Master of Science in Civil Engineering Department, Middle East
Technical University** by,

Prof. Dr. Canan Özgen

Dean, Graduate School of **Natural and Applied Sciences** _____

Prof. Dr. Ahmet Cevdet Yalçiner

Head of Department, **Civil Engineering** _____

Assoc. Prof. Dr. Murat Güler

Supervisor, **Civil Engineering Dept., METU** _____

Examining Committee Members

Prof. Dr. İsmail Özgür Yaman

Civil Engineering Dept., METU _____

Assoc. Prof. Dr. Murat Güler

Civil Engineering Dept., METU _____

Asst. Prof. Dr. Onur Pekcan

Civil Engineering Dept., METU _____

Inst. Dr. Soner Osman Acar

Civil Engineering Dept., METU _____

Assoc. Prof. Dr. Mustafa **Şahmaran**

Civil Engineering Dept., Gazi University _____

Date: July 22, 2014

I hereby declare that all information in this document has been obtained and presented in accordance with academic rules and ethical conduct. I also declare that, as required by these rules and conduct, I have fully cited and referenced all material and results that are not original to this work.

Name, Last name:

Signature :

ABSTRACT

THE INFLUENCE OF DIFFERENT MIXTURE DESIGN VARIABLES ON THERMAL FATIGUE CRACKING OF ASPHALT CONCRETE PAVEMENTS

Arabzadeh, Ali

M. S., Department of Civil Engineering

Supervisor: Assoc. Prof. Dr. Murat Güler

August 2015, 166 pages

In this study, in order to investigate the thermal fatigue resistance of naturally-aged asphalt concrete specimens, an experimental setup is developed. Mixture design variables, selected according the superpave method of design, include asphalt content, asphalt type, aggregate type, gradation and modification. In the course of this study, using the developed setup, thermal coefficients and thermal fatigue life of the asphalt concrete specimens are measured. Then, using the analysis of variance tests the significant mixture design variables affecting the two types of tests are identified. According to the statistical analyses, aggregate type, gradation, asphalt type and asphalt content significantly affect the thermal coefficient of asphalt concrete. The thermal fatigue resistance is significantly affected by aggregate type, asphalt content and the asphalt type. The results of this study provide a solution to minimize the thermal fatigue cracking in asphalt concrete pavements.

Keywords: Thermal Fatigue Resistance, Asphalt Concrete, Thermal Expansion Coefficient, Strain Loading

ÖZ

ASFALT BETON KAPLAMALARIN TERMAL YORULMA KIRIKLARINA FARKLI KARIŞIM DİZAYNLARININ ETKİSİ

Arabzadeh, Ali

Yüksek Lisans, İnşaat Mühendisliği Bölümü

Tez Yöneticisi: Doç. Dr. Murat Güler

Ağustos 2014, 166 Sayfa

Bu çalışmada doğal yaşlandırılmış asfalt beton numunelerinin termal yorulma dayanımının araştırılması ve simule edilmesi için deney düzeneği geliştirilmiştir. Karışım dizayn değişkenleri (asfalt oranı ve çeşidi, agregaya kaynağı ve nitelikleri) Superpave dizayn yöntemine göre seçilmiştir. Bu çalışmanın amacı geliştirilen deney düzeneğini kullanarak asfalt beton numunelerinin termal katsayı ve termal yorulma ömrünün belirlenmesidir. Farklı deneylerin analiziyle karışım dizaynına etki eden iki çeşit deney belirlenmiştir. İstatistik analizlere göre agregaya tipi, agregaya boyutu, asphalt çeşidi ve asphalt oranı asphalt betonunun termal katsayısını gözle görülür bir şekilde etkilemektedir. Termal yorulma direnci belirgin olarak agregaya çeşidi, asphalt oranı, asphalt içeriği ve asphalt çeşidi tarafından etkilenmektedir. Çalışmanın sonuçları asphalt beton kaplamalarındaki termal yorulma çatlaklarını en aza indirmek için çözüm sunmaktadır.

Anahtar Kelimeler: Termal yorulma direnci, asphalt betonu, Termal genişleme katsayısı, gerilme yüklemesi

To my parents

ACKNOWLEDGEMENTS

Foremost, I would like to express my deep gratitude to my patient advisor and guru Assoc. Prof. Dr. Güler whose supervision during this study transformed my naiveté to sophistication, and it was because of his directions that I feel the confidence I have today.

Besides my advisor, I would like to thank the rest of my thesis committee: Prof. Dr. İsmail Özgür Yaman, Asst. Prof. Dr. Onur Pekcan, Inst. Dr. Soner Osman Acar, and Assoc. Prof. Dr. Mustafa Şahmaran for their insightful comments and hard questions.

I thank my fellow lab mates in Transportation Laboratory: Başak Varlı and Yalçın Karakaya for their helps and all the fun we have had together during my research.

The last but not the least, I would like to thank my parents for giving birth to me at the first place and then supporting me emotionally during the hard times. It was because of their sincere supports that I was able to sail through the difficulties I had during this study.

TABLE OF CONTENTS

ABSTRACT.....	v
ÖZ	vi
ACKNOWLEDGEMENTS.....	viii
TABLE OF CONTENTS	ix
LIST OF TABLES.....	xiii
LIST OF FIGUERS.....	xiv
LIST OF ABBREVIATIONS USED.....	xix
CHAPTERS	
1. INTRODUCTION.....	1
1.1 Background.....	1
1.2 Research Objectives.....	3
1.3 Scope.....	4
1.4 Outline of Research.....	4
2. LITERATURE REVIEW.....	7
2.1 Introduction.....	7
2.2 Thermal cracking of asphalt concrete pavements.....	7
2.3 Significance of thermal cracking in asphalt concrete pavements	10
2.4 Thermal fatigue cracking of asphalt concrete pavements.....	13
2.4.1 Factors affecting thermal fatigue cracking	15
2.5 Methods for measuring thermal fatigue performance of asphalt concrete pavements.....	29

2.5.1 Phenomenological approach.....	29
2.5.2 Mechanistic approach.....	29
2.6 Previous studies on measurement of thermal fatigue performance of asphalt concrete.....	30
2.6.1 Thermal Stress Restrained Specimen Test (TSRST).....	30
2.6.2 Two-point bending beam fatigue test.....	31
2.6.3 Four-point bending beam fatigue test.....	32
3. METHODOLOGY.....	35
3.1 Introduction.....	35
3.2 Preparation of TSRST machine	35
3.2.1 Design and fabrication.....	35
3.2.2 Programming	42
3.3 The temperature range for measuring the thermal fatigue resistance of asphalt concrete.....	49
3.4 Measurement of thermal strains for applying the cyclic sinusoidal loads	50
3.5 Sample preparation	51
3.5.1 Selection of the materials for the study	51
3.5.2 Superpave mixture design	53
3.5.3 Sample preparation for the measurement of thermal coefficient and the thermal fatigue resistance	55
3.6 Laboratory testing of the specimens	59
3.6.1 Testing for the measurement of thermal coefficient of contraction	59
3.6.2 Testing for the measurement of thermal fatigue resistance	60

4. DATA ANALYSIS.....	61
4.1 Introduction.....	61
4.2 Analysis of experimental data for measuring the thermal coefficients 61	
4.3 Analysis of experimental data for thermal fatigue performance	63
4.3.1 Reduction of stiffness to 35% of its initial value	66
4.3.2 Extrapolating the number of cycles to 50% reduction using power model	67
4.3.3 Calculating the slope of the linear line fitted to log-log scale data.....	71
5. RESULTS AND DISCUSSION.....	73
5.1 Introduction.....	73
5.2 Mixture design variables for performing ANOVA.....	73
5.3 Analysis of variance tests (ANOVA) for the measured thermal coefficients	74
5.4 Calculating the natural logarithm of the number of cycles.....	80
5.5 Analysis of variance tests (ANOVA) for the number of cycles at 35% reduction in stiffness	81
5.6 Analysis of variance tests (ANOVA) for the extrapolated number of cycles at 50% reduction in stiffness using power model	89
5.7 Analysis of variance tests (ANOVA) for slopes of the linear lines fitted to log-log scale data of stiffness versus number of cycles	94
6. CONCLUSIONS AND RECOMMENDATIONS.....	99
6.1 Introduction.....	99
6.2 Conclusions.....	99
6.3 Recommendations for future work	102

REFERENCES	105
APPENDICES	
A. THERMAL STRAIN PLOTS.....	109
B. STIFFNESS REDUCTION PLOTS	119
C. BEST LINEAR REGION PLOTS	129
D. POWER MODEL PLOTS	139
E. MAXIMUM CALCULATED VALUES OF COEFFICIENT OF DETERMINATION FOR EACH SPECIMEN, FOR FINDING THE BEST LINEAR FIT IN LOG-LOG SCALE DATA	149
F. THE PLOTS SHOWING THE EFFECT OF DIFFERENT MIX DESIGN VARIABLE ON THE RESPONSES TAKEN FROM ALL 26 SPECIMEN.....	151
G. SOFTWARE MANUALS	161

LIST OF TABLES

TABLES

Table 3.1 Aggregate properties	52
Table 3.2: Asphalt properties	52
Table 3.3: summary of calculated asphalt contents (Qadir, 2010).....	55
Table 4.1: The values of thermal strains measured for each specimen.....	63
Table 5.1: Types of specimens and their replicate numbers	74
Table 5.2: ANOVA analysis for the measured thermal coefficients.....	75
Table 5.3: The averaged measured thermal coefficients	75
Table 5.4: ANOVA analysis for the number of cycles at 35% reduction in stiffness	82
Table 5.5: The average measured number of cycles at 35% reduction in stiffness	82
Table 5.6: ANOVA analysis for the extrapolated number of cycles to 50% reduction in stiffness	90
Table 5.7: The average measured number of cycles at 50% reduction in stiffness	90
Table 5.8: ANOVA analysis for the slopes of the fitted linear lines.....	94
Table 5.9: The average measured slopes	95
Table E.1: The maximum values of measured R2s.....	149

LIST OF FIGUERS

FIGURES

Figure 2.1: Phenomenon of low temperature cracking in AC pavements (FHWA courses,1998).....	8
Figure 2.2: Thermal stress gradients (Haas, Meyer, Assaf, & Lee, 1987).	9
Figure 2.3 An example of a severely developed thermal crack in an asphalt concrete pavement.	10
Figure 2.4 The effect of frost action on asphalt concrete pavements.	11
Figure 2.5 The expulsion of water through the cracks.	12
Figure 2.6 Free body diagram of a pavement section under thermal loading.	14
Figure 2.7 Approximate temperature range of thermal fatigue cracking (Carpenter & H., 1983).....	14
Figure 2.8 Stiffness behavior of asphalt binder (Robert et al.1996).....	20
Figure 2.9 Behavior of asphalt according to temperature (Breen & Stephens, 1967).....	21
Figure 2.10 Ideal temperature range for good asphalt pavement performance (Bureau of Materials and Physical Research, 2005).....	22
Figure 2.11 Fatigue paths obtained from uniaxial testing under sinusoidal loading (Lundstrom, Bendetto, & Isacson, 2004).....	25
Figure 2.12 Principle of 2-point bending fatigue test.....	32
Figure 2.13 Schematic of the four-point bending beam fatigue test.	33
Figure 3.1: TSRST machine for measuring thermal coefficient and thermal fatigue resistance of asphalt concrete specimens.....	36
Figure 3.2: refrigerating chamber.	37

Figure 3.3: General schematic of the refrigerating chamber for measuring thermal fatigue resistance.	38
Figure 3.4: General schematic of the refrigerating chamber for measuring thermal coefficient.	39
Figure 3.5: LVDT set up for measuring thermal coefficient and thermal fatigue resistance.	41
Figure 3.6: The dummy specimens placed beside the test specimens.....	42
Figure 3.7: The program for the measurement of thermal coefficient	44
Figure 3.8: The program for the measurement of thermal fatigue cracking.	46
Figure 3.9: Frequency versus temperature range.	50
Figure 3.10: Waveform for the constant amplitude sinusoidal strain loading.	51
Figure 3.11: The gradation of aggregates according to the standards of TGDH (Qadir, 2010).	53
Figure 3.12: The method for sticking the plastic mounting studs on the sides of specimens.	57
Figure 3.13: Ensuring the concentricity of the specimen and plates with the help of a metal O-ring.....	58
Figure 3.14: The board used for sticking the specimens to the plates.....	59
Figure 4.1: Axial thermal strain versus temperature	62
Figure 4.2: The data of applied axial strain on one of the specimens	64
Figure 4.3: The data of axial stress recorded in one of the fatigue tests	64
Figure 4.4: The stiffness path calculated for one of the specimens.	65
Figure 4.5: Stiffness reduction (in percent) for three different test specimens.	67
Figure 4.6: The data of stiffness versus number of cycles in a log-log scale.....	68
Figure 4.7: The plot showing the values of coefficient of determination for the whole range of cycles according to the selected number of cycles.....	70
Figure 4.8: The power model fitted to the portion of data with the best fatigue behavior.	71
Figure 4.9: Comparison of the slopes of two linear lines fitted to the log-log scale data.	72

Figure 5.1: The average thermal coefficient measured for the test specimens grouped according to the asphalt content.	77
Figure 5.2: The average thermal coefficient measured for the test specimens grouped according to the asphalt type.	78
Figure 5.3: The average thermal coefficient measured for the test specimens grouped according to the gradation.	79
Figure 5.4: The average thermal coefficient measured for the test specimens grouped according to the aggregate type.	80
Figure 5.5: The average number of cycles for different types of specimens grouped according to the asphalt content.	83
Figure 5.6: The natural logarithm of average number of cycles for different types of specimens grouped according to the asphalt content.	84
Figure 5.7: The average number of cycles for different types of specimens grouped according to the asphalt type.	85
Figure 5.8: The natural logarithm of average number of cycles for different types of specimens grouped according to the asphalt type.	86
Figure 5.9: The average number of cycles for different types of specimens grouped according to the aggregate type.	88
Figure 5.10: The natural logarithm of average number of cycles for different types of specimens grouped according to the aggregate type.	88
Figure 5.11: The average number of cycles for different types of specimens grouped according to the asphalt content.	91
Figure 5.12: The natural logarithm of average number of cycles for different types of specimens grouped according to the asphalt content.	92
Figure 5.13: The average number of cycles for different types of specimens grouped according to the aggregate type.	93
Figure 5.14: The natural logarithm of average number of cycles for different types of specimens grouped according to the aggregate type.	93
Figure 5.15: The average slope for different types of specimens grouped according to the aggregate type.	95

Figure 5.16: The average slope for different types of specimens grouped according to the asphalt content.	97
Figure 5.17: The average slope for different types of specimens grouped according to the asphalt type.	97
Figure A.1: Thermal strain plots for all the specimens.	109
Figure B.1: Stiffness reduction plots for all the specimens.	119
Figure C.1: The logarithmic data of stiffness vs. number of cycles for the specimens	129
Figure D.1: The power model fitted to the data in the selected region for all the specimens.	139
Figure F.1: The measured thermal coefficients for all the specimens grouped according to asphalt content.	151
Figure F.2: The measured thermal coefficients for all the specimens grouped according to asphalt type.	152
Figure F.3: The measured thermal coefficients for all the specimens grouped according to aggregate type.	152
Figure F.4: The measured thermal coefficients for all the specimens grouped according to gradation	153
Figure F.5: The measured number of cycles at 35% reduction in stiffness for all the specimens grouped according to asphalt content.	153
Figure F.6: The natural logarithm of measured number of cycles at 35% reduction in stiffness for all the specimens grouped according to asphalt content.	154
Figure F.7: The measured number of cycles at 35% reduction in stiffness for all the specimens grouped according to asphalt type.	154
Figure F.8: The natural logarithm of measured number of cycles at 35% reduction in stiffness for all the specimens grouped according to asphalt type.	155
Figure F.9: The measured number of cycles at 35% reduction in stiffness for all the specimens grouped according to aggregate type.	155
Figure F.10: The natural logarithm of measured number of cycles at 35% reduction in stiffness for all the specimens grouped according to aggregate type.	156

Figure F.11: The measured number of cycles at extrapolated 50% reduction in stiffness for all the specimens grouped according to asphalt content..... 156

Figure F.12: The natural logarithm of extrapolated number of cycles at 50% reduction in stiffness for all the specimens grouped according to asphalt content. 157

Figure F.13: The measured number of cycles at extrapolated 50% reduction in stiffness for all the specimens grouped according to aggregate type. 157

Figure F.14: The natural logarithm of extrapolated number of cycles at 50% reduction in stiffness for all the specimens grouped according to aggregate type. 158

Figure F.15: The slopes measured for all the specimens grouped according to the aggregate type..... 158

Figure F.16: The slopes measured for all the specimens grouped according to the asphalt content. 159

Figure F.17: The slopes measured for all the specimens grouped according to the asphalt type. 159

Figure G.1: Manual for the thermal strain test. 161

Figure G.2: Manual for the thermal fatigue test. 164

LIST OF ABBREVIATIONS

- ANOVA:** Analysis of Variance
- α_g :** Thermal coefficient after glass transition temperature
- α_l :** Thermal coefficient before glass transition temperature
- B:** Basalt Aggregate
- C:** Coarse Gradation
- F:** Fine Gradation
- FHWA:** Federal Highway Administration
- HMA:** Hot Mix Asphalt
- L:** Limestone Aggregate
- LCPC:** Laboratoire Central des Ponts et Chaussées
- LVDT:** Linear Variable Displacement Transducer
- O-:** Optimum Asphalt Content - 0.5%
- O+:** Optimum Asphalt Content + 0.5%
- PG:** Performance Grade
- RTD:** Resistance Temperature Detectors
- R²:** Coefficient of determination
- S:** SBS Modification
- SBS:** Styrene Butadiene Styrene
- Superpave:** Superior PERforming Asphalt PAVements
- TGDH:** Turkish General Directorate of Highways
- TSRST:** Thermal Stress Restrained Specimen Tests
- Z:** Neat or non-modified asphalt

CHAPTER 1

INTRODUCTION

1.1 Background

In Turkey, the majority of roadway pavements are made of asphalt concrete. As a result, the authorities responsible for the construction and maintenance of asphalt pavements are concerned with pavement deteriorations due to a wide range of distresses. Among the type of deteriorations, cracking is the most detrimental factor that causes severe damages in pavement structure and degradation of service quality. Pavement cracking can occur as a result of either traffic loading or strains developed due to temperature differentials in the field. Thermally induced cracks manifest themselves in regions where severely low temperatures take place causing low temperature cracking; or considerable oscillations in air temperature causing thermal fatigue cracking. The former manifests itself in regions such as Canada, United States of America, Europe and some parts of Asia experiencing severely low temperatures. The latter, on the other hand, can occur in anywhere having considerable periodic temperature changes especially during spring times. Because of their significant impacts on pavement performance, investigating the mechanism of thermally induced cracks and mitigating their detrimental effects have drawn the attention of many researchers.

Asphalt concrete like other materials contracts when cools down and expands when heats up due to air temperature. Thermally induced cracks occur in two different ways; low temperature cracking under extremely cold temperatures and thermal fatigue cracking due to large diurnal temperature cycles (Sugawara and Moriyoshi, 1984, Gerristen, et al. 1988, and Vinson, et al., 1989). Low temperature cracking

occurs when the thermally induced stresses exceed the tensile strength of asphalt concrete. The induction of thermal stress is due to the stress build-up through the shrinkage of surface course which is restrained by the friction between the surface course and the underlying layer. Thermal fatigue cracking, at first, was not thought to be of paramount importance until the researchers in 1970s observed severe transverse cracks in some of the roads in Texas where the low temperature cracking was not the primary reason for deterioration, because the climate of the state is classified as mild. This showed that the thermal fatigue can even occur under any temperature conditions other than hot weather. Since the asphalt mixture has a visco-elastic behavior under high temperatures and the energy of thermally induced stress is dissipated through the viscous characteristic of asphalt mixture; thermal fatigue cracks cannot be developed. The findings of previous researches showed that thermal fatigue takes place approximately between -7 $+21$ °C, and that its occurrence is dependent on the fluctuations in air temperature resulting in different ranges of tensile strains.

Once a crack is initiated on the surface of asphalt concrete pavement, rainfalls accumulated on the surface can penetrate through the pavement foundation having crack openings ranging from 2.5 to 3.5 mm, and eventually cause serious structural failures in the subgrade. The seepage of rainfalls will also lead to the formation of ice lenses, resulting in strength loss due to thawing during spring seasons or deterioration in the roadway profile if the subgrade includes swelling soil. Another problem originated from thermal fatigue cracks is the pumping which results from the loss of fine materials in the saturated subgrades by the effect of wheel loads. Each time a vehicle tire moves over the crack location, the pore pressure in the subgrade is increased. In order to dissipate the pressure, the water is expelled through the cracks, and during this process fine soil particles are pumped out with water, which will result in loss of support under the pavement surface. The result of this process is the depressions or uplifts over the wearing course causing significant reduction in the driving quality and hence pavement serviceability. To

recover the structural performance of wearing course, a comprehensive rehabilitation would be needed, causing a huge amount of investment to be spent. For example, millions of dollars are annually allocated to renovating the pavements in US and Canada just because of thermal cracking.

Previous studies reveal that the thermal fatigue cracking is mainly associated with the strain range generated during the thermal changes in the field. It manifests itself in the form of transverse cracks perpendicular to the road axis, causing crack patterns pertaining to low temperature cracking. It has been mentioned by different researchers that thermal fatigue cracks are dependent upon temperature variations, mix properties, i.e. aggregate source, AC types, gradation, air void content and polymer modification. Since only a few researchers have worked on thermal fatigue cracking and each of them applied their own way of testing, there is still no a well-developed test method to characterize thermal fatigue cracking. As a result, the measurement of asphalt concrete behavior under thermal fatigue has been an active research area in which significant developments in the testing and characterization procedures are still needed. The main aim of this study is therefore to fabricate an apparatus for simulating thermal fatigue cracking in short time scales together with investigating effects of different mix variables on this type of distress.

1.2 Research Objectives

The objective of this research is summarized as follows:

- 1- Design and set up of a test configuration that allows simulation of thermal fatigue in a short time scale compared with the long time that takes place in the field. It is worth mentioning that, cyclic variation of temperature causes thermal fatigue cracking, and the period of each cycle is one day in the field.
- 2- Identify significant mix variables for thermal fatigue cracking of asphalt concrete using statistical design of experiments.

According to the results of this research, it is expected that mix variables that play a significant role in thermal fatigue cracking could be identified using a well-set up testing procedure. Also, it is anticipated that the outcomes of this investigation would assist my counterparts in doing more profound and further researches on the thermal fatigue cracking; thus, the potential for the detrimental effects of this type of distress could be reduced, if not eliminated.

1.3 Scope

This research was conducted as follows:

- 1- Designing and development of a test apparatus for simulating the thermal fatigue cracking of asphalt concretes in a short time scale compared with the thermal fatigue occurring in the field.
- 2- Analyzing the outcome of experiments and identifying significant testing parameters and mix variables on the basis of statistical analysis.

In this research, in order to measure the thermal fatigue resistance of asphalt concrete beams a completely modified version of TSRT equipment is used. In the previous studies, TSRT was used to measure the thermally induced stresses due to the reduction of temperature. However, in this research, TSRST device is utilized to apply the thermally induced stresses mechanically. Details pertaining to the configuration of the testing device and its performance are presented in chapter three. In order to analyze the resulting data a suitable statistical design of experiments was conducted.

1.4 Outline of Research

A literature review of the researches, each conducting an investigation, on the thermal fatigue cracking of asphalt concrete pavements is presented in chapter two. A summary of research outcomes together with the methods used by the previous researchers to simulate thermal fatigue cracking are also discussed. The chapter

also contains the effect of mix properties and environmental conditions on the on the result of experiments.

Chapter three explains all testing variables and mix designs concerning the test specimens. Moreover, this chapter contains the procedure by which the specimens were prepared. Test set-up and testing asphalt concrete specimens for thermal fatigue cracking are exhaustively described in chapter three.

In chapter four, an analysis of experimental data for thermal fatigue cracking is proposed. Moreover, this chapter includes a computation of parameters for determining the thermal fatigue performance of asphalt concrete specimens.

Chapter five includes the discussion of a numbers of response parameters such as number of cycles to 35% and 50% reduction in stiffness and slope of the power model. In addition, the thermal strain level reached during the thermal cycles is also presented in this chapter.

Chapter 6 includes conclusions and recommendations for future studies respectively.

CHAPTER 2

LITERATURE REVIEW

2.1 Introduction

In this chapter, the mechanism and the concept of thermal cracking in asphalt concrete pavements are elaborated. Moreover, described herein are the methods for measuring thermal fatigue performance of asphalt concrete based on the previous studies and the significance of thermal fatigue in terms of field performance of asphalt concrete.

2.2 Thermal cracking of asphalt concrete pavements

Asphalt concrete like other materials expands or contracts depending on the thermal changes in the environment. While the expansion behavior of asphalt concrete becomes critical for spalling, its contraction is responsible for the development of transverse cracks in the wearing courses. Hence, the volumetric contraction of asphalt concrete pavements has always been an intriguing issue for the pavement engineers. When the upper most layer of a flexible pavement contracts, it is restrained by its underlying layer. The existence of this restraint is the result of generated friction between the two layers during the construction of pavement layers. As a result, under low environment temperatures in the field, the tension stresses are induced in the asphalt concrete pavement, which results in transverse thermal cracking (Figure 2.1). Thermal cracking of asphalt concrete pavements is one of the major distresses attributed to asphalt concrete pavements due to monotonic or cyclic tensions. The monotonic tension is ascribed to low temperature cracking of asphalt concrete pavement. As the environmental temperature

decreases, the tension due to the thermally induced stress increases. If the environment temperature goes down to an extreme level, the generated stress will exceed the fracture strength of asphalt concrete pavement, and hence the low temperature cracking occurs eventually (Janoo, Bayer Jr, & Walsh, 1993).

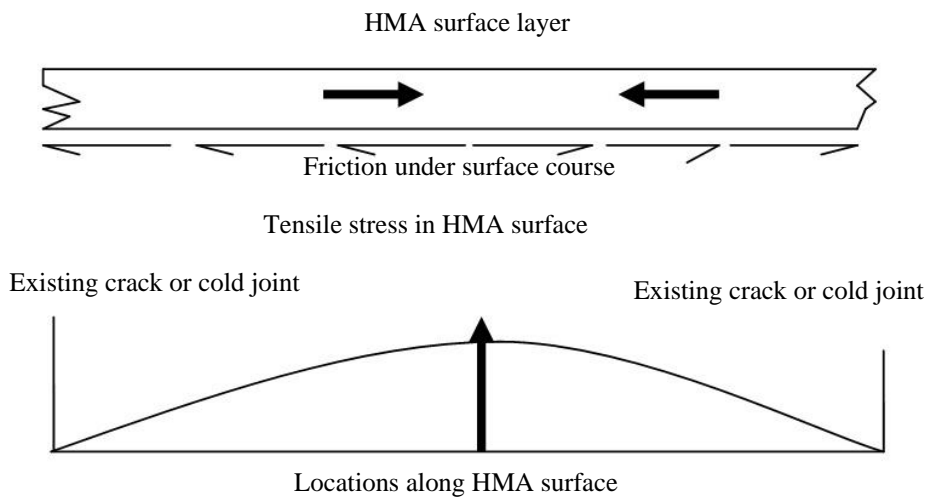


Figure 2.1: Phenomenon of low temperature cracking in AC pavements (FHWA courses,1998).

Researchers (Vinson, Janoo, & Haas,1989) believe that low temperature cracking occurs more frequently in temperatures below the glass temperature at which asphalt concrete behavior goes from elasto-plastic to elastic phase.

Although some researchers believe that thermal fatigue cracking is a special case of low temperature cracking (Jackson & Vinson, 1996), the others claim that thermal fatigue cracking due to cyclic tensions is a different type of thermal cracking, which resembles to traffic-load associated fatigue cracking (Epps, 1999). They claim that the thermal fatigue cracking is analogous to the traffic-load

associated fatigue in which the failure occurs solely because of repetition of transient traffic loads. In thermal fatigue, loads due to repetition of thermal tensions cause fatigue in asphalt concrete pavement. Although both types of mentioned fatigue cracking are similar in mechanism, their initiation and propagation is vastly different. The cracks attributed to the traffic-load associated fatigue initiate from under the bottom of the asphalt concrete and then gradually propagate until they appear on the surface. In contrast, thermally induced fatigue cracks initially occur on the surface of the asphalt concrete pavement then propagate until they reach the bottom of surface layer (Gerritsen & Jongeneel, 1988). It is worth mentioning that the same mechanism of cracking exists for the low temperature cracking.

The crack initiation in thermal fatigue is due to the existence of temperature gradient in the surface layer, in that the thermally induced tension stress is the maximum on the surface, and it decreases parabolically through the lift thickness. The reduction of thermal stress as a function of depth is illustrated by Haas et al.,(1987) in Figure 2.2. The closer the upper layer is to the surface, the more prone it is to thermal cracking. That is the reason why cracks attributed to both types of thermal cracking, in terms of initiation and propagation, are called “top to bottom cracking”.

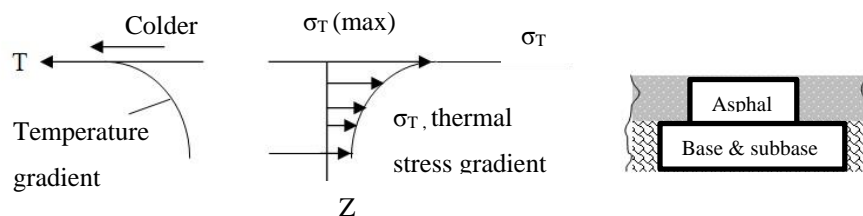


Figure 2.2: Thermal stress gradients (Haas, Meyer, Assaf, & Lee, 1987).

2.3 Significance of thermal cracking in asphalt concrete pavements

Cracks ascribed to low temperature and thermal fatigue develop transversely and are almost perpendicular to the road axis (Figure 2.3). The reason why thermal cracks are not developed longitudinally is that the length of the pavement is much greater than its width; as a result, the asphalt concrete layer shrinks more in its length compared to its width. Whatever the responsible mechanism is for of the occurrence of cracks, once they are developed they start accelerating the pavement deterioration. Crack openings around 2.5-3.5 mm can easily let the water into the pavement foundation and, consequently cause serious structural problems. The infiltration of water to the pavement subgrade is the main reason for pavement deteriorations associated with freeze-thaw cycles during spring.



Figure 2.3 An example of a severely developed thermal crack in an asphalt concrete pavement.

The frost action consists of two phases: freezing the soil water, and thawing the subgrade soil. The freeze phase is accompanied by conspicuous heaving on the road surface, and the thaw phase is associated with a noticeable softening of the road bed. An example of frost action on the road is illustrated in Figure 2.4.



Figure 2.4 The effect of frost action on asphalt concrete pavements.

In addition to frost action, there is another problem associated with the existence of water in the pavement structure; it can make the base saturated; as a result, the passage of transient loads over the pavement surface increases the water pressure. The easiest way for the induced pressure to dissipate is through expelling the water from the cracks; therefore, some soil particles are pumped out by the water (Figure 2.5). Consequently, due to loss of soil, the support beneath the asphalt concrete pavement becomes deficient, and additional cracks will develop around the

transverse thermal cracks under traffic loading. The results of this process is the formation of depressions, heaves and softened roadbeds that all lower the serviceability of the pavement, and hence the driving quality.



Figure 2.5 The expulsion of water through the cracks.

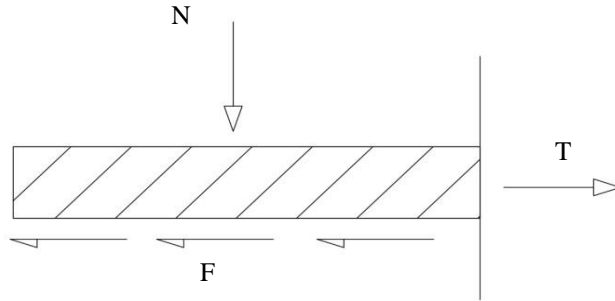
Thermally induced cracks are often sealed by using special sealants, results in spending a lot of money for road maintenance, and if the sealant is not applied on time, deteriorations will accelerate in the pavement and the rehabilitation costs even get higher. For this reason, the justification of rehabilitation cost for thermal cracking has taken the attraction of many researchers for many years.

2.4 Thermal fatigue cracking of asphalt concrete pavements

From mid-seventies, thermal fatigue cracking has been under observation. This thermally induced cracking, probably, has nothing to do with extremely cold climatic conditions or traffic loading. In moderate climates, this type of cracking is not able to induce high enough amounts of thermal stress to cause instantaneous cracking. However, cyclic thermal fluctuations above the fracture temperature might cause fatigue in the pavement, and make it more susceptible to cracking under subsequent thermal and/or traffic induced stresses (Gerritsen & Jongeneel, 1988). The main reason for the development of severe transverse thermal cracking in the pavements located in west Texas was attributed to thermal fatigue cracking of the asphalt concrete (Carpenter, S.H., Lytton, & Epps., 1974). However, the results of researches done later, suggested that other factors might be significant as well (Carpenter, H., & Lytton, 1977) & (Anderson, O., & Epps, 1983).

Conventional traffic-load associated fatigue tests performed in laboratory demonstrated that fatigue could also occur in asphalt concrete under low loading frequencies, exactly like the low cyclic load induced by variations in temperature (Gerritsen & Jongeneel, 1988). A free-body diagram showing the forces acting on a fully restrained asphalt concrete layer is presented in Figure 2.6.

The temperature range attributed to thermal fatigue cracking is estimated to be approximately between -7°C (20°F) and 21°C (70°F), which is represented in Figure 2.7 (Carpenter & H., 1983). Above this range, thermal stresses are dissipated due to the relaxation of asphalt concrete. Below this range, the dominant mode of distress is known to be low temperature cracking (Carpenter & H., 1983).



T = Tensile force induced due to thermal contraction.
 N = Normal force representing the mass of pavement section.
 F = Fiction force between pavement and base course.

Figure 2.6 Free body diagram of a pavement section under thermal loading.

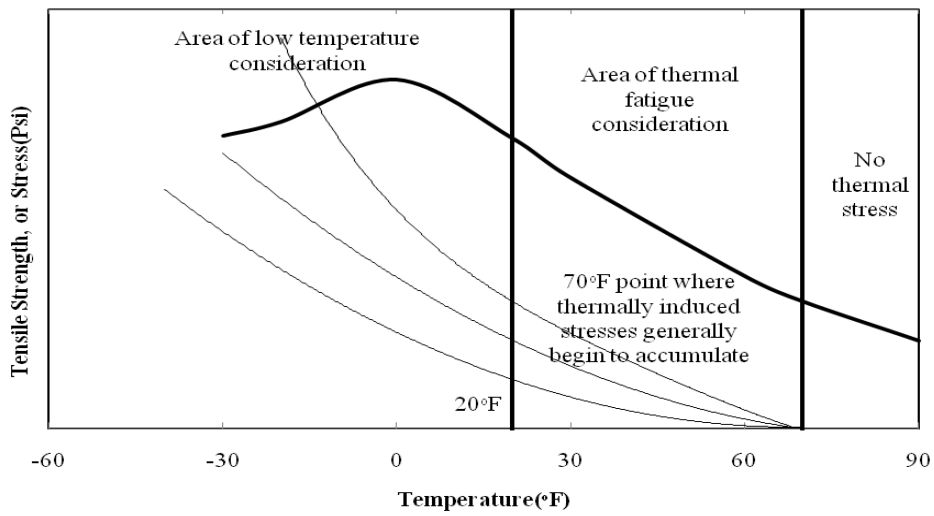


Figure 2.7 Approximate temperature range of thermal fatigue cracking (Carpenter & H., 1983).

As it was illustrated in the Figure 2.6, the failure mechanism ascribed to thermal fatigue is tension related, meaning that as Vinson et al.(1996) suggested, it is possible to postulate that thermal fatigue cracking is a special type of low temperature cracking. As a result, under some circumstances, it would be possible to make analogies between the test results of works done on low temperature and thermal fatigue cracking.

2.4.1 Factors affecting thermal fatigue cracking

Since yet there is no standard or established way of doing thermal fatigue test, it is not possible to make a comprehensive argument about the factors influencing that mode of distress. However, due to the fact that the repeated thermal tension applied to the asphalt concrete might resemble the thermally induced tension in low temperature cracking (Jackson & Vinson, 1996), it is possible to discuss over the factors affecting the low temperature cracking. It is worth mentioning that, these discussions are not readily made unless there is a definite similarity between the two modes of thermal cracking, in terms of conditions and materials used. Among the factors categorized by Haas et al. (1987) for low temperature cracking, there are three general elements that are likely to influence the thermal fatigue: climate, component material properties and asphalt mixture properties, which are discussed in detail in the following sections.

2.4.1.1 Climate

Unlike the low temperature cracking that takes place in severely cold regions, the thermal fatigue cracking happens in the places having moderate climates. The factors affecting thermal fatigue in the context of climate are temperature and pavement aging. Although aging is somehow dependent on the temperature, it is appropriate to discuss each of them independently.

a-Temperature

The temperature is of paramount importance and is a controlling parameter for thermal fatigue (Al-Qadi, Hassan, & Elseifi, 2005). The fluctuations in temperature

bring about thermally induced strains in the semi-restraint flexible pavements, causing eventually thermal fatigue. If the temperature is below -7°C low temperature cracking is the dominant mode of thermal cracking and if it is more than 21°C due to relaxation no thermal cracking would occur (Carpenter & H., 1983). As a result, -7°C to 21°C is a suitable range for investigating the effect of temperature on thermal fatigue. In addition, Gerritsen et al. (1988) also claimed that thermal fatigue occurs in moderate temperatures. After analyzing data gathered from the instrumented Virginia Smart Road, an interstate highway in the US, Al-Qadi et al. (2005) concluded that the effect of temperature fluctuations on the flexible pavements is most common in the spring, a season in which daily temperature keeps oscillating within a moderate range. It is worth mentioning that, the strain range reached in the spring was around $350\mu\text{m/m}$. In order to investigate the effect of temperature change on asphalt concrete researchers have to apply thermal alterations on the asphalt concrete specimens in the laboratory. Since the thermal conductivity of asphalt concrete is low, the temperature changes applied on the specimens need a long time to diffuse thoroughly in the specimen and then equilibrate. Although Jackson et al. (1996) have applied thermal cycles using TSRST machine to observe thermal fatigue, other researchers because of the financial problems and the hardships concerning the long time needed for performing the experiments, have applied mechanical cyclic loads to simulate thermal fluctuations. It is worth mentioning that Jackson et al. (1996) were not able to do a comprehensive research on thermal fatigue performance of asphalt concrete because of the explained problems, the details of mechanical application of thermal changes will be discussed comprehensively later in this chapter.

b-Pavement aging

Chemical transformation of asphalt cement due to the induction of maximum temperature in the pavement, oxidation, solar radiation etc. causes the asphalt concrete to be age-hardened. As the asphalt concrete is aged, it will suffer from thermal cracking because of the increased stiffness if the maximum temperature on

the pavement surface increases, the amount of aging in asphalt concrete will also be increased (Keliewer & Zeng, 1996). It is hypothesized that aging of the asphalt cement could influence the number of cycles to failure, the initial stiffness and the rate of damage evaluation during thermal fatigue. Moreover, it is widely accepted that thermal cracks initiate and then propagate in the aged pavements much more quickly compared with the new ones. Aging of asphalt concrete pavements was one of the many reasons for the Strategic Highway Research Program (SHRP) to introduce the performance based binder grading system. For example, the asphalt cement graded with PG 58-22 indicates that a flexible pavement can perform well in the temperature range between of -22°C and 58°C.

Thermal fatigue cracking is not a viable mode of distress without considering the effect of environmental aging on the asphalt concrete (Jackson & Vinson, 1996). In addition, Vinson et al. (1996) claimed that in the absence of environmental aging the time needed for asphalt concrete to develop a single crack would be at least 8 years in a severely harsh condition. Gerritsen et al. (1988) performed thermal fatigue experiment at the two temperatures of 0°C and 10°C and investigated the effect of aging. They observed that at 10°C the aged asphalt concrete specimens sustained less thermal cycles before failure and at 0°C they noticed that the behavior of aged specimens became much more brittle compared with the unaged ones; finally, they witnessed that the failure of each aged specimen was accompanied by an abrupt fracture. Moreover, age-hardening of asphalt mixtures increases the levels of thermal stress that are generated due to the temperature differentials (Epps, 1999). Rapid short aging due to plant mixing and during construction as well as long age hardening will all contribute to increasing the thermal stresses induced in the flexible pavements.

2.4.1.2 Component material properties

Asphalt concrete is a heterogeneous material that is mainly made of aggregate and asphalt cement. Moreover, asphalt cement modifiers are sometimes added to the binder in order to improve temperature related properties. , so that it can resist in a

better way against certain types of distresses. Components of material properties are the only factors by which researchers can control the thermal fatigue cracking behavior of asphalt concrete. They, unlike the effects of climate and environment, can be controlled to reduce the detrimental effects of severe climatic and environmental conditions.

a-Aggregate

The major part of asphalt mixture, both in terms of volume and weight, consists of aggregate. With respect to quantity and solidness, aggregate is the backbone of asphalt concrete and it literally works like a skeleton in the mixture. Some of the researchers believe that low temperature cracking had nothing to do with aggregates and it is the binder that plays the instrumental role in thermal cracking. However, many researchers still refuse the theory of sole effect of asphalt cement on low temperature cracking by proving that the aggregate's role could be at least as important as the binder's.

Unlike the vast literature available for low temperature cracking that investigates the effect of aggregate, there is not enough research dealing with the influence of aggregate on thermal fatigue. Just Epps et al. (1999), for example, studied the effect of aggregate gradation on thermal fatigue and found that gap-graded aggregates outperformed the dense graded mixtures under average climatic conditions.

So far, there is no work on the effect of aggregate size and source on thermal fatigue cracking, which could have considerable influence on the number of cycles sustained before failure.

b- Asphalt cement

Apart from the importance of aggregate, it has always been emphasized that the asphalt cement has a key role in the behavior of asphalt mixture. Its performance under temperature variations is largely dependent upon its mechanical properties, thermal properties and also on its interactions with other materials, which are discussed in the following sessions.

1-Asphalt cement stiffness

Stiffness is describes the rigidity of an object and determines to which extent it can resist deformation in response to an induced force. The complementary concept to rigidity is the flexibility. Stiffness of asphalt binder is a material property usually derived from dividing the stress induced in the substance by its corresponding strain. It is widely used in determining the behavior of asphalt mixtures to rate its thermal performance. Stiffness of asphalt cement is completely independent of time for very short periods of loading; in other words, it reaches the modulus of elasticity. On the contrary, for long loading periods its behavior is completely viscous. For intermediate loading times, the behavior of asphalt cement becomes visco-elastic. The relationship between asphalt cement stiffness and time is illustrated in Figure 2.8. The stiffness of the asphalt binder is influenced by the state of stress, rate of applied strain, temperature, moisture and other effects causing the asphalt cement to be age-hardened. Moreover, the stiffness of the asphalt concrete highly depends on the stiffness of the asphalt binder and for low temperature cracking a binder with low stiffness performs better (Roberts, Kandhal, Brown, & Lee, 1996).

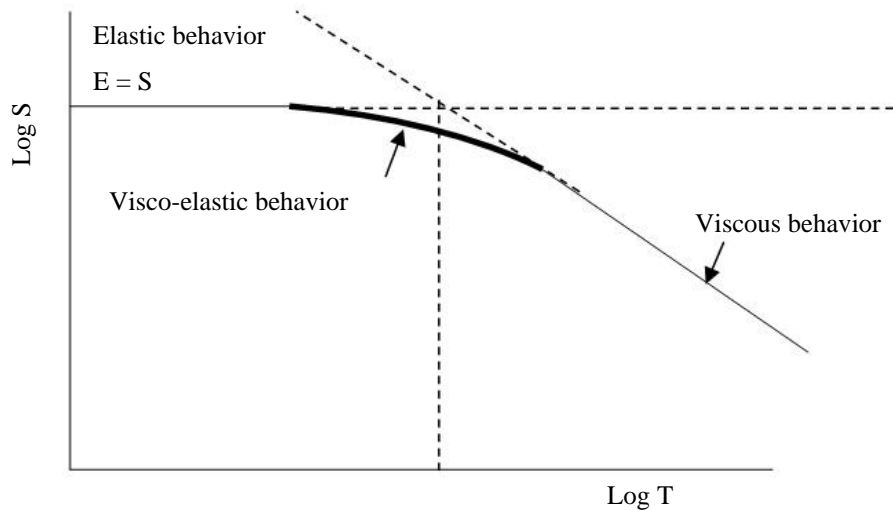


Figure 2.8 Stiffness behavior of asphalt binder (Robert et al.1996).

2-Asphalt cement thermal properties

Thermal properties of asphalt cement play a key role in thermal cracking and specifically in thermal fatigue cracking of asphalt concrete. Asphalt cement shows three types of behavior when it is exposed to a wide range of temperatures. As shown in Figure 2.9, the behavior of asphalt cement consists of three states: liquid, rubbery and glassy. In the figure, T_g represents the glass transition temperature; the temperature at which asphalt concrete moves from visco-elastic state to completely elastic state or vice versa. When the change in the volume goes into a discontinuous state the glass transition occurs (Breen & Stephens, 1967). If the temperature range at which thermal fatigue happens falls within the glassy state, it is postulated that the failure due to repetition of load occurs in a brittle manner, similar to low temperature cracking. If the temperature range falls within the visco-elastic state

the dominant factor of failure due to repetition of loading would probably be the thermal fatigue. If the temperature range falls within the viscous state, due to relaxation of asphalt no thermal fatigue cracking would occur.

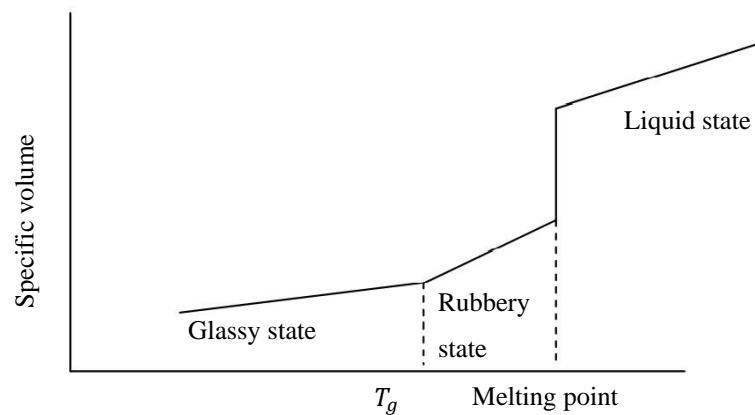


Figure 2.9 Behavior of asphalt according to temperature (Breen & Stephens, 1967).

3-Asphalt cement modification

Asphalt cement is a visco-elastic material that can show both solid-like and liquid-like characteristics depending on temperature. Asphalt binder, as a result, can act like a solid and liquid in cold and warm temperatures, respectively. Its liquid behavior makes it prone to rutting and the solid behavior increases potential to cracking. As a result, asphalt modifiers are used to improve temperature dependent properties and help the asphalt pavements perform better if exposed to harsh climatic conditions (Figure 2.10). As illustrated in the figure, binder III has a narrow range of temperature in which a good performance without any type of distress is

obtained. In order to improve its temperature performance, certain type of modifiers can be added to the asphalt binder. After the modification, for example, binder II outperforms binder III and binder I becomes far better than the others. There are different types of modifiers available on the market, such as polymers, crumb rubber modifier (CRM), etc. Polymer modifiers are divided into two main classes: elastomers and plastomers. The first improves strength at high temperatures as well as elasticity at low temperatures, and the latter enhances the strength but elasticity. It is worth noting that, styrene-butadiene-styrene (SBS) used in this research work is one type of elastomer.

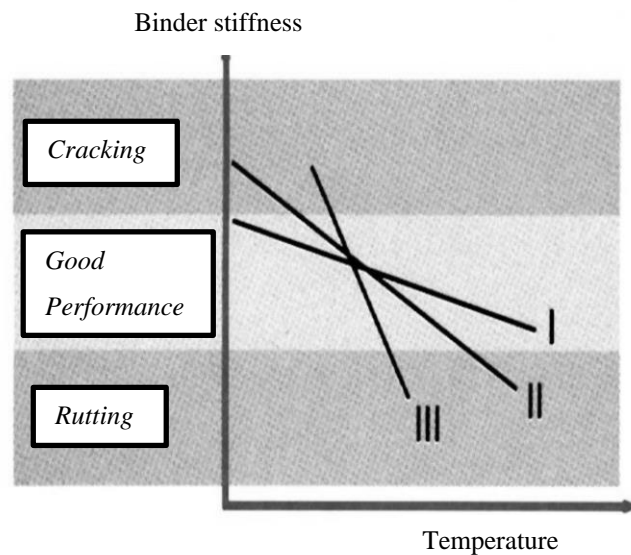


Figure 2.10 Ideal temperature range for good asphalt pavement performance (Bureau of Materials and Physical Research, 2005)

Epps et al. (1999) were one of the few researchers who evaluated the effect of CRM on the number of cycles that asphalt concrete sustains until failure. After analyzing the data, they proved that CRM modification enhanced the asphalt concrete resistance to thermal fatigue in moderate climatic conditions. However, Qadir (2010) investigated the effect of SBS on low temperature cracking using statistical analysis proved that its influence is not significant.

2.4.1.3 Asphalt mixture properties

In addition to the effects of component material properties on thermal fatigue, the combined effect of these components describing the asphalt mixture is also important for the thermal fatigue performance of asphalt concrete pavements. Asphalt mixture is a heterogeneous material consisting of aggregate, asphalt cement and air voids. The percentage of each of these components has a significant effect on the resistance of asphalt concrete against distresses. The following sections deal comprehensively with the properties of asphalt mixture.

1- Stiffness of asphalt mixture

Stiffness of asphalt concrete is of the utmost significance in determining the performance of flexible pavements under service conditions. The stiffness of asphalt concrete is determined exactly the same way as described in the previous sections; it is the result of dividing the stress by the corresponding strain. Stiffness is an important property to determine asphalt concrete resistance against both thermal fatigue and load associated fatigue. Its reduction in bending, shear and uniaxial fatigue tests is an indication of the micro crack coalescence. In uniaxial load-associated fatigue testing, the test procedure is used to assume a 50% reduction in the pseudo stiffness as an acceptable failure criterion (Lee, 1996). It is worth noting that, the reduction of stiffness is the result of applying cyclic load in the constant strain mode.

In the context of thermal fatigue, the stiffness reduction is divided into two stages: initial stage and the second stage. In the former, there is a drastic drop in stiffness

reduction path during the first few cycles that is ascribed to the rheological behavior of asphalt concrete; the latter is representative of the fatigue behavior (Gerritsen & Jongeneel, 1988). The second stage, in terms of the rate of decrease in stiffness, vastly depends upon the environmental temperature and the penetration grade of the asphalt cement. Lundstrom et al (2004), who worked on the conventional fatigue found that at a cold temperature like 0°C the reduction of stiffness is approximately linear and generally it could not exceed 20%. Moreover, they proved that asphalt concrete is capable of sustaining more thermal cycles at warmer climates like 10°C compared with 0°C. In terms of penetration grade, they verified that higher penetration grades sustain more thermal cycles before failure.

Apart from the importance of stiffness reduction rate in the second stage, the path that is followed is of paramount significance. As it is illustrated in Figure 2.11 by Lundstrom et al (2004), in the uniaxial fatigue tests performed on asphalt concrete specimens four typical paths are generally obtained.

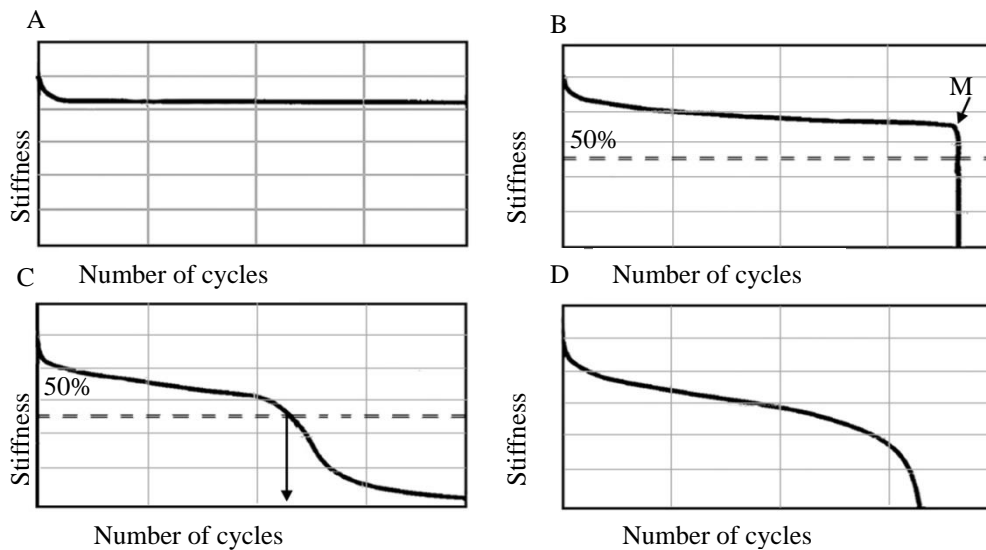


Figure 2.11 Fatigue paths obtained from uniaxial testing under sinusoidal loading (Lundstrom, Bendetto, & Isacsson, 2004).

Path A is obtained in the controlled strain amplitude when the amplitude of the strain applied is too low. As a result, after a few cycles the number of load applications would not affect the stiffness reduction and the experiment might go on for a great number of cycles without any more reduction of stiffness or any failure in the time allocated for the test.

Fatigue path B is the most favorable in the controlled strain amplitude mode. The smooth reduction rate of stiffness until either 50% reduction in stiffness or a sudden failure is an indication of a unified strain field existing in the specimen.

Path C having an s-shaped curve is an adverse path ascribed to the non-uniform strain field induced in a specimen. The stiffness reduction rate decreases in this type, but only for a certain number of load application; after that, it starts to increase then approaches an inflection point and again decreases until it tends to zero. Since

this type of path is representative of a non-uniform strain field, it is not possible to discuss about it.

Fatigue path D is representative of the stress controlled fatigue test with uniform strain field. The stiffness reduction rate starts to decrease from the beginning until it approaches an inflection point then increases until it approaches zero. The increase in the stiffness reduction rate at the last stage of the path is due to the fact that strain amplitude together with the internal temperature keep increasing.

In order to determine the stiffness or the relation between stress and strain in viscoelastic materials, dynamic complex modulus method is used. It is a complex quantity which has two parts: real and imaginary. Its real part is representative of the elastic stiffness and its imaginary part shows the internal damping (Huang, 2004). The absolute value of the complex modulus is referred to as the dynamic modulus, which is the ratio of the peak to peak stress to pertaining peak to peak strain. It is highly dependent upon the frequency and temperature applied during the test. The frequency should well simulate the way the load is applied. For simulating thermal fatigue, it is not practical to apply thermal cycles, because the thermal conductivity of asphalt is low, so that it is not possible to make quick fluctuations in temperature within the test specimen. Instead, it is possible to apply the thermal fluctuations mechanically in relatively higher frequencies compared with the thermal frequency that needs one day to complete each cycle. Frequency and temperature are interchangeable in load-associated fatigue tests with the S-mix as the key parameter. Using a limited number of test specimens, Gerritsen et al (1988) found that this interchangeability works for very low frequencies as well. As a result, it is possible to conduct thermal fatigue in frequencies and temperatures other than the ones occurring in the pavements exposed to climatic conditions. It is worth noting that, while they are interchangeable it is better to stay as close as possible to real conditions of the field. Most of complex modulus tests are performed by inducing compressive sinusoidal or haversine loads in the test specimens, but if the specimens are viscoelastic, then any type of loading will give

the same results (Huang, 2004). Therefore, loading condition should also be in tension-compression or only in tension mode

2- Thermal properties of asphalt concrete

Asphalt is a viscoelastic material, and like other engineering materials it contracts or expands under temperature variations. . As a result, in the prediction of thermal strain and stress, the thermal coefficient of material is required, which is denoted by the constant α . In general, the coefficient α is termed as the coefficient of thermal expansion-contraction, but in pavement engineering it is termed as the thermal coefficient of contraction, since in this discipline of engineering the concern is the stress built up due to contraction. Thermal coefficient of contraction is used to describe the relationship between temperature change and the thermally induced strain, which is generally defined by

$$\alpha = \frac{d\varepsilon^T(T)}{dT} \quad (2.1)$$

Where:

ε^T = the thermal strain, and

T = temperature (Collieu & Powney, 1973).

If the relationship between T and ε^T is linear α becomes constant, otherwise the strain is calculated by

$$\varepsilon^T = \int_{T_i}^T \alpha(T')dT' = \int_0^t \alpha [T(t')] \frac{dT(t')}{dt'} dt' \quad (2.2)$$

Where:

T_i = the initial temperature at zero time,

T' = the temperature integral variable, and

t' = the time integral variable.

The thermal coefficient of materials is usually temperature dependent, meaning that it decreases when temperature decreases (Collieu & Powney, 1973). In asphalt mixtures the same rule exists but the reduction in the thermal coefficient consists of two stages: before and after the glass transition. As a result, it would be possible to estimate a constant thermal coefficient for each stage. Bahia et al. (1993) fit a five-parameter curve (Equation 2.3) to the data of volume change versus temperature change, and obtained the thermal coefficient before and after the glass transition temperature.

$$v = C_v + \alpha_g(T - T_g) + R(\alpha_l - \alpha_g) \ln \left[1 + \exp \left(\frac{T - T_g}{R} \right) \right] \quad (2.3)$$

Where:

v = specific volume at temperature T ,

C_v = volume at a given temperature,

T_g = glass transition temperature,

R = constant defining the curvature,

α_l = thermal coefficient for $T > T_g$, and

α_g = thermal coefficient for $T < T_g$.

3- Air void content and quantity of binder in asphalt mixtures

Gerritsen et al. (1988) concluded that increasing the binder content of asphalt concrete from 5.3% to 6.3% of aggregate weight enhanced the thermal fatigue resistance up to a factor of 6. Moreover, they proved that air void content or binder content affects the age hardening of the asphalt mixtures. If the amount of air voids increases the asphalt mixture becomes more prone to age-hardening. In other words, if the binder content increases the asphalt concrete becomes less age hardened. In addition, an increase in binder content results in the decrease of initial stiffness (Gerritsen & Jongeneel, 1988). Shah (2004) found that the asphalt concrete pavements with 4 and 7 percent void contents did not manifest vast differences in the frequency of thermal cracks.

2.5 Methods for measuring thermal fatigue performance of asphalt concrete pavements

There are two approaches for evaluating the thermal fatigue performance of asphalt concrete: phenomenological and mechanistic approach (Vinson, Janoo, & Haas, 1989). Those approaches are explicated in the following sections.

2.5.1 Phenomenological approach

Phenomenological approaches generally try to simulate field performance using suitable laboratory test procedures. These approaches typically correlate documented field distress with laboratory test results. Phenomenological approaches generally apply Miner's hypothesis (1945) (Equation 2.4) for the fatigue analysis. The hypothesis suggests that the damage due to fatigue accumulates and the failure does not happen unless the sum of ratios of fatigue life is equal or greater than unity.

$$\sum_i \frac{n_i}{N_i} = 1 \quad (2.4)$$

Where:

n_i = the number of cycles accumulated at stress i , and

N_i = the average number of cycles to failure.

2.5.2 Mechanistic approach

Mechanistic approaches make a correlation between pavement distress and substantial material properties like time, temperature, stress, strain, etc. The majority of the mechanistic thermal cracking models are on the basis of fracture mechanics. These models correlate thermal cracking of asphalt to fracture mechanics parameters: like energy release rate integral (c*-line integral) and stress intensity factor or j-integral. Since discussing about the fracture mechanics is beyond the scope of this thesis work, it is not appropriate here to go through more details.

2.6 Previous studies on measurement of thermal fatigue performance of asphalt concrete

In previous studies, numerous researchers have investigated the low temperature cracking of asphalt concrete in many different ways. However, because there is no a standardized test method available yet, only a limited number of studies exist to investigate the thermal fatigue behavior of asphalt concrete. There only exist a limited number of researches in this area. The details of these few research efforts for measuring the thermal fatigue are discussed in the following subsections.

2.6.1 Thermal Stress Restrained Specimen Test (TSRST)

TSRST is the most common phenomenological approach for measuring the thermal cracking of asphalt concrete, because it closely simulates this type of distress. For low temperature cracking performance, it has been shown by a number of researchers that it can provide satisfactory results; however, this test setup for thermal fatigue may not be a feasible option because of the prolonged testing durations. Each thermal cycle lasts one day in the field and if one wants to evaluate thermal fatigue, at least one year is needed to complete the testing. Jackson et al. (1996) claimed that TSRT is a controlled strain test and can be used to evaluate the thermal fatigue cracking within a temperature range of 0°C to -12°C. It is worth mentioning that they accelerated the rate of temperature change from 10 to 20 °C/h. In their test, the length of the cylindrical specimens were kept constant which means that they did not let them expand or contract while applying thermal cycles, and then they measured the thermally induced stress. They found that the level of stress induced decreased as the number of cycles increased, no thermal crack was observed at the end of testing. The stress decrease was ascribed to either stress relaxation or the coalescence of micro cracks. It is worth noting that due to power outage during the tests they were not able to make a comprehensive study.

2.6.2 Two-point bending beam fatigue test

In this test, trapezoidal specimens are mounted like a vertical cantilever. Their bases are fixed and their tops are actuated sinusoidally at a constant strain. The schematic diagram of two-point bending apparatus is presented in the Figure 2.12.

Gerritsen et al (1988) used two-point bending beam test to measure the thermal fatigue of asphalt concrete specimens at two temperatures of 0 and 10°C. The frequency used in their experiment was 0.0004 Hz, and the high levels of constant strain they applied were from 2 to 5 mm/m. They noticed 2 stages in the reduction of stiffness: initial stage and the rest. The former showed a drastic drop in the stiffness in approximately first ten cycles, which was attributed to the rheological properties of the bitumen. The latter represented the fatigue behavior of asphalt concrete. As a result, in order to determine the number cycles for measuring the fatigue life of asphalt mixes, they discarded the first ten cycles and evaluated the thermal fatigue resistance from the 11th cycle. It is worth noting that the criteria they used for determining the fatigue life of each specimen was based on the cycle number at which its stiffness was equal to 50 percent of the 11th cycle's stiffness.

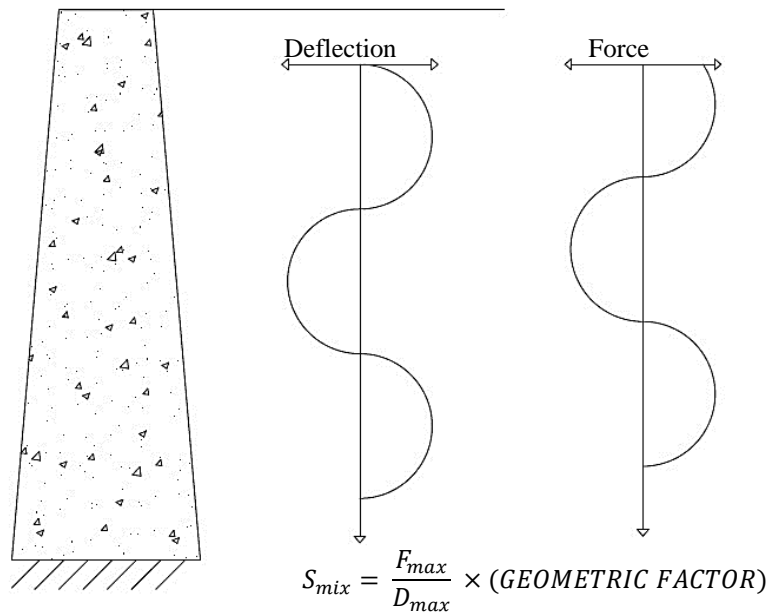


Figure 2.12 Principle of 2-point bending fatigue test.

2.6.3 Four-point bending beam fatigue test

Four-point bending beam fatigue test is a more advanced method of evaluating fatigue resistance of asphalt concrete specimens compared with the two-point bending beam fatigue test. It is favored because failure can occur between the two center loads, an area in which the stress is distributed uniformly (Figure 2.13).

Epps (1999) using a four-point bending beam fatigue test measured the resistance of rectangular beam specimens against thermal fatigue cracking at a temperature of 4°C. She conducted the tests at a frequency of 0.05 Hz at two levels of constant strain, which were applied sinusoidally. One of the levels was used to represent average weather conditions and the other was used for simulating extreme climatic conditions. The levels of strain were representative of the thermally induced stress in asphalt concrete pavement. In order to select the thermal stress levels, she used

the COLD program. The inputs of the program included a description of the pavement structure, its thermal properties, weather data at the site and relationships describing the temperature dependence and tensile strength of asphalt concrete. It is worth noting that the temperature fluctuations considered for the extreme and average environmental conditions were 22 and 14°C respectively. The failure criterion she used was the reduction of stiffness to 50% of its initial value.

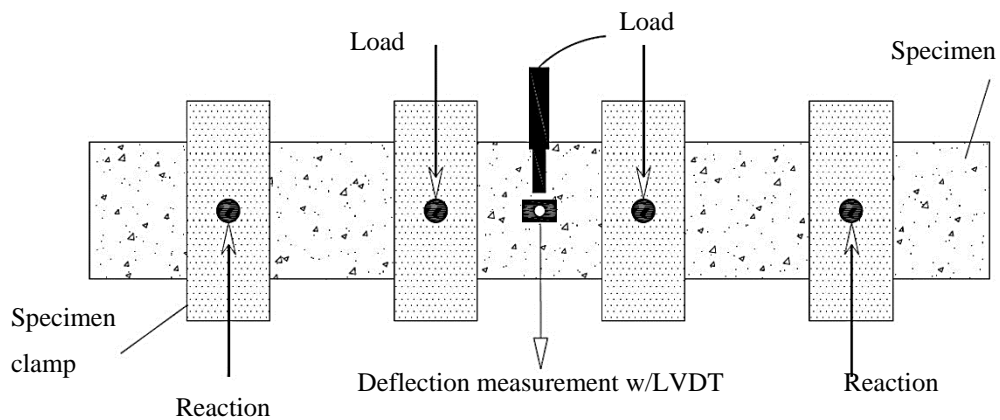


Figure 2.13 Schematic of the four-point bending beam fatigue test.

CHAPTER 3

METHODOLOGY

3.1 Introduction

This chapter is allocated to the methodology used in this research. The main topics of this chapter are revising, manufacturing, programming and calibrating the TSRST machine, estimating the quantity of materials, mixing, compacting and cutting the samples.

3.2 Preparation of TSRST machine

TSRST device has been used by numerous researchers for the measurement of low temperature cracking, and each of them has designed their own apparatus. For the measurement of thermal fatigue, Jackson et al. (1996) were the first and only researchers who designed a TSRST machine. As a result, in this thesis work a TSRST device is revised for measuring thermal fatigue cracking.

3.2.1 Design and fabrication

The first step in this research is to use a TSRST machine for measuring thermal coefficient, and then revise it for measuring the thermal fatigue resistance of asphalt concrete samples.

The TSRST used in this study is made up of three main parts: refrigerating chamber, servo motor for actuation and a compressor unit for decreasing temperature. In addition, in order to control the test and gather data, a computer and a data acquisition system are used (Figures 3.1, 3.3 and 3.4).

The refrigerating chamber is made up of two layers. The internal layer, which is used for insulation is made of a certain foam material, and the external layer whose function is structural is made of a steel frame (Figure 3.2).

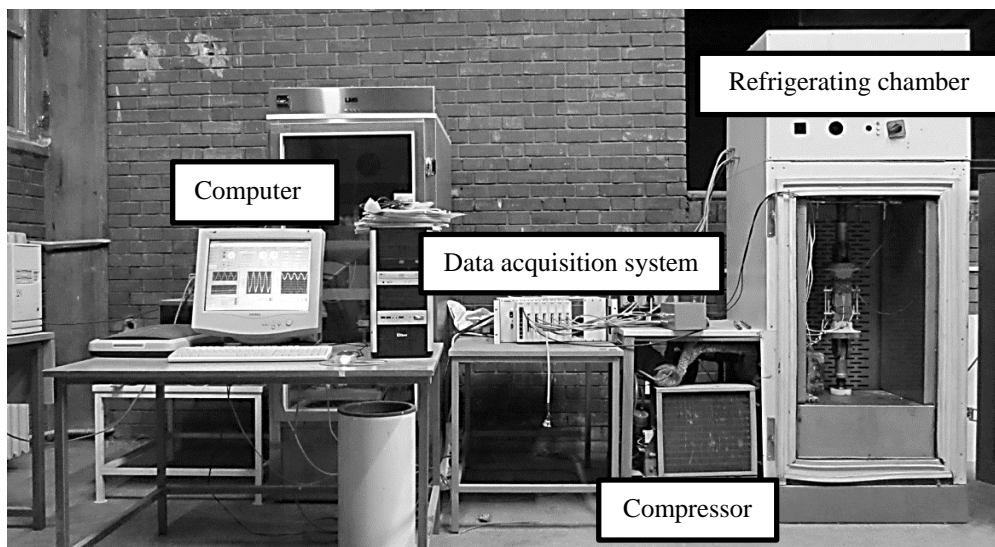


Figure 3.1: TSRST machine for measuring thermal coefficient and thermal fatigue resistance of asphalt concrete specimens.

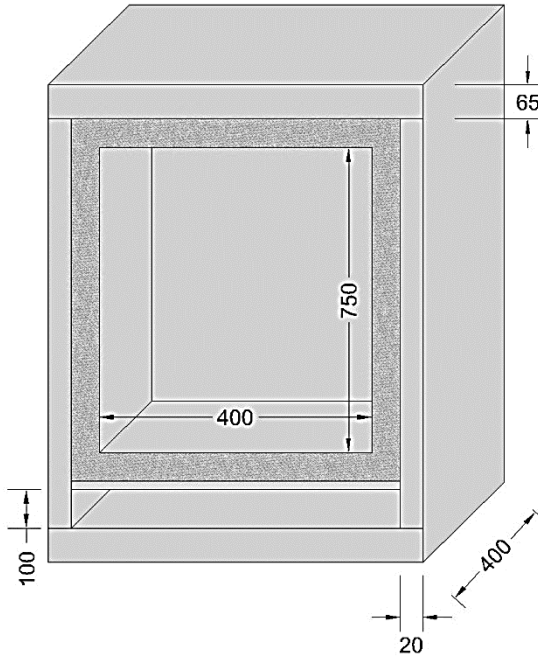


Figure 3.2: refrigerating chamber.

As it is seen in Figure 3.2, two steel plates each having 65 mm thickness are welded to top and bottom of the two vertical 20 mm thick steel plates in order to make the structural frame of the chamber. A foam material having 170 mm thickness is used in the inner part of the chamber for insulation against heat transfer. If the maximum load applied by the actuator on the specimen reaches 30 kN, which is the loading capacity of the load cell, the pertaining maximum vertical deflection of the structure of chamber reaches to 90 microns that is considered to be infinitesimal (Qadir, 2010). In addition, the vertical deflection has no effect on the measurement of thermal fatigue, because in the constant strain mode the load is recorded proportional to the applied strain that is measured within the gage length on the specimen.

Figures 3.3 and 3.4 represent general schematic of refrigerating chamber used for measuring the thermal fatigue resistance and the thermal coefficient of asphalt concrete specimens.

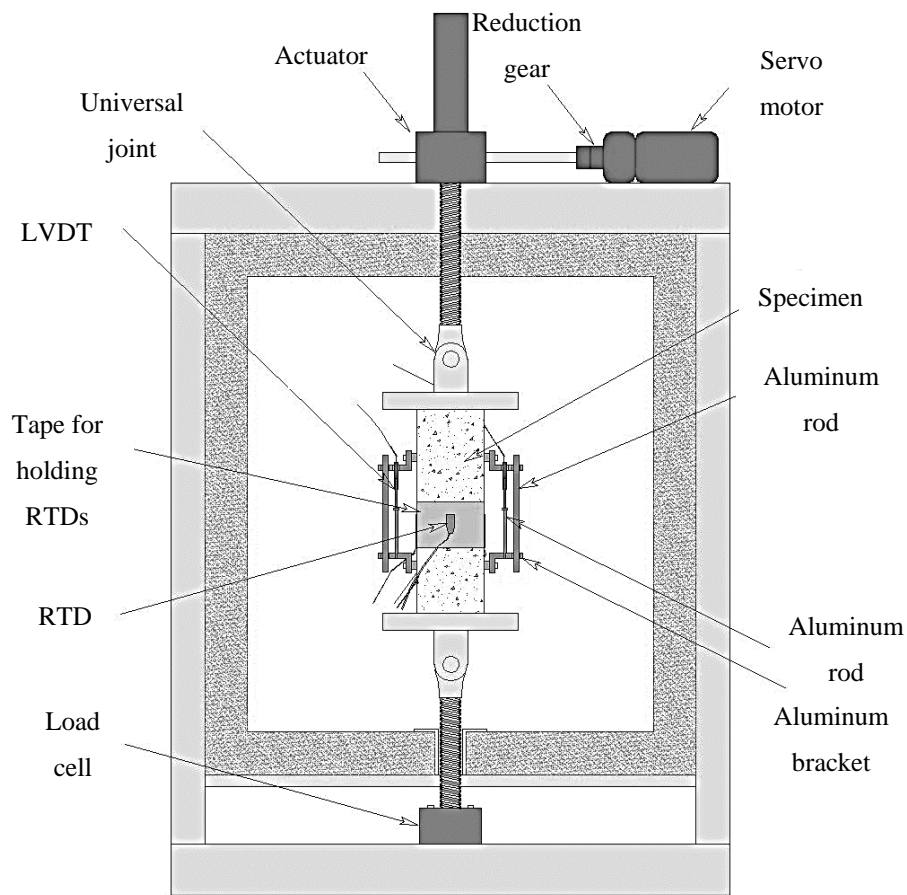


Figure 3.3: General schematic of the refrigerating chamber for measuring thermal fatigue resistance.

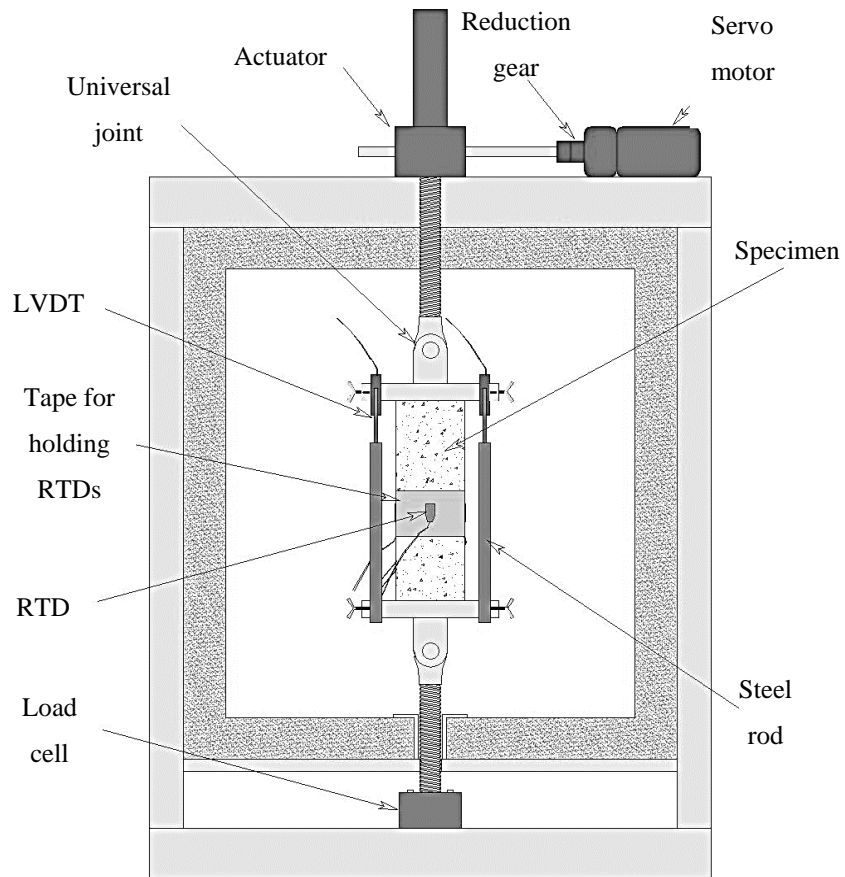


Figure 3.4: General schematic of the refrigerating chamber for measuring thermal coefficient.

The servo motor used in this study is used for both the measurement of thermal coefficient and cyclic application of load on the specimen in the measurement of thermal fatigue cracking. In measuring the thermal coefficient, it constantly applies a compressive amount of -5.25 kg on the specimen in order to compensate the dead weight of the specimen. In the measurement of thermal fatigue cracking the servo motor is capable of applying 30 kN on the specimen, which is the load capacity of

the load cell. It is worth noting that the servo motor used in this research work is potentially able to apply 50 kN on the specimen.

The compressor unit (Figure 3.1) has a key role in both the measurement of thermal fatigue resistance and the determination of thermal coefficient. In the former, it constantly keeps the temperature of the chamber at 5 C° while in the latter it decreases the temperature of the chamber from 15 to -25 so that the thermal coefficient can be measured.

The data acquisition system (Figure 3.1) is used for gathering data from transducers and for controlling the TSRST machine. In thermal fatigue test, for example, data acquisition system is capable of applying a desired cyclic strain on the specimen by serving as a terminal that connects the computer to the actuator and the LVDTs. Moreover, the stress data are simultaneously gathered by the data acquisition system and then recorded in the computer.

The computer (Figure 3.1) is used for entering the inputs and recording the outputs from the data acquisition system.

LVDTs are used in measurement of thermal coefficient and evaluating the thermal fatigue resistance of the specimens. In the former, two LVDTs capable of resisting cold temperatures are fixed into the top platen in a way that their tips touch the top of two steel rods fixed at the other end in the bottom platen. In the latter, the LVDTs are attached on the specimen using an aluminum fixture (Figure 3.5).

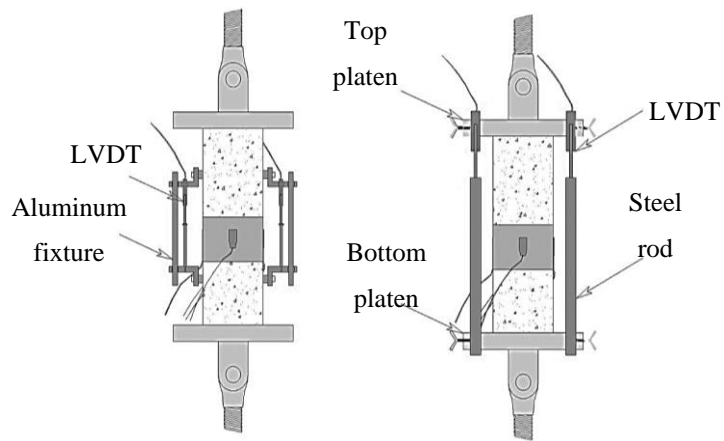


Figure 3.5: LVDT set up for measuring thermal coefficient and thermal fatigue resistance.

RTDs (Figures 3.3 & 3.4) are used in the test setup for measuring the thermal coefficient and the thermal fatigue resistance of the asphalt concrete specimens. These sensors are used to accurately measure the temperature at the surface and the core of the test specimens better than 0.3 °C. During the tests, a dummy specimen is placed vertically within the environmental chamber to measure the core temperature of each specimen. These measurements are performed using a probe RTD that is placed in the core of the dummy specimen (Figure 3.6).

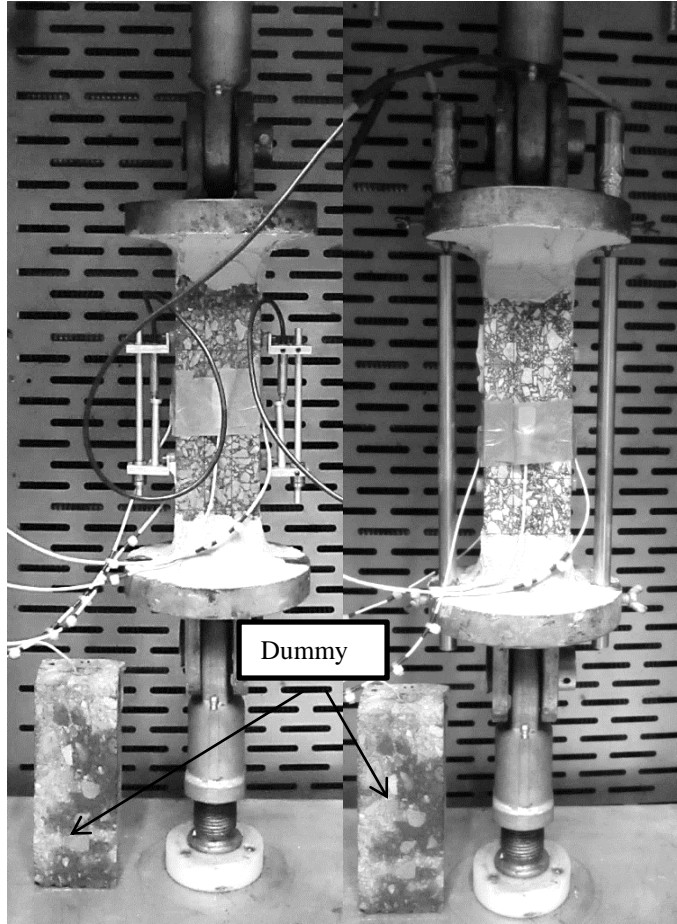


Figure 3.6: The dummy specimens placed beside the test specimens.

3.2.2 Programming

The program used in this research work was written in Labview® language, which facilitates the measurement and controlling of the test. The program is used in two modes: measuring the thermal coefficient and evaluating the thermal fatigue resistance. A comprehensive procedure for applying both modes is explained in the appendix section of this thesis.

3.2.2.1 Program for measurement of thermal coefficient

In this mode, at first the specimen is preconditioned at a target temperature until the target temperature is stabilized within the specimen. After that, the temperature is decreased to result in the shrinkage of the specimen. During the temperature reduction a negligible compressive load is applied on the specimen in order to guarantee free shrinkage of the specimen. During the test, the data of temperature reduction versus axial deformation are recorded by the program, which also is used for the measurement of thermal coefficient. The panel of the program consists of two parts: the section for entering input data manually, and the section showing the outputs in the form of plots. The input section consists of system control, motor control, test control mode, displacement control, and temperature data control. The output section includes the plots showing deformation versus time, temperature versus time, and instantaneous thermal coefficient versus time (Figure 3.7).

1- The system control

The system control consists of buttons for turning on and off the power, motor, fan and cooler. During the test, all of the buttons must be turned on.

2- The motor control

The motor control as its name implies controls the motor speed, the amount of load it applies and the direction to which it should rotate. For example, in order to mount the specimen in the machine, the speed and direction of moving the top platen are set in a way that enable the operator to reach a desired space between the top and bottom platens, so that the specimen can be mounted between them. In addition, during the thermal coefficient test the motor constantly applies a compressive 50N load on the specimen to ensure the free shrinkage of the specimen. The amount of applied load on the specimen is adjustable through the box that is in the motor control section.

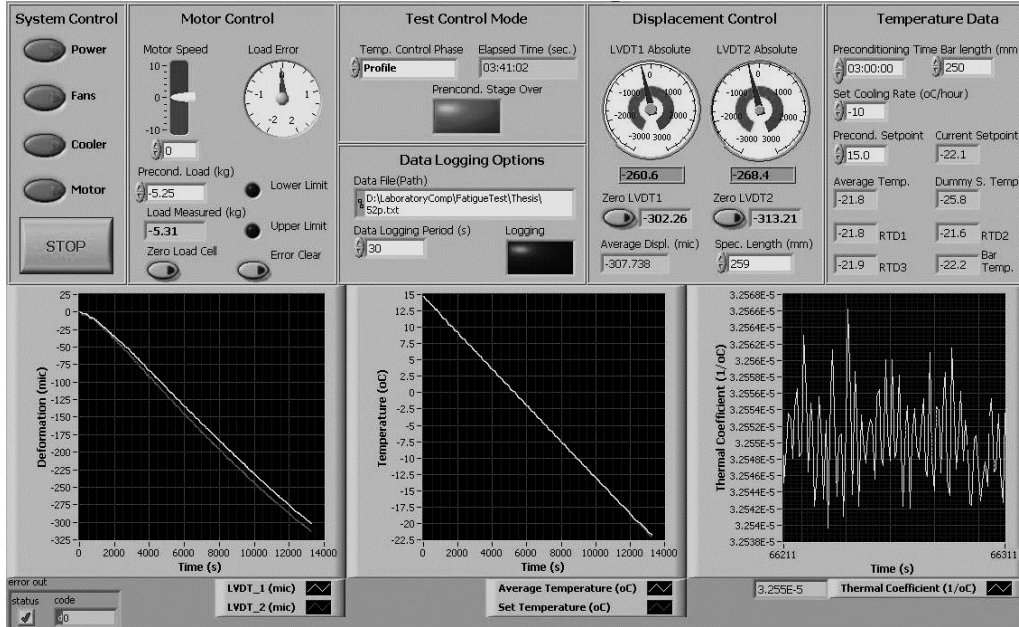


Figure 3.7: The program for the measurement of thermal coefficient

3- The test control mode

The main part of the test control mode is the control phase which lets the user to choose the mode of testing. It enables the operator to choose between the jugging mode, preconditioning mode and the profile mode. The preconditioning mode is 3 hours for this research which allows the target temperature of 15 °C to be stabilized within the specimen, then by choosing the profile mode the software starts to decrease the temperature, so that the thermal coefficient could be calculated by using the data of thermal strain versus temperature which is recorded by the software .The program does not let the operator to start the profile mode until the green blinker representing the end of stage for preconditioning starts blinking.

In addition to the control mode, there are other parts in the test control mode: the box showing the elapsed time during the test, the data file directory, the box showing data logging period and a green blinker blinking each time that the data is

recorded. In this research, the data logging period is set to record the data in each 30 seconds.

4- Displacement control

This section is totally related to LVDTs. The LVDTs are set to zero when the profile mode is started. Due to the decrease in temperature both the specimen and extension bars start to shrink. The shrinkage of extension bars results in getting erroneous results from LVDT readings. The software eliminates the error by subtracting the shrinkage length of extension bars from LVDT readings. This section also includes a box showing the average displacement of LVDTs.

5- The temperature data control

This section allows the operator to enter the preconditioning time, the cooling rate and the preconditioning temperature. The preconditioning time, cooling rate and preconditioning temperature considered for this research work are 3 hours, -10°C/h and 15°C respectively.

This section also shows the readings from the four RTDs placed on the surfaces of the prismatic specimens together with the temperature of rod RTD placed in the core of the dummy specimen.

3.2.2.2 The program for measuring the thermal fatigue resistance

In this mode, like the program written for measuring the thermal coefficient, at first the specimen is preconditioned at a target temperature until the aimed temperature is stabilized within the asphalt concrete. After the preconditioning, according to the program, a certain sinusoidal displacement is applied on the specimen and the test goes on for a defined period of time or until the specimen breaks. During the test, the data of stress, time, temperature and strain are recorded by the program. The panel of the program consists of two parts: the section for entering input data manually, and the section showing the outputs in the form of plots. The input section consists of system control, motor control, test control mode, displacement control, load control and temperature data control. The output section includes the plots

showing load versus time, deformation versus time, temperature versus time, and amplitude versus time (Figure 3.8).

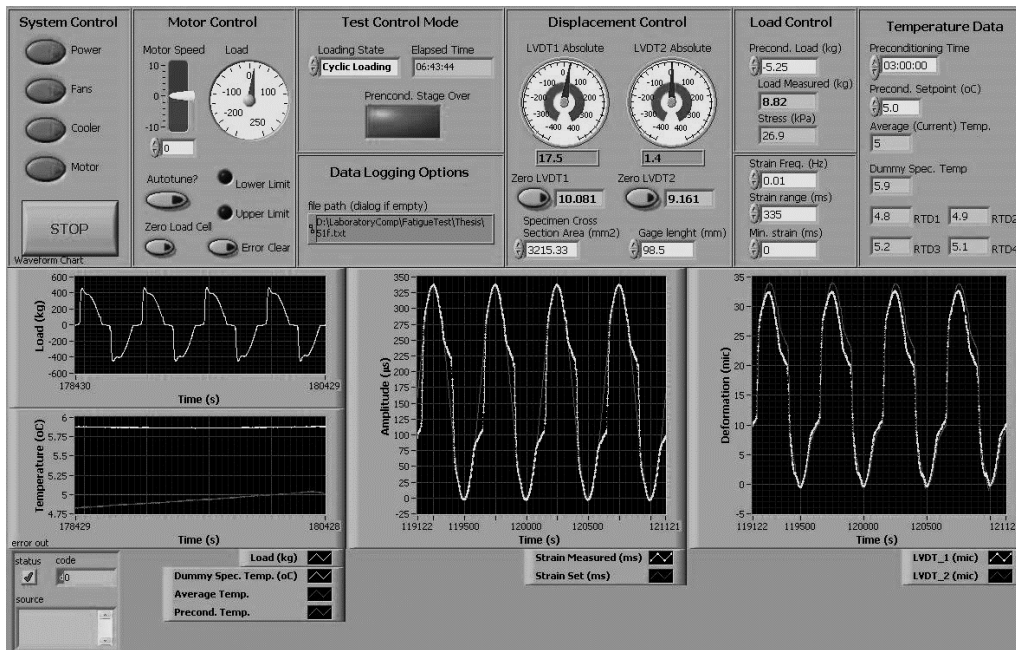


Figure 3.8: The program for the measurement of thermal fatigue cracking.

1- The system control

The system control consists of buttons for turning on and off the power, motor, fan and cooler. During the test all of the buttons must be turned on.

2- The motor control

The motor control in the thermal fatigue mode, serves exactly like motor control section in the thermal coefficient mode.

3- The test control mode

The main part of the test control mode is the loading state which lets the user to choose the mode of testing. It enables the operator to choose between the jugging mode, preconditioning mode and the cyclic loading mode. The preconditioning mode is 3 hours for this research work which allows the target temperature of 5 °C to be stabilized within the specimen, then by choosing the cyclic loading mode the software starts to apply sinusoidal load on the specimen that is commensurate with the amplitude of displacement in microns which is entered as input into the program. The amount of constant sinusoidal displacement is calculated after finding the thermal coefficient. The thermal coefficient is calculated from the data recorded in the thermal coefficient mode of the program.

In addition to the loading state, there is a box showing the elapsed time during the test and also a green blinker that whenever starts blinking indicates that the program is ready for applying cyclic load. There also is a part for entering the directory of the file and its name so that after writing the address in the pertaining box the file is recorded there during the test. The data are recorded at each second.

4- The displacement control

This section includes the part showing LVDT reading, the part for entering the average cross section area of the specimen measured at three sections in squared millimeters and a box for entering the gage length in millimeters which is always 98.5 mm. The LVDTs are set to zero when the cyclic loading mode is started. During the test, the program applies the cyclic loading according to the average value of the two LVDT readings. Their average must oscillate between the amplitude of the strain entered by the operator in the load control mode and zero. Therefore, the program pulls and pushes the specimen to the extent that the average range of the two LVDT readings at the maximums and minimums becomes equal to the amplitude of strain entered by the user and zero respectively.

5- The load control

This section includes the parts for pre-conditioning loading, load measured, stress, strain frequency, strain range and the minimum strain.

The preconditioning loading which is -5.25 kg is entered to the pertaining box by the operator. It is a trivial amount, which ensures that there would not be any excessive load and the specimen would be pre-conditioned as it is free at both ends.

The part representing the load measured shows the amount of load applied on the specimen in response to the applied cyclic strain, and the part allocated to the stress represents the division of the measured load by the input cross section area of the specimen and shows the value of stress in kPa.

Strain frequency is entered to the program by the operator and its value for this research work is 0.01Hz. The strain range is calculated on the basis of the maximum generated thermal strain in the specimen, and its unit is micron. The strain range is calculated by multiplying the thermal coefficient of asphalt concrete in a certain temperature range of interest and is the maximum amount up to which the specimen is pulled. The minimum strain is chosen to be zero for this research because it is not intended to make the specimen undergo pretension.

6- The temperature data

This section allows the operator to enter the preconditioning time and the preconditioning temperature. The preconditioning time and temperature considered for this research work are 3 hours and 5°C respectively. During the preconditioning mode, when the temperature of the specimen is over 5°C the program keeps the cooler and fans running until it reaches 5°C, and when the temperature of the chamber falls below 5°C the program still does not let the fans and cooler operate until the temperature exceeds the target temperature again.

This section also shows the readings from the four RTDs placed on the surfaces of the prismatic specimen together with value of the rod RTD placed in the core of the dummy specimen.

3.3 The temperature range for measuring the thermal fatigue resistance of asphalt concrete

The pavements made of asphalt concrete undergo thermal fatigue cracking whenever subjected to cyclic temperature changes while being restrained by the layer beneath them. The range of daily temperature change and the frequency of its occurrence depend on the locality in which the pavement is constructed. For this thesis work, the province of Ankara located in Turkey is the area in which the thermal fatigue resistance is investigated. As a result, the weather data gathered by the Weather Bureau were analyzed from 2000 to 2013 inclusively. Using a code written in MATLAB® environment, the range of temperature was calculated for each day during the 13 years and then the results of the frequency versus temperature range for all of the days of that period were plotted in the Figure 3.9. As it is seen in the graph, the range of 10°C is the mode with a frequency of occurrence of more than 200.

Due to the result of this analysis, the measurement of thermal fatigue resistance in this study was founded on a temperature range with a value of 10°C.

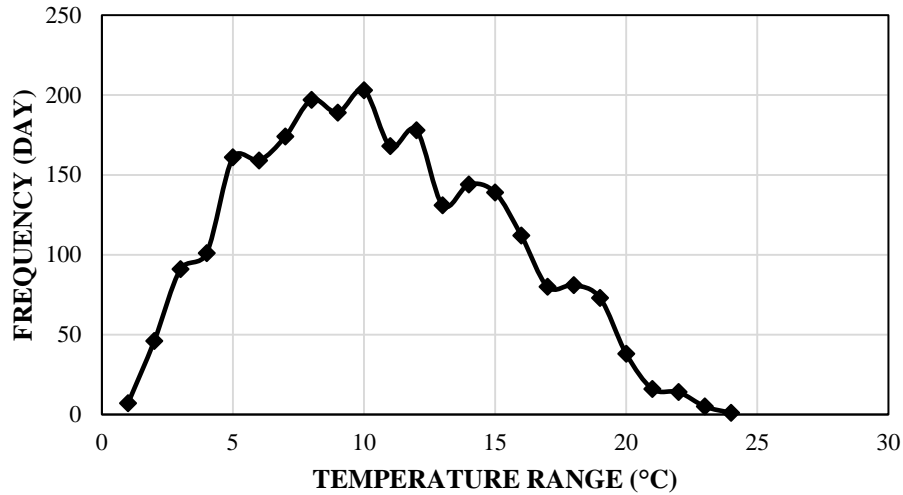


Figure 3.9: Frequency versus temperature range.

3.4 Measurement of thermal strains for applying the cyclic sinusoidal loads

After finding the temperature differential of 10°C, and measuring the thermal coefficients of the specimens, the maximum thermal strains pertaining to each specimen were calculated through using Equation 3.1. In this study, it was assumed that the minimum strain level is zero implying a complete strain reversal only at the initial cycle for each load application. Then, for evaluating the thermal fatigue resistance, the cyclic sinusoidal loads (0.01Hz) were applied on the specimens at the calculated constant strain amplitudes specific to each specimen.

$$\varepsilon = \alpha\Delta T \tag{3.1}$$

Where:

ε = thermal strain at the selected temperature range;

α = Thermal coefficient; and T = temperature.

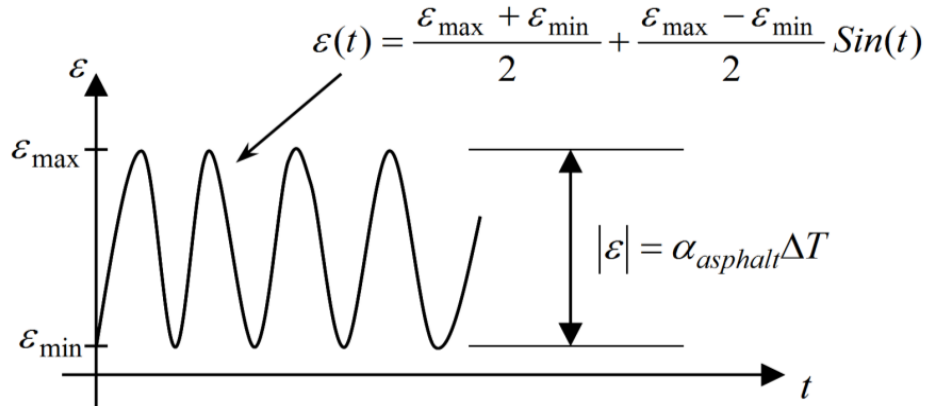


Figure 3.10: Waveform for the constant amplitude sinusoidal strain loading.

3.5 Sample preparation

Sample preparation consists of selecting the mix design variables, statistical design of variables, compacting the mixtures in the form of slabs, cutting the beam specimens from the slabs, and finally measuring the mix volumetric properties of the beam specimens. The samples that were used in this study were statistically designed and prepared for the measurement of low temperature cracking and the ones remaining from that experiment are utilized in this study. To achieve a complete aging of the test specimens, they were kept in the laboratory environment for five years. Since the specimens used by other researchers for the measurement of thermal cracking were not aged in such a way, the results of this study are unique as the aging process was completed in a natural way. Several authors stated that the thermal fatigue cracking of asphalt concrete is not a viable mode of distress without considering the effect of aging (Jackson & Vinson, 1996).

3.5.1 Selection of the materials for the study

In order to satisfy the design requirements the aggregates were obtained from an asphalt plant in the vicinity of Ankara. The modified and unmodified asphalt cements used in this study are in accordance with the standards of Turkish General

Directorate of Highways (TGDH). The properties of the materials used in this research work are presented in Tables 3.1 and 3.2.

Table 3.1 Aggregate properties

Measured properties	Aggregates	
	Basalt	Limestone
Specific gravity	2.93	2.75
Average absorption, %	1.00	1.45
LA abrasion value, %	15	28

Table 3.2: Asphalt properties

Measured properties	Asphalt	
	50/70	71/100
Specific gravity	1.025	1.034
Penetration (0.1 mm)	54	73

The gradation of aggregates as well as the grades of asphalt were chosen in a way that the requirements of TGDH were met. According to the TGDH, wearing course

consists of either coarse or fine aggregates, which are named as Type I and Type II, respectively. This classification is for considering the extreme values of gradation to meet that demands of the construction sector. Using a 0.45 gradation chart, the selected gradation for this study are presented in the Figure 3.10.

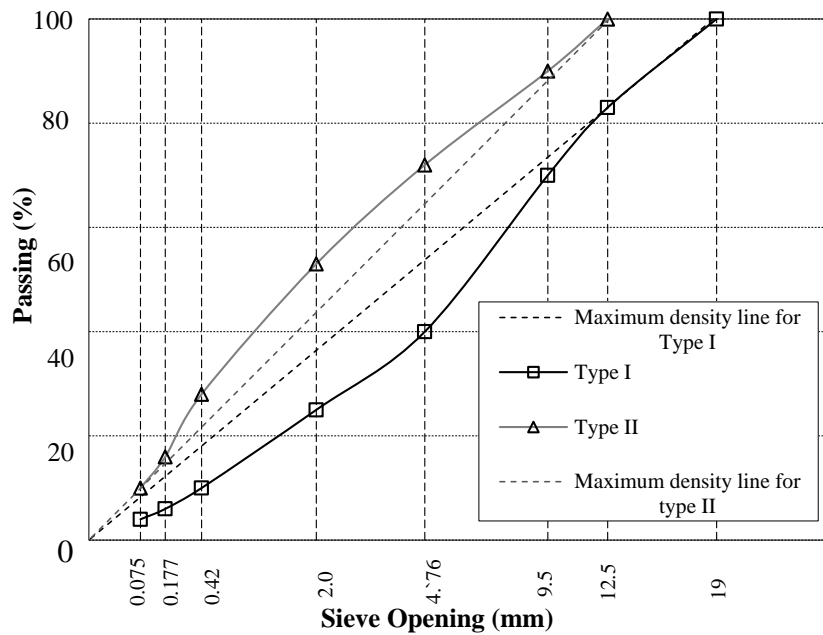


Figure 3.11: The gradation of aggregates according to the standards of TGDH (Qadir, 2010).

3.5.2 Superpave mixture design

Superpave is a design method that stands for Superior Performing Pavements, and supersedes the Marshal mix design. In this study, the optimum asphalt content was achieved by using the Superpave method of mixture design. In this study, except

the optimum asphalt content which was achieved in accordance with the standards of Superpave, the selection of asphalt cement grade, aggregate gradation and asphalt content were all according to the standards and requirements of TGDH (Qadir, 2010). Qadir, (2010) according to the standards of Superpave, prepared three samples for each combination and tested them for the optimum asphalt content at an approximate air void content of 4%. In order to compensate for the alterations in the design of air void contents, he considered a tolerance margin of $\pm 0.5\%$. For measuring the optimum asphalt contents at the target air voids, the values of theoretical maximum specific gravities, maximum density and the specimen bulk specific gravities were measured according to the codes of AASHTO T 166 & AASHTO T 209.

After finding the values of optimum asphalt contents, the weight required for combination of mixes, the voids filled with asphalt (VFA) and the voids in mineral aggregates (VMA) were calculated. A total of different 16 mix designs were prepared at the optimum asphalt contents (Table 3.3).

Table 3.3: summary of calculated asphalt contents (Qadir, 2010)

No.	Aggregate	Asphalt	Modification	Gradation	Optimum AC %	Air voids %	Weight Required (Kg)
1	B	57	Z	F	5.0	4.0	20.90
2	B	57	Z	C	4.4	4.0	20.93
3	B	57	S	F	5.2	4.0	20.21
4	B	57	S	C	4.8	3.6	20.71
5	B	71	Z	F	5.3	4.0	20.63
6	B	71	Z	C	4.5	3.9	20.35
7	B	71	S	F	5.4	4.0	20.87
8	B	71	S	C	5.0	3.9	21.07
9	F	57	Z	C	4.5	3.9	22.41
10	F	57	Z	F	5.3	4.0	22.14
11	F	57	S	C	5.0	4.0	22.14
12	F	57	S	F	5.5	4.0	22.09
13	F	71	Z	C	4.8	4.0	21.8
14	F	71	Z	F	5.4	4.0	22.46
15	F	71	S	C	5.5	4.0	21.92
16	F	71	S	F	5.1	3.9	22.5
AASHTO 2001 Criteria				12.5 mm (Maximum size of aggregate)			
VMA (%)				14			
VFA (%)				65-75			
Symbol used: Aggregate Type: L-limestone, B-basalt; Gradation: C-coarse, F-fine; Modification: Z- No Modifications, S-SBS Modification; Asphalt Type: 57-(50/70), 71-(71/100); VMA- voids in mineral aggregates; VFA- voids filled with asphalt.							

3.5.3 Sample preparation for the measurement of thermal coefficient and the thermal fatigue resistance

The mixtures were prepared according to the specifications presented in the Table 3.3 and then using a French (LCPC) slab compactor, they were compacted in the

form of slabs with dimensions of $50 \times 18 \times 10$ cm. In order to simulate the short term aging, the mixtures were subjected to heat for three hours.

a – Preparation of beam specimens

Using a saw diamond machine, the dimensions of $50 \times 65 \times 250$ mm were cut out of the slabs. The cross section of 50×65 was chosen for maintaining an aspect ratio between 4 and 6 in order to eliminate any adverse effect on the response variables of the test (Vinson et al., 1989). It should be noted that after applying epoxy for sticking the specimens to the plates the length of each specimen becomes 260mm. Some of the beams were tested for measuring the resistance of asphalt concrete against the low temperature cracking and the measurement of the glass transition (Qadir, 2010), and the rest was left for laboratory aging for 5 years. This time period let the remaining specimens to age gradually and made them perfectly ready to be utilized for the measurement of thermal fatigue cracking in this research work.

b– Sticking and mounting studs on the specimens

In order to mount the aluminum fixtures on the specimens for the purpose of measuring the thermal fatigue resistance of asphalt concrete, at first, the plastic mounting studs must be attached on the specimens. For this reason, two straight lines are drawn on the two axes of each specimen surface. Then through the aid of an aluminum frame the plastic mounting studs are attached on the prismatic test specimens by using epoxy. The aluminum frame has two holes with exactly the same diameter as that of the studs. The longitudinal axes of the holes and the transversal axis of the frame must coincide with the longitudinal and transversal axes of the specimen surfaces, respectively (Figure 3.11).

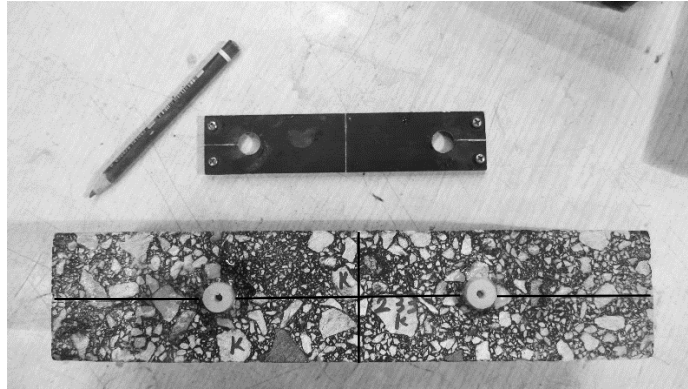


Figure 3.12: The method for sticking the plastic mounting studs on the sides of specimens.

c- Mounting the beam specimens between the top and bottom plates

Precision during adhesion of the specimens to the plates is crucial for the framework of accuracy in the test results. On the contrary, if this process had been done in a perfunctory manner, some situations could have arisen. For example, if the beam specimens and the plates were eccentric at either the top or bottom, unnecessary moments could have been induced within the specimens, and can lead to premature failures or significant reductions in the stiffness during the thermal fatigue test.

In order to ensure that the cross sections of each specimen at the top and bottom are concentric with the plates, before gluing them together using epoxy, a metal O-ring with a diameter of 15mm is glued on the center of both ends of the specimens. The O-ring acts as a female connector which receives the protrusions stuck out of the center of the plates and let the platens sit tightly and concentrically on the both ends of the specimens when they are mounted between the plates (Figure 3.12).

In order to glue the specimens to the plates by means of epoxy the bottom platens are fixed on a channel's flange supported on a board (Figure 3.13). Next some epoxy is applied on each plate and the specimens are seated on the epoxy. While seating the specimens on the plates, it has to be ensured that the protrusions of the

plates and the metal O-rings are interlocked well together. When the alignment is secured then some epoxy is applied on top of the specimens and the top platens are seated on the top of each specimen.

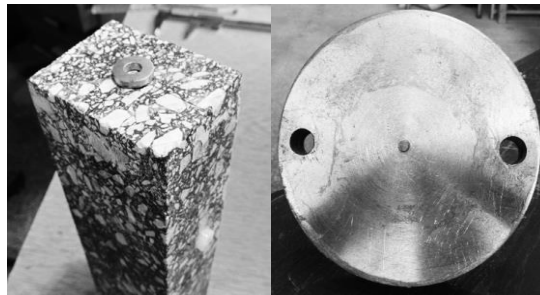


Figure 3.13: Ensuring the concentricity of the specimen and plates with the help of a metal O-ring.

Again while seating the top platens on the specimens, it has to be assured that the protrusions and the metal O-rings are joint well together. After that, in order to guarantee the robustness, some more epoxy, which increases the area of adhesion, is spread on the plates and the top and bottom of the specimens. Finally, the specimens are kept on the channels for at least 12 hours in order to let the epoxy cure and become strong enough to be tested for the measurement of thermal coefficient and consequently thermal fatigue resistance. It is worth noting that, in order to guarantee the adhesiveness of the epoxy to the surface of the plates and specimens, acetone and trichloroethylene are used respectively for cleaning the surfaces prior to starting the sticking process.

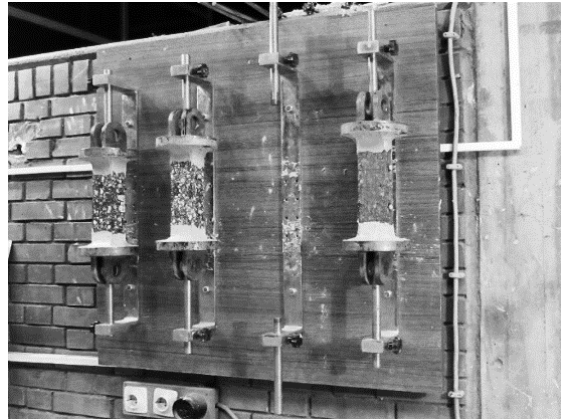


Figure 3.14: The board used for sticking the specimens to the plates.

3.6 Laboratory testing of the specimens

In this study two types of tests are performed: the measurement of thermal coefficient in order to find the amplitude of thermal cyclic strain, and the measurement of thermal fatigue cracking resistance of the beam specimens on the basis of the of thermal strain amplitude.

3.6.1 Testing for the measurement of thermal coefficient of contraction

The beam specimens stuck to the bottom and top plates are mounted in the TSRST machine and then the LVDTs and RTDs are attached on them. After the mounting, specimens were preconditioned at 15°C for three hours; then, according to the program written for the measurement of thermal coefficients, the temperature is dropped at a rate of -10°C/hour until it reaches -25°C. During the reduction of

temperature the specimens shrink freely and the data of axial deformation versus temperature for each specimen are recorded in each 30 seconds.

3.6.2 Testing for the measurement of thermal fatigue resistance

After recording the data for the measurement of thermal coefficient of contraction concerning the temperatures above the glass transition, the specimens are dismantled from the TSRST machine and left to warm in room temperature for at least 12 hours. Then the specimens are put back to the machine and the RTDs and LVDTs are mounted. After that, the specimens are preconditioned at 5°C for three hours. After the preconditioning time is over, constant cyclic strains with the frequency of 0.01Hz are applied on each specimen on the basis of their measured thermal strains. Thermal strains are measured according to the thermal coefficient of each specimen and the temperature differential of 10°C. The tests continue until either a breakage happens or the time spent for each run exceeds 3 days. During the thermal fatigue cracking tests, the data of stress and applied strain versus time are recorded for each beam specimen.

CHAPTER 4

DATA ANALYSIS

4.1 Introduction

This chapter presents the methods used for measuring the thermal coefficient and, consequently, the thermal fatigue resistance of the prismatic test specimens.

4.2 Analysis of experimental data for measuring the thermal coefficients

The relationship between thermal strain and temperature for one of the specimens is presented in Figure 4.1. In order to show the correlation between the thermal strain and temperature, a five-parameter curve (Equation 4.1), using the least square method, was fit to the test data (Bahia & Anderson, 1993). As it can be seen in Figure 4.1, there is a curvature at -12°C indicating the glass transition temperature lying in the applied temperature range. This shows that the thermal coefficient must be calculated before and after the glass transition temperature to characterize the thermo-volumetric properties of the specimen (Zeng & Sields, 1998). Because of the selected temperature range in the testing program, Equation 4.1 was therefore used to calculate the thermal coefficients of each specimen falling above the glass transition temperatures.

$$v = C_v + \alpha_g(T - T_g) + R(\alpha_l - \alpha_g) \ln \left[1 + \exp \left(\frac{T - T_g}{R} \right) \right] \quad (4.1)$$

Where:

v = specific volume at temperature T ; C_v = volume at a given temperature;

T_g = glass transition temperature; R = constant defining the curvature; α_l = thermal coefficient for $T > T_g$, and α_g = thermal coefficient for $T < T_g$.

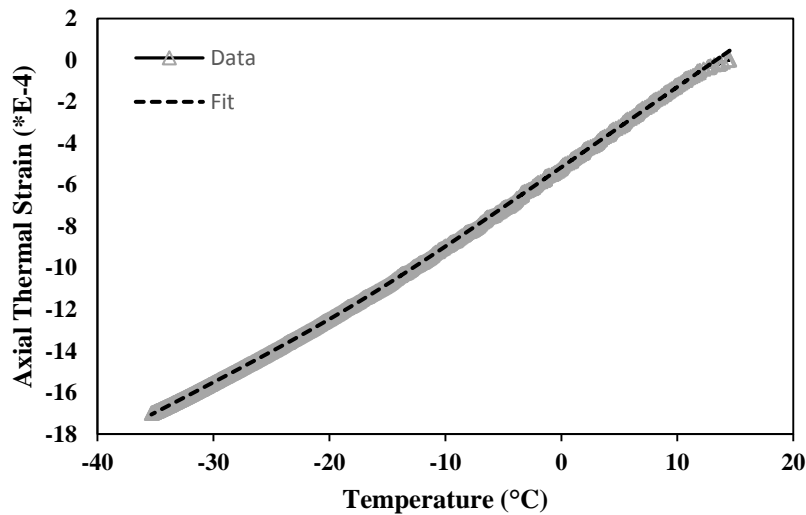


Figure 4.1: Axial thermal strain versus temperature

It should be emphasized that since the temperature range of interest for measuring the thermal fatigue resistance of beam specimens was within 0-10°C, the thermal coefficients for above the glass transition (α_l) were calculated for each specimen. The reason for selecting that temperature range is that the thermal fatigue cracking experiment had to be performed at 5°C and the most frequent temperature range during 2000-2013 that was calculated in Section 3.3 and it turned out to be 10°C.

In order to evaluate the thermal fatigue resistance of each specimen at the constant strain mode, it was necessary to measure the thermal strain that will be applied to each specimen (Table 4.1). These measurements were performed through Equation

4.2. It is worth noting that the thermal strains were calculated at the selected temperature differential of 10°C and according to each specimen's thermal coefficient.

$$\varepsilon = \alpha \Delta T \quad (4.2)$$

Where:

ε = thermal strain at the selected temperature range;

α = Thermal coefficient; and T = temperature.

Table 4.1: The values of thermal strains measured for each specimen.

Specimen Code	Replicate No.	Thermal Strain ($\mu\text{m/m}$)	Specimen Code	Replicate No.	Thermal Strain ($\mu\text{m/m}$)
LF54ZO	I	333	LF73ZO-	II	407
LF54ZO	II	298	BF54ZO+	I	361
LF54ZO+	I	379	BF54ZO+	II	385
LF54ZO+	II	380	BC73ZO-	I	386
LC54SO-	I	347	BC73ZO-	II	384
LC54SO-	II	337	BC73ZO-	III	387
LF54SO+	I	374	BF73ZO+	I	388
LF54SO+	II	377	BF73ZO+	II	384
LF54SO+	III	367	BF73ZO-	I	305
LF73ZO	I	355	BF73ZO-	II	355
LF73ZO	II	382	BF73ZO-	III	376
LF73ZO	III	364	BC73SO+	I	444
LF73ZO-	I	385	BC73SO+	II	422

4.3 Analysis of experimental data for thermal fatigue performance

During the thermal fatigue tests, according to the program written in the Labview[®] environment, the data of cyclic strain and stress versus time were recorded for each test specimen. Figures 4.2 and 4.3 represent an initial part of the data recorded for one of the specimens. The peaks of the cyclic data are underscored by the circles

because they play an instrumental role for determining the stiffness path for each of the specimens. The stiffness is calculated through dividing peak-to-peak stress by peak-to-peak strain.

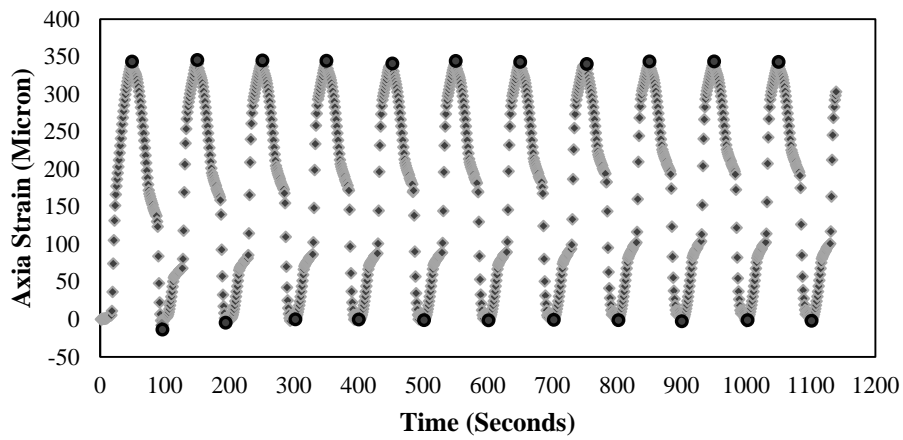


Figure 4.2: The data of applied axial strain on one of the specimens

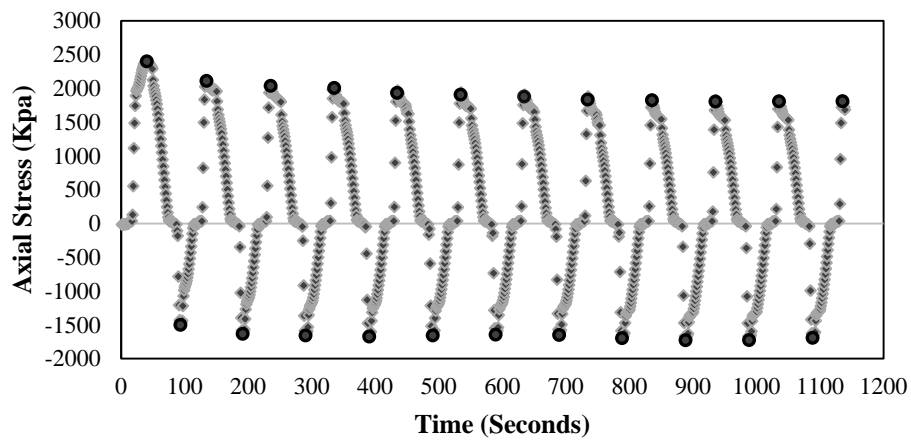


Figure 4.3: The data of axial stress recorded in one of the fatigue tests

Figure 4.4 represents the stiffness reduction path calculated in Matlab® environment for the same specimen under constant strain loading. It is worth noting that the stiffness reduction path shown in Figure 4.4 is calculated for the entire duration of the run and the horizontal axis represents the number of cycles. The test went on until the specimen broke at 1200th cycle. Since the frequency of the strain applied on the specimens is 0.01 Hz, each cycle needs 100 seconds to complete. For example, 1200 cycles in terms of duration is equal to 120000 seconds or 33 hours and 20 minutes.

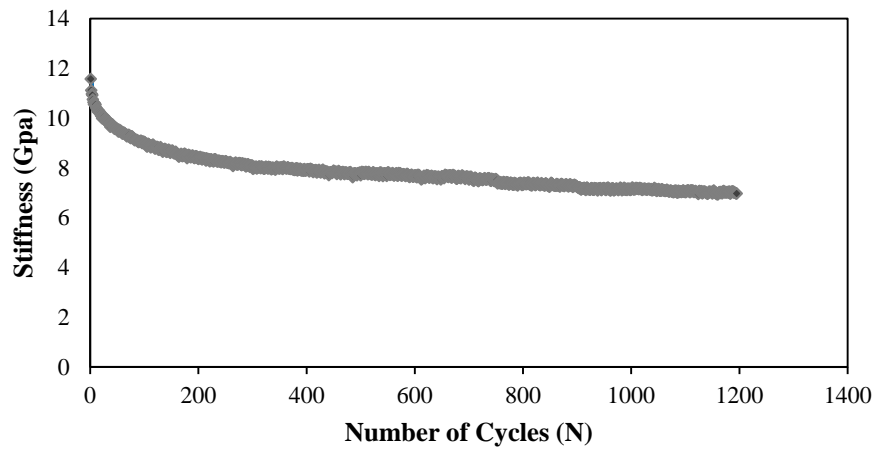


Figure 4.4: The stiffness path calculated for one of the specimens.

The stiffness paths calculated for all of the specimens are presented in the appendix part of this study.

In order to analyze the responses taken from all of the specimens, different approaches were used in this study which are explained in details in the following subsections.

4.3.1 Reduction of stiffness to 35% of its initial value

In conventional load-associated fatigue tests with the applied frequencies in the range of 10-50 Hz, the criteria for ending the tests is either 50% reduction in stiffness or when the specimen breaks. However, in the tests associated with thermal fatigue cracking, due to the low frequencies applied, it is not possible to carry on the tests until they approach to 50% reduction in stiffness. For instance, since the applied frequency was 0.01 Hz it was not practical to wait for each test to approach 50% reduction in stiffness. If the specimens did not break or approach to 50% reduction in stiffness, the cyclic applied strain was not removed earlier than 72 hours. The specimens generally approached to a range of stiffness reduction from 35 to 50%. Between the approached ranges of strains the minimum reduction of 35%, was chosen; then, the number of cycles and their natural logarithm pertaining to the selected stiffness reduction were taken as the response variable. Figure 4.5 represents the stiffness reduction path in terms of percent for three different test specimens. The stiffness reduction paths for all of the specimens are attached to the appendix section of this study.

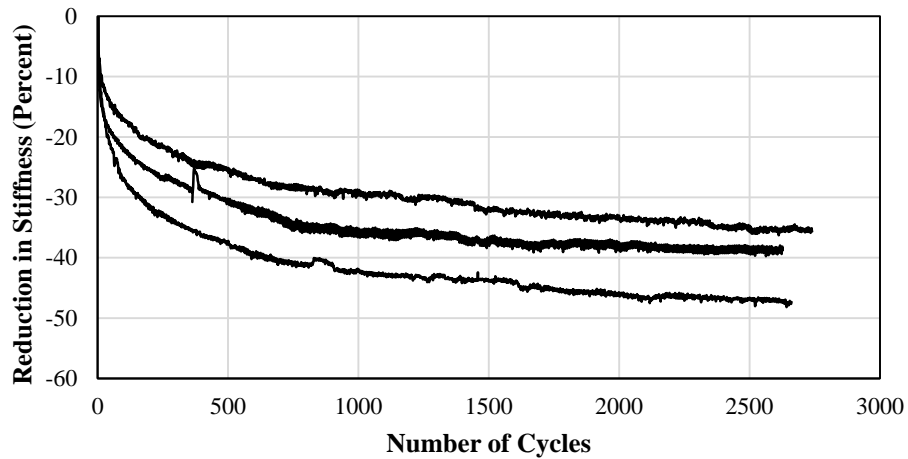


Figure 4.5: Stiffness reduction (in percent) for three different test specimens.

4.3.2 Extrapolating the number of cycles to 50% reduction using power model

Because it was not possible to carry on the tests for each specimen to approach 50% reduction in stiffness, it was decided to extrapolate the number of cycles to 50% reduction using a power model that is conventionally used for load-associated fatigue (Equation 4.3).

$$S = AN^B \quad (4.3)$$

Where:

S = Stiffness at cycle N ; and A & B are fatigue constants.

In order to fit the power model, at first the data of stiffness versus number of cycles were plotted in a log-log scale (Figure 4.6); as it is apparent in the figure, there is a region between the two circles in which the stiffness reduction approximately

follows a linear behavior; the linear region is labeled with the number 2 and is ascribed to fatigue performance of asphalt concrete. The first and the third region do not represent the fatigue behavior of asphalt concrete (Gerritsen & Jongeneel, 1988). The first portion represents an accelerating rate of reduction in stiffness which is due to the change in aggregate skeleton in the first few cycles; this change is because of the big amplitude of the constant cyclic strain that was applied on the test specimen. The third part of the graph in which the rate of stiffness reduction accelerates again is attributed to the rapid crack growth in the asphalt concrete.

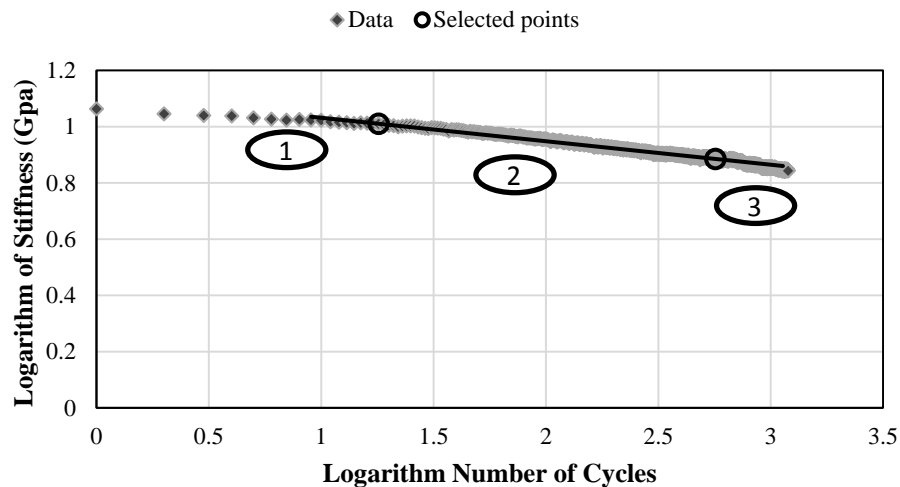


Figure 4.6: The data of stiffness versus number of cycles in a log-log scale.

The length and location of the linear portion of the log-log scale data that represent the fatigue behavior of the asphalt concrete differs from specimen to specimen. As

a result, for finding the best linear region, at first the log-log scale graphs obtained from the test specimens were observed visually in order to estimate the number of cycles belonging to a region that resulted in the best linear trend in reduction of stiffness. After that, by using a code that was written in Matlab® environment, the whole range of data was examined in order to find the exact location of the linear region. The best region was selected on the basis of the maximum value of coefficient of determination (Figure 4.7) that was obtained from performing linear regression for each investigated region. Figure 4.7, which is an output taken from Matlab®, shows the results of investigation in the form of the values of coefficients of determination for the specimen from which the log-log scale data was obtained and presented in the previous figure. As it can be seen in the figure, the written code starts to calculate the values of coefficients of determination from the first cycle up to the last one. The number of cycles, in each selected span from which the coefficients were calculated, is 550 and the best region start from the 18th cycle. As a result, the best span representing the fatigue behavior of 550 cycles starts from the 18th cycle and ends up in 568th cycle.

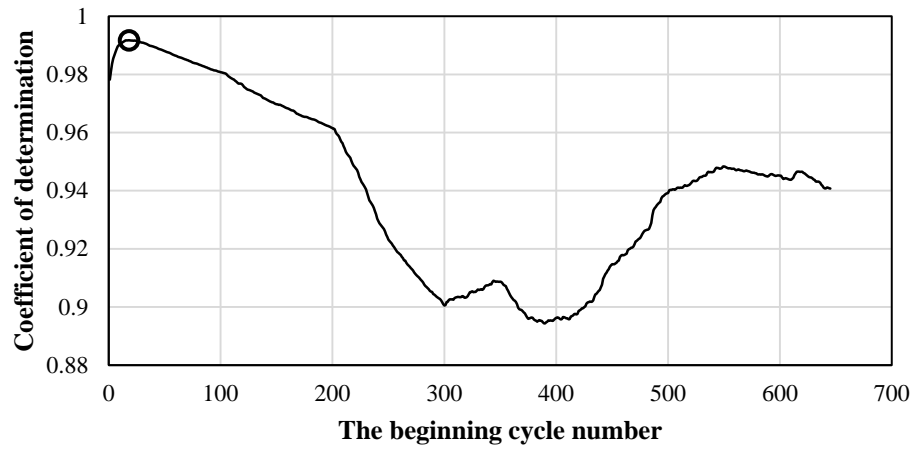


Figure 4.7: The plot showing the values of coefficient of determination for the whole range of cycles according to the selected number of cycles.

After finding the best region, the power model (Equation 4.3) was fit to the non-logarithmic scale of data which were within the best region (Figure 4.8). As it is obvious, the model presents the fatigue behavior very well.

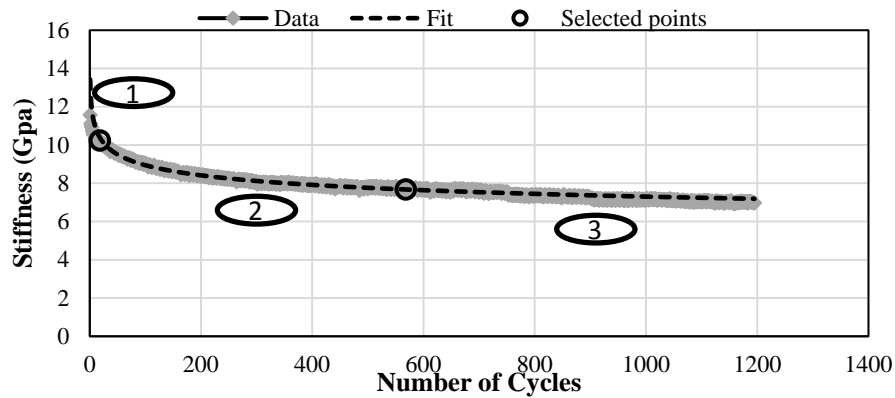


Figure 4.8: The power model fitted to the portion of data with the best fatigue behavior.

It is worth mentioning that the same graphs that were given as examples for one specimen in this subsection are made for all of the specimens and are attached to the appendix section of this study. In addition, the maximum calculated coefficients of determination for each specimen are attached in a tabular format to the appendix section.

4.3.3 Calculating the slope of the linear line fitted to log-log scale data

Another approach used for analyzing the data of thermal fatigue was evaluating the slope of the linear line that was fitted to the log-log scale data. The way of fitting the linear line was explained in details in the previous subsection.

The slope of the linear line calculated for each test specimen shows the rate at which micro cracks developed within the specimen during each test. Bigger absolute value of slope of the line results in quicker propagation of micro cracks and, consequently, the shorter fatigue life of the specimen (Figure 4.9).

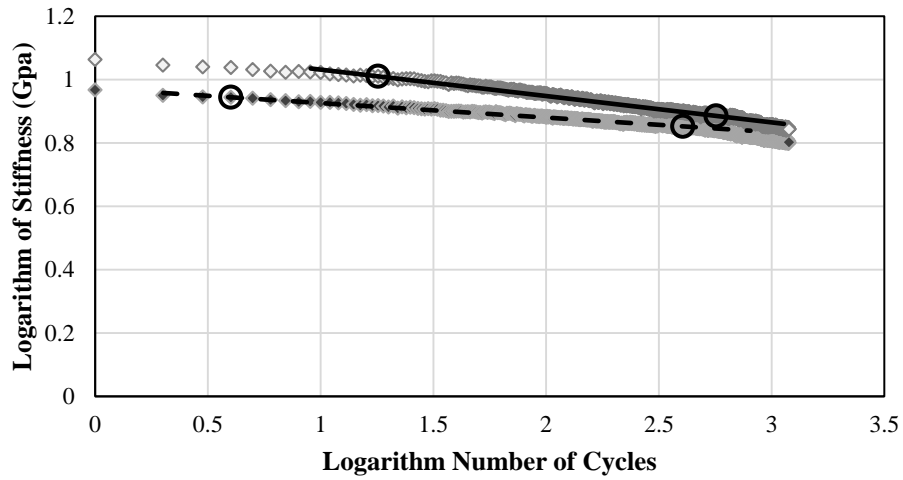


Figure 4.9: Comparison of the slopes of two linear lines fitted to the log-log scale data.

Figure 4.9 clearly illustrates the difference between the slopes of two lines fitted to the log-log scale data gathered from two test specimens. The specimen's fatigue behavior with the dashed line outperforms the continuous one because its slope is smaller and, as a result of that, it resists thermal fatigue cracking better.

CHAPTER 5

RESULTS AND DISCUSSION

5.1 Introduction

This chapter deals with the statistical analysis of the test results taken from the measurement of thermal coefficient and thermal fatigue resistance of the test specimens. The results were analyzed through analysis of variance (ANOVA) technique in Matlab[®] environment.

5.2 Mixture design variables for performing ANOVA

The beam specimens used in this study were statistically designed and fabricated for the measurement of low temperature cracking, and the remaining ones from the previous experiment were utilized for the measurement of thermal coefficients and thermal fatigue resistance of asphalt concrete beam specimens. The following statistical variables with their assigned symbols were included in this research: 1- Aggregate type: basalt and limestone with the assigned symbols of B and L respectively. 2- Gradation: coarse and fine with the assigned symbols of C and F respectively. 3- Asphalt grade: with penetration values 54 and 73 (0.1mm) and the symbols assigned to them is the same as their values. Modification: modified with SBS with the symbol S and not modified with the symbol Z. 4- Asphalt content: optimum asphalt content with the symbol O, 0.5% more than optimum asphalt content with the symbol O+ and 0.5% less than optimum asphalt content with the symbol O-. For example, a specimen with the code LF54SO+, consists of Limestone, Fine gradation, an asphalt type with a penetration value of 54, SBS modifier and an asphalt content that is 0.5% more than the optimum asphalt content.

It is worth noting that some of the specimens had two replicates while others had three (Table 5.1).

Table 5.1: Types of specimens and their replicate numbers

Specimen code	No. of replicates	Specimen code	No. of replicates
BC73ZO-	3	LF73ZO-	2
BC73SO+	2	LF73ZO	3
BF54ZO+	2	LF54SO+	3
BF73ZO-	3	LF54ZO	2
BF73ZO+	2	LF54ZO+	2
LC54SO-	2		

5.3 Analysis of variance tests (ANOVA) for the measured thermal coefficients

A total of 26 specimens (Table 5.1) were tested in order to measure the thermal coefficients, and then they were statistically analyzed for finding the significant mixture design variables affecting the thermal coefficient of asphalt concrete. Table 5.2 presents the probability values calculated through ANOVA. As it is apparent from the ANOVA results, asphalt content and aggregate type are the most significant design variables since their p-values for a confidence interval of 5% ($p < 0.05$) are approximately zero. In addition, aggregate type and gradation are also significant because their p-values are less than 0.05. Table 5.3 represents the average thermal coefficients pertaining to each type of mixture.

Table 5.2: ANOVA analysis for the measured thermal coefficients

Design variable	Probability
Aggregate type	0.0203
Gradation	0.0115
Asphalt type	0.0001
Modification	0.2667
Asphalt content	0.0001

Table 5.3: The averaged measured thermal coefficients

Specimen code	Thermal coefficient (1/°C)	Specimen code	Thermal coefficient (1/°C)
BC73ZO-	3.86E-5	LF73ZO-	3.96 E-5
BC73SO+	4.3 E-5	LF73ZO	3.67 E-5
BF54ZO+	3.73 E-5	LF54SO+	3.73 E-5
BF73ZO-	3.45 E-5	LF54ZO	3.16 E-5
BF73ZO+	3.86 E-5	LF54ZO+	3.8 E-5
LC54SO-	3.42 E-5		

Since the thermal coefficient of asphalt concrete can represent its behavior associated with thermal cracking (Arabzadeh & Guler, 2014), lower thermal coefficients can result in better performance in terms of thermal cracking. If they are lower, they will result in lower thermal strains and as a result of that lower thermal stresses can be generated within asphalt concrete pavements when they are exposed to temperature differentials.

As it is apparent in Figure 5.1, the variations in the asphalt content caused drastic changes in average values of thermal coefficient and the smallest thermal coefficients were obtained when the value of asphalt content was optimum. Thermal coefficients measured for the asphalt content which was 0.5% higher than optimum turned out to be the largest and the asphalt content which was 0.5% less than the optimum resulted in values of thermal coefficient which were between the other two values. As it can be seen in the figure, variation in the average values of thermal coefficient among the specimens with the highest asphalt content is minimum, which indicates that the amount of asphalt content is a dominating factor in determining the value of thermal coefficient. The results obtained for the thermal coefficient approximately agree with the conclusion made by Xu et al., (2008). They examined the effect of two types of asphalt content: 3.8 and 5% at 4 and 4.1% airvoid contents respectively and concluded that higher asphalt content results in a higher thermal coefficient. In addition, Vinson et al., (1989) concluded that small changes in asphalt content increases the thermal coefficient and decreases the strength of the asphalt concrete. The result of this thesis work concerning the effect of asphalt content on thermal coefficient is compatible with the research performed by Qadir (2010) in which he investigated the effect of variations in asphalt content on low temperature cracking; he found that the optimum asphalt content results in the highest fracture strength and the lowest fracture temperature.

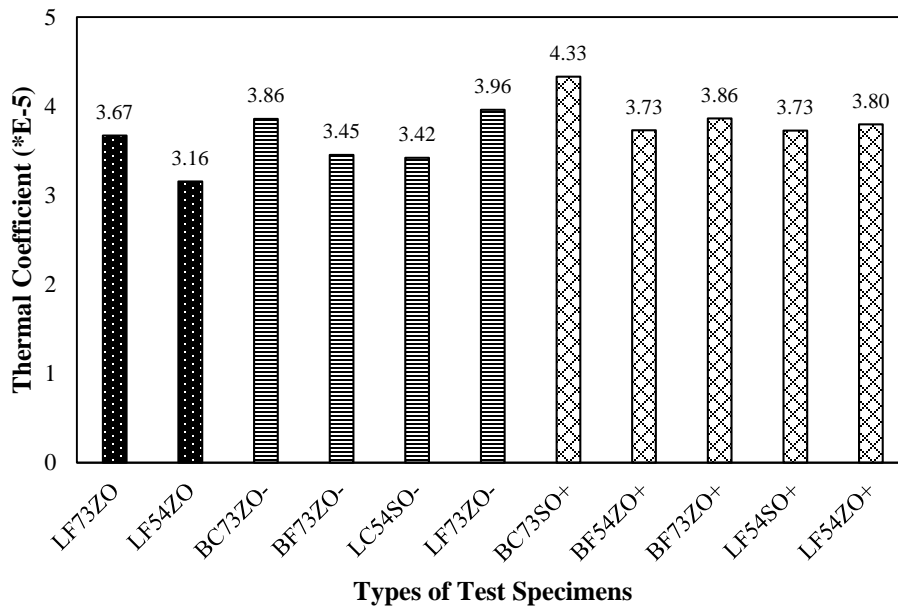


Figure 5.1: The average thermal coefficient measured for the test specimens grouped according to the asphalt content.

A figure similar to Figure 5.1, in which all of the 26 specimens are grouped according to the asphalt content, is attached to the appendix section of this study.

The asphalt type with lower penetration value resulted in smaller thermal coefficients in the test specimens (Figure 5.2) which may be ascribed to the change in the chemical compounds of the two types of asphalt that were used in this study. However, it is believed that softer asphalts outperform the harder ones against thermal cracking (Wang, Wayoe, & Anderson, 1992). The reason for this discrepancy can be because of the long period of aging during which may be the higher grade asphalt showed more susceptibility to the aging and became more aged. A figure similar to Figure 5.2, in which all of the 26 specimens are grouped according to the asphalt type, is attached to the appendix section of this study.

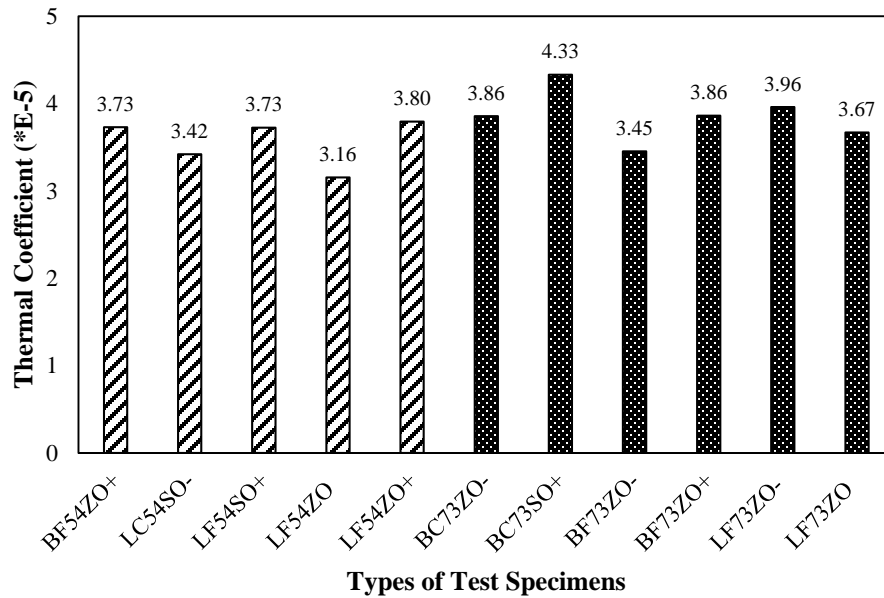


Figure 5.2: The average thermal coefficient measured for the test specimens grouped according to the asphalt type.

Another outcome of the analysis is the behavior that fine graded mixture displayed by showing relatively lower thermal coefficients (Figure 5.3); this behavior may be is due to the fact that finer aggregates offer a better degree of interlock in the aggregate skeleton. The results concerning the gradation type are in agreement with the findings of Tan et al., (2008). A figure similar to Figure 5.3, in which all of the 26 specimens are grouped according to the gradation, is attached to the appendix section of this study.

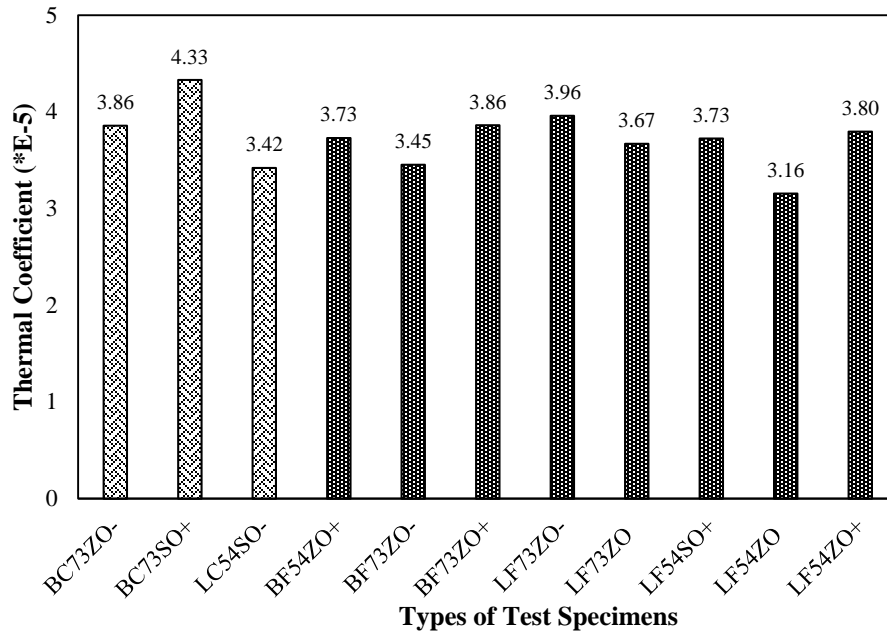


Figure 5.3: The average thermal coefficient measured for the test specimens grouped according to the gradation.

In comparison with the basalt aggregate, limestone outperformed by causing lower thermal coefficients in the test mixtures (Figure 5.4) which is compatible with the findings of Qadir (2010); he proved that limestone outperforms basalt both in terms of fracture strength and fracture temperature. The reason for this behavior can be ascribed to the thermal properties of aggregates which means that the thermal coefficient of limestone can be smaller than basalt's. A figure similar to Figure 5.4, in which all of the 26 specimens are grouped according to the aggregate type, is attached to the appendix section of this study.

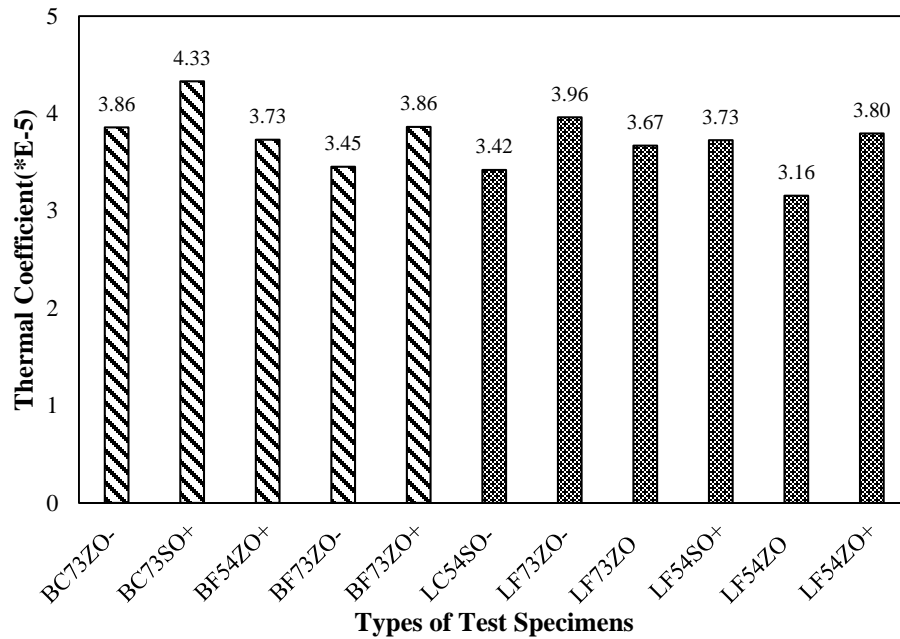


Figure 5.4: The average thermal coefficient measured for the test specimens grouped according to the aggregate type.

As it is obvious from the Table 5.2, modifying asphalt concrete has no significant effect on its thermal coefficient. The results, associated with modification, are in complete agreement with the findings of Nam et al. (2009). They found that no clear trend and difference could be seen between types of modification in terms of affecting the thermal coefficient of asphalt concrete.

5.4 Calculating the natural logarithm of the number of cycles

Because of the nature of thermal fatigue cracking there could be a considerably big difference between the results (number of cycles) taken from the specimens. If the data are presented using a column chart, sometimes the height of columns for some specimens becomes very short which makes it difficult for one to make comparisons between them or even see them at some occasions. As a result, it was decided to

calculate the natural logarithm of the responses obtained from the experiments, so that the data interpretation and presentation of the graphs became clearer. It is possible to do statistical analysis for the natural logarithm of the number of cycles in thermal fatigue cracking (Epps, 1999) , and this method was applied in this study and the taken results were compatible with ANOVA performed on the non-logarithmic number of cycles; moreover, the natural logarithm of the number of cycles was assumed to be normally distributed. Although the analysis of variance was performed on the logarithmic number of cycles, the results of ANOVA taken from them were not included in this thesis work. Figure 5.6, for instance, is a converted form of Figure 5.5 and its vertical axis is the natural logarithm of the number of cycles at 35% reduction in stiffness. The length of short columns in logarithmic scale is increased and it is easier to see them and to make comparison between the specimen types affected by mix design variables.

5.5 Analysis of variance tests (ANOVA) for the number of cycles at 35% reduction in stiffness

A total of 26 specimens (Table 5.1) were tested in order to measure the number of cycles at 35% reduction in stiffness, and then they were statistically analyzed for finding the significant mixture variables affecting the thermal fatigue performance of asphalt concrete. Table 5.4 presents the probability values calculated through ANOVA. As it is obvious from the ANOVA results, the asphalt content is the most significant design variable since its p-value for a confidence interval of 5% ($p < 0.05$) is 0.0055. Aggregate and asphalt type with the p-values of 0.0691 and 0.0621 respectively, are also important although their p-values are more than 0.05. Table 5.5 represents the average number of cycles at 35% reduction in stiffness pertaining to each type of mixture.

Table 5.4: ANOVA analysis for the number of cycles at 35% reduction in stiffness

Design variable	Probability
Aggregate type	0.0691
Gradation	0.6186
Asphalt type	0.0621
Modification	0.3214
Asphalt content	0.0055

Table 5.5: The average measured number of cycles at 35% reduction in stiffness

Specimen code	No. of cycles	Specimen code	No. of cycles
BC73ZO-	76	LF73ZO-	476
BC73SO+	2230	LF73ZO	1387
BF54ZO+	460	LF54SO+	1835
BF73ZO-	43	LF54ZO	520
BF73ZO+	451	LF54ZO+	1751
LC54SO-	184		

Figures 5.5 and 5.6 in which the specimen types are divided to three groups according to the effect of asphalt contents, show the response of each specimen type to variations in asphalt content. The responses are the average number of cycles of replicates at 35% reduction in stiffness. Similar figures, in which all of the 26 specimens are grouped according to the asphalt content, are attached to the appendix section of this thesis. The figures includes the number of cycles at 35% reduction in stiffness for each replicate.

As it is observable from Figures 5.5 and 5.6, variations in asphalt content causes drastic changes in the number of cycles at 35% reduction in stiffness. The asphalt

content with 0.5% less than optimum results in the shortest fatigue life, and with each 0.5% increment in asphalt content the fatigue life of asphalt concrete increases. The outcomes of this study are in complete agreement with the findings of Gerritsen et al. (1988). They found that increasing the binder content of asphalt concrete from 5.3% to 6.3% of aggregate weight enhances the thermal fatigue resistance up to a factor of 6.

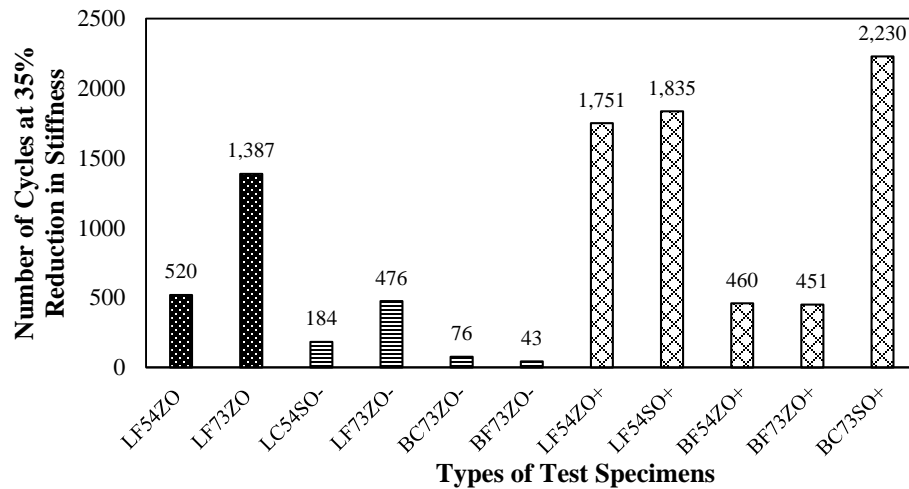


Figure 5.5: The average number of cycles for different types of specimens grouped according to the asphalt content.

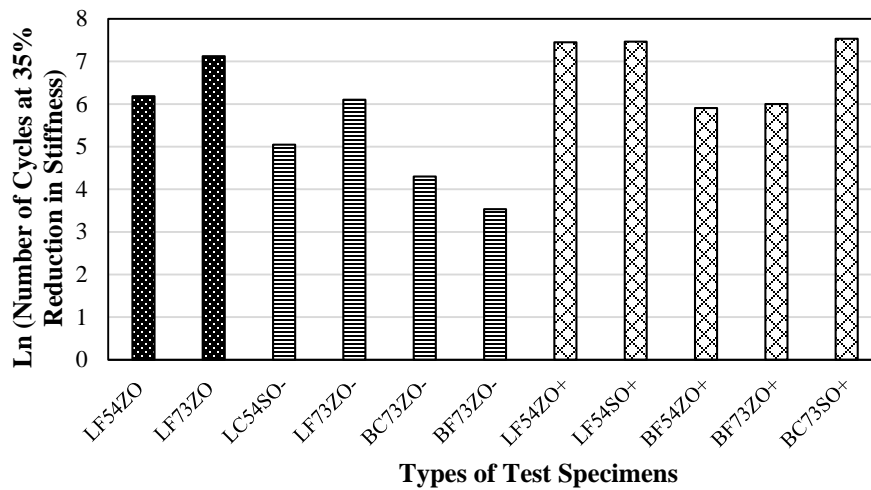


Figure 5.6: The natural logarithm of average number of cycles for different types of specimens grouped according to the asphalt content.

It is believed that air void content or binder content affects the age hardening of the asphalt mixtures. The more the air voids are the more prone is the asphalt mixture to be age hardened (Gerritsen & Jongeneel, 1988). In other words, if the binder content increases the asphalt concrete becomes less age hardened. The 5-year period of natural age hardening applied to the test specimens used in this study lays a solid cornerstone to the framework of accuracy of the findings of this study and the other former researches in which the effect of asphalt content on thermal fatigue life of asphalt concrete was investigated. During this period the voids had enough time to gradually oxidize the asphalt binder without the need to apply any heat to artificially accelerate the oxidation process.

Figures 5.7 and 5.8 in which the specimen types are divided to two groups according to the effect of asphalt types, show the response of each specimen type to different asphalt types. The responses are the average number of cycles of replicates at 35% reduction in stiffness. Similar figures, in which all of the 26 specimens are grouped

according to the asphalt type, are attached to the appendix section of this thesis. The figures include the number of cycles at 35% reduction in stiffness for each replicate.

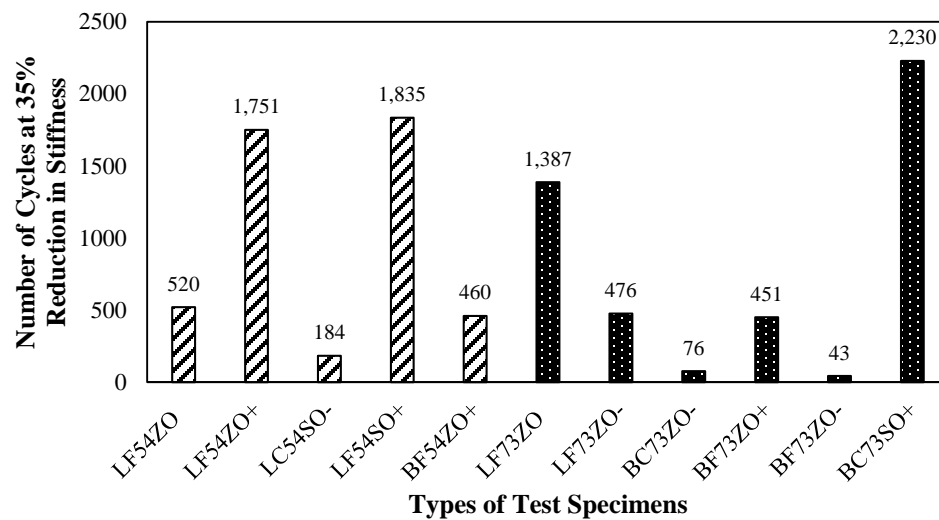


Figure 5.7: The average number of cycles for different types of specimens grouped according to the asphalt type.

As it can be seen from the Figures 5.7 and 5.8, the test specimens that have an asphalt type with the penetration value of 54 sustain more number of cycles until they approach to 35% reduction in stiffness. The results of this research are not in agreement with the findings of Lundstrom et al. (2004) because they found that the softer asphalt sustains more number of cycles before failure. Moreover, Roberts et al. (1996) believed that the softer asphalt cement provides more resistance to thermal cracking when compared with the stiffer one. The reason why the test specimens with a lower penetration grade outperformed the other ones can be

attributed to the long 5-year period of natural age hardening. During this period may be the chemical compounds of the asphalts changed due to the gradual oxidation and this change could have the worst effect on the asphalt with the higher penetration grade. It is worth mentioning that, the effect of the long term aging on the specimens was proved by comparing the glass transition temperatures of the specimens after and before the long term aging. The glass transition temperature drastically dropped after the aging period for all of the specimens.

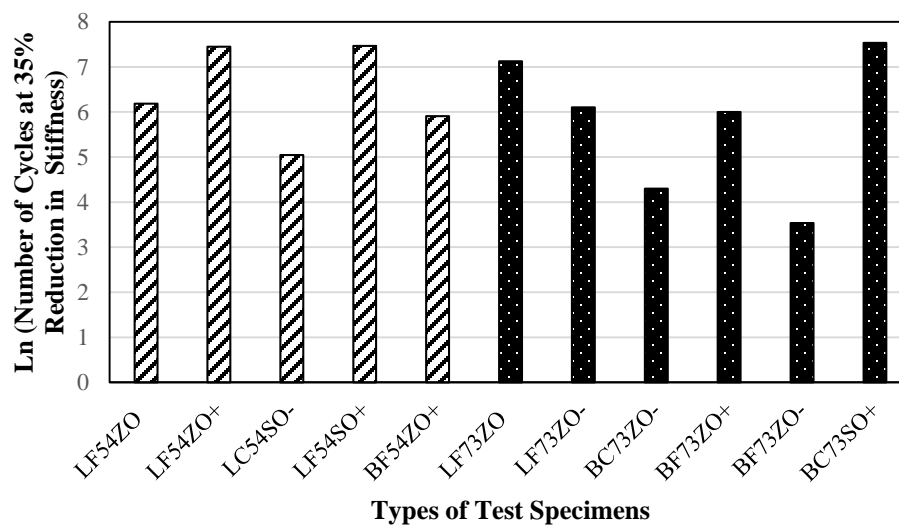


Figure 5.8: The natural logarithm of average number of cycles for different types of specimens grouped according to the asphalt type.

In addition, there could be another scenario in which the results related to the effect of asphalt type can be related. The chemical reaction between the aggregates and

the asphalt cement during the long period of age hardening could have affected the asphalt types.

Figures 5.7 and 5.8 in which the specimen types are divided to two groups according to the effect of aggregate types, show the response of each specimen type to different aggregate types. The responses are the average number of cycles of replicates at 35% reduction in stiffness. Similar figures, in which all of the 26 specimens are grouped according to the aggregate type, are attached to the appendix section of this thesis. The figures include the number of cycles at 35% reduction in stiffness for each replicate.

It is interpretable from the Figures 5.9 and 5.10 that the limestone, if used in asphalt concrete, performs better than basalt in resisting against thermal fatigue cracking. Limestone is proved to be a good type of aggregate for temperature cracking and also for creep performance (Qudais & Shweily, 2007). In addition, Qadir (2010) concluded that the asphalt concrete composed of limestone outperforms basalt in resisting against low temperature cracking; he worked on the test specimens with the same mixture design variables that were used in this study.

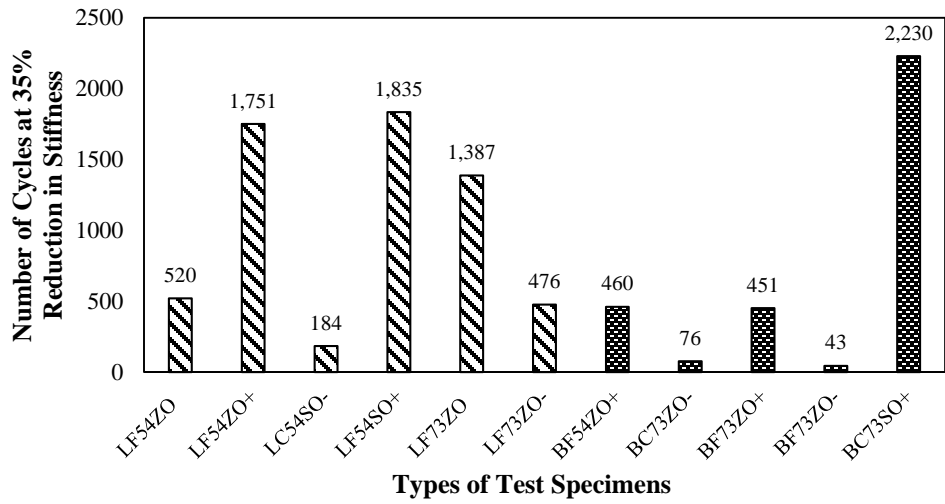


Figure 5.9: The average number of cycles for different types of specimens grouped according to the aggregate type.

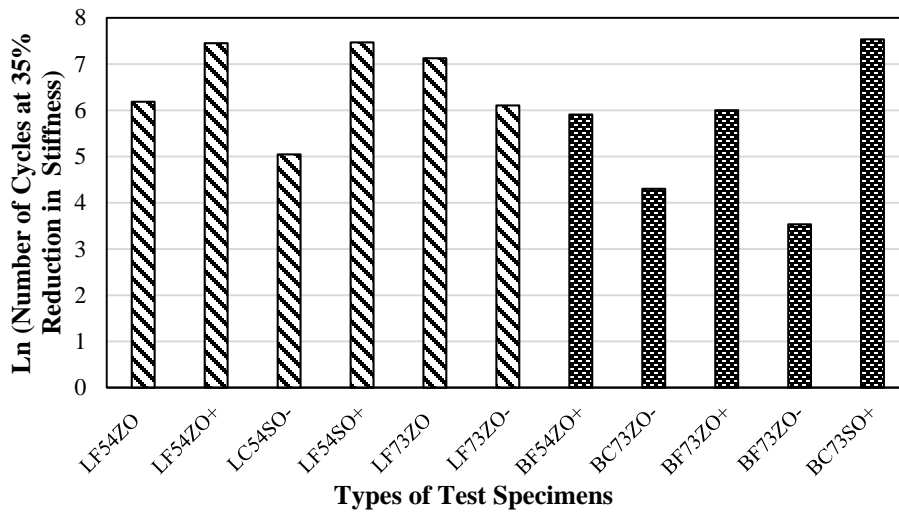


Figure 5.10: The natural logarithm of average number of cycles for different types of specimens grouped according to the aggregate type.

The difference between the effects of the two types of aggregate can be because of the surface texture and shape of each aggregate type which all are capable of influencing the bonding strength of asphalt cement (Nam & Bahia, 2009).

For gradation, the p-value according to Table 5.3 is equal to 0.6186 which is far greater than 0.05; as a result, it had no significant effect on thermal fatigue performance of asphalt mixtures tested in this study. Moreover, Vinson et al. (1989) found that the gradation has no effect on thermal cracking potential of asphalt concrete.

Like gradation, modification had no effect on thermal fatigue performance; its p-value is 0.3214 which is bigger than 0.05 (Table 5.3). The reason that the modifier had no effect on thermal fatigue performance of asphalt concrete can be attributed to the amount of modifier; if the added amount was more, may be it could show significance in ANOVA results. In addition, may be changing the type of modifier could affect the thermal fatigue behavior of asphalt concrete. Epps, (1999) found that adding CRM causes an improvement in thermal fatigue performance of asphalt concrete. Moreover, Qadir (2010) found that adding SBS modifier has no significant effect on low temperature cracking of asphalt concrete pavements. It is worth mentioning that, the specimens he tested were composed of the mixture design variables that were used in this study.

5.6 Analysis of variance tests (ANOVA) for the extrapolated number of cycles at 50% reduction in stiffness using power model

Along with analysis of the number of cycles at 35% reduction in stiffness, the 26 specimens were analyzed on the basis of extrapolated number of cycles, using the power model, to 50% reduction in stiffness. Then, they were statistically evaluated for finding the significant mixture design variables affecting the thermal fatigue performance of asphalt concrete. Table 5.6 presents the probability values calculated through ANOVA. As it is obvious from the ANOVA results, the asphalt content is the most significant design variable since its p-value for a confidence

interval of 5% ($p < 0.05$) is 0.0237. The aggregate type with the p-values of 0.0539 is also important although its p-values is slightly more than 0.05. Table 5.7 represents the average number of cycles at 50% reduction in stiffness pertaining to each type of mixture.

Table 5.6: ANOVA analysis for the extrapolated number of cycles to 50% reduction in stiffness

Design variable	Probability
Aggregate type	0.0539
Gradation	0.5288
Asphalt type	0.5844
Modification	0.105
Asphalt content	0.0237

Table 5.7: The average measured number of cycles at 50% reduction in stiffness

Specimen code	No. of cycles	Specimen code	No. of cycles
BC73ZO-	25,657	LF73ZO-	38,127
BC73SO+	62,057	LF73ZO	117,695
BF54ZO+	3,573	LF54SO+	396,174
BF73ZO-	822	LF54ZO	9,502
BF73ZO+	595,867	LF54ZO+	1,070,147
LC54SO-	11,330		

Figures 5.11 and 5.12 in which the specimen types are divided to three groups according to the effect of asphalt contents, show the response of each specimen type to variations in asphalt content. The responses are the average number of cycles of replicates at extrapolated 50% reduction in stiffness. Similar figures, in which all of the 26 specimens are grouped according to the asphalt content, are attached to the appendix section of this thesis. The figures includes the number of cycles at extrapolated 50% reduction in stiffness for each replicate.

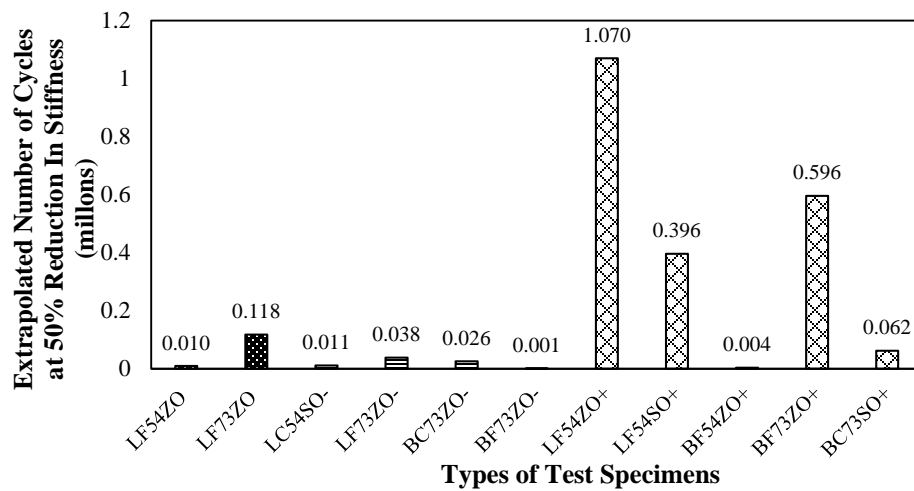


Figure 5.11: The average number of cycles for different types of specimens grouped according to the asphalt content.

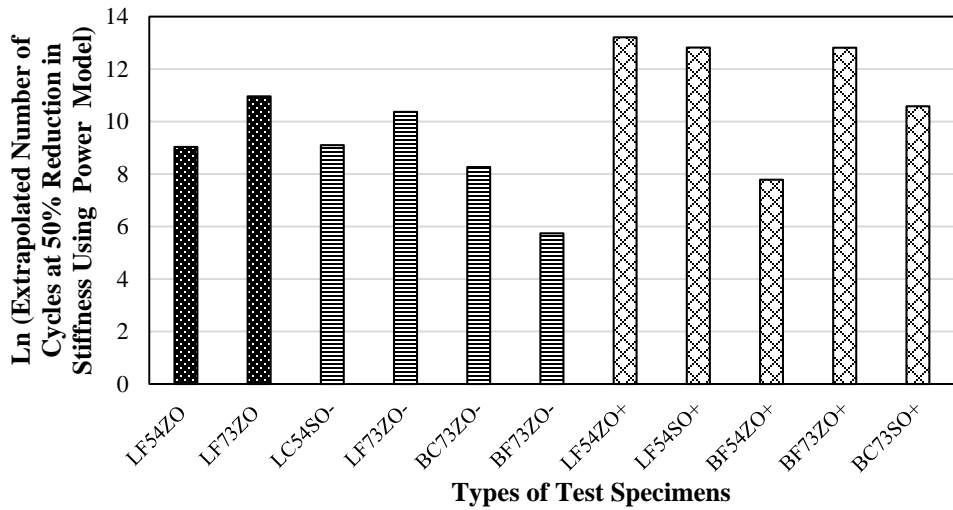


Figure 5.12: The natural logarithm of average number of cycles for different types of specimens grouped according to the asphalt content.

Figures 5.13 and 5.14 in which the specimen types are divided to two groups according to the effect of aggregate types, show the response of each specimen type to variations in aggregate type. The responses are the average number of cycles of replicates at extrapolated 50% reduction in stiffness. Similar figures showing the number of cycles at extrapolated 50% reduction in stiffness for each replicate, in which all of the 26 specimens are grouped according to the asphalt content, are attached to the appendix section of this thesis.

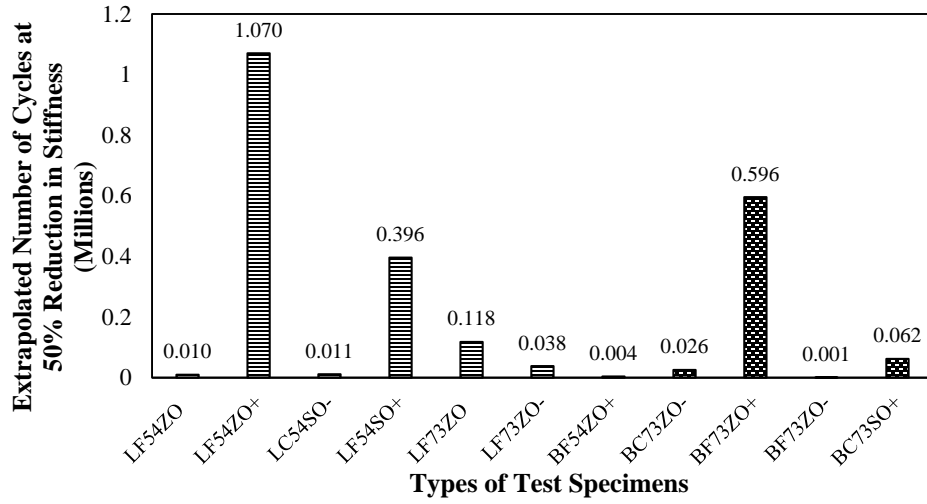


Figure 5.13: The average number of cycles for different types of specimens grouped according to the aggregate type.

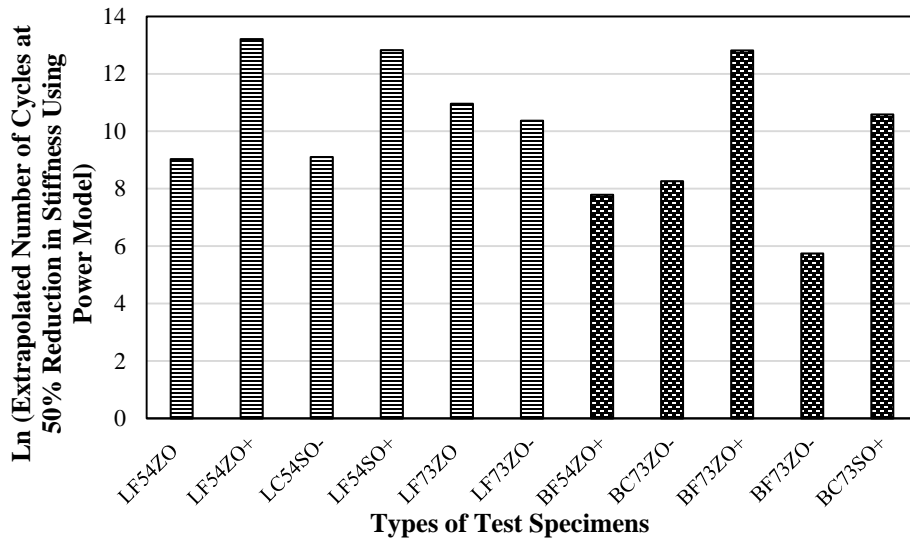


Figure 5.14: The natural logarithm of average number of cycles for different types of specimens grouped according to the aggregate type.

5.7 Analysis of variance tests (ANOVA) for slopes of the linear lines fitted to log-log scale data of stiffness versus number of cycles

The 26 specimens were also investigated on the basis of the slope of the linear line fitted to the log-log scale data of stiffness versus number of cycles. Then, they were statistically analyzed for finding the significant mixture design variables affecting the thermal fatigue performance of asphalt concrete. Table 5.8 presents the probability values calculated through ANOVA. As it is obvious from the ANOVA results, the aggregate type is the most significant design variable since its p-value for a confidence interval of 5% ($p < 0.05$) is 0.0027. The asphalt content and asphalt type with the p-values of 0.0611 and 0.0845 are also important although their p-values are slightly more than 0.05. Table 5.9 represents the average slopes pertaining to each type of mixture.

Table 5.8: ANOVA analysis for the slopes of the fitted linear lines

Design variable	Probability
Aggregate type	0.0027
Gradation	0.333
Asphalt type	0.0845
Modification	0.6419
Asphalt content	0.0611

Table 5.9: The average measured slopes

Specimen code	Slope	Specimen code	Slope
BC73ZO-	0.116	LF73ZO-	0.064
BC73SO+	0.092	LF73ZO	0.083
BF54ZO+	0.147	LF54SO+	0.055
BF73ZO-	0.151	LF54ZO	0.093
BF73ZO+	0.058	LF54ZO+	0.056
LC54SO-	0.079		

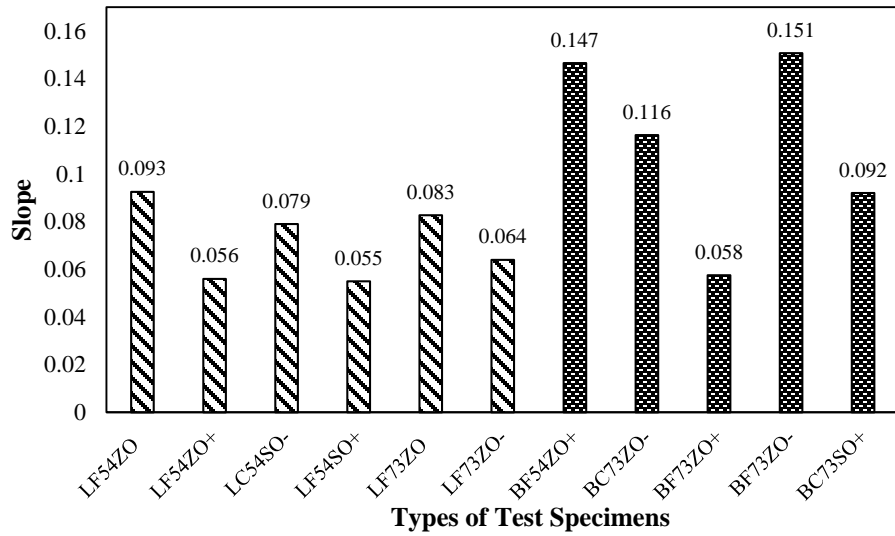


Figure 5.15: The average slope for different types of specimens grouped according to the aggregate type.

Figure 5.15 in which the specimen types are divided to two groups according to the effect of aggregate type, shows the response of each specimen type to different kinds of aggregate. The responses are the average of slopes of the fitted linear lines.

A similar figure in which all of the 26 specimens are grouped according to the aggregate type, is attached to the appendix section of this thesis.

As it can be seen in the Figure 5.15, changes in the aggregate type vastly affects the slope of the fitted linear line. The results pertaining to the aggregate type are in complete agreement with findings discussed in the two previous subsections. All of the findings are consistent in relation to the significance of the aggregate type and also the way that limestone outperforms basalt. The magnitude of slopes represents the rate at which the micro cracks develop within the asphalt concrete specimens. Basalt, for example, has a shorter life according to thermal fatigue cracking because the slopes pertaining to this type of aggregate are bigger than limestone.

Changes in the asphalt content considerably affects the slope of the fitted linear lines (Figure 5.16). The results obtained in this subsection are in complete agreement with the findings discussed in the two previous subsections; all of the findings are in agreement according to the significance of the asphalt content and also the way that its variations influences the thermal fatigue life of asphalt concrete. The biggest slope belongs to the asphalt content that is 0.5% less than optimum which means that, the rate at which the micro cracks develop within the specimen made with this asphalt content is the highest. With the 0.5% increments in the asphalt contents the rate of the development of micro cracks decreases. In other words, increasing the asphalt content improves the thermal fatigue life of asphalt concrete. A similar figure, in which all of the 26 specimens are grouped according to the asphalt content, is attached to the appendix section of this study.

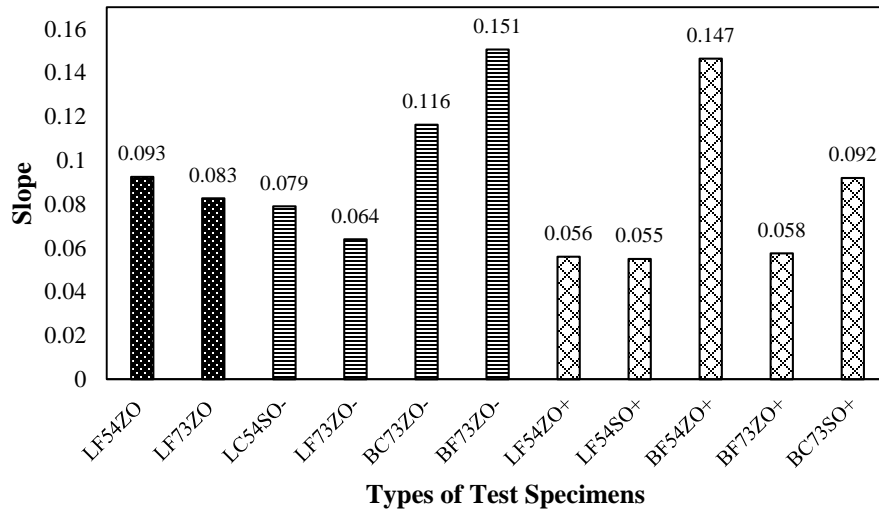


Figure 5.16: The average slope for different types of specimens grouped according to the asphalt content.

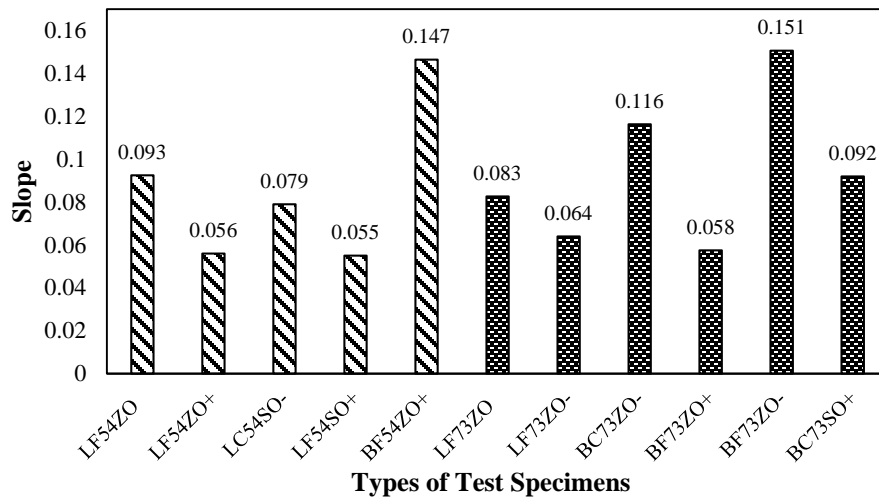


Figure 5.17: The average slope for different types of specimens grouped according to the asphalt type.

As it can be seen in the Figure 5.17, changes in the asphalt type affect the slopes of the fitted linear lines. The results pertaining to the asphalt type are in complete agreement with findings discussed for the effect of asphalt type on the number of cycles at 35% reduction in stiffness. A similar figure, in which all of the 26 specimens are grouped according to the asphalt type, is attached to the appendix section of this study.

CHAPTER 6

CONCLUSIONS AND RECOMMENDATIONS

6.1 Introduction

The summarized findings of this research together with recommendations for future work are included in this chapter. It is hoped that the recommendations made in this study help develop the future researches associated with thermal cracking. The methods, used in this study, for the measurement of thermal coefficient and, especially, the thermal fatigue resistance of asphalt concrete are unique; nonetheless, the summarized findings in this research depend on the selected mixture design variables, test procedures and conditions, and, as a result, there is no guarantee to expect that the conclusions of this study to be completely compatible with the findings of the other researches.

6.2 Conclusions

In this research a TSRST machine was revised for measuring the thermal fatigue performance of asphalt concrete. At first the thermal coefficients of the test specimens were calculated and then on the basis of the measured thermal coefficients and the pertaining thermal strains, the cyclic loads were applied on the specimens in the constant strain mode; then their thermal fatigue performance was evaluated. A total of 26 specimens were used in this research and the outcomes of the experiments were analyzed by applying ANOVA method. The results of the statistical analysis revealed the significant mixture design variables affecting the thermal coefficient and thermal fatigue performance of asphalt concrete. The findings of the research are as follows:

- The aggregate type was proved to be an important factor affecting the thermal coefficient of asphalt concrete. Limestone outperformed basalt by resulting in smaller values of thermal coefficients calculated for the asphalt concrete specimens. The reason for this behavior can be attributed to the thermal coefficient of aggregates themselves.
- The effect of gradation on thermal coefficient of asphalt concrete turned out to be important and fine aggregates resulted in smaller coefficients of contraction compared with the coarse ones. The reason of this behavior can be attributed to the degree of interlock of aggregates. Fine aggregates have a higher degree of optimum interlock, and consequently bring about smaller thermal coefficients.
- Asphalt type had a strongly significant effect on the thermal coefficient of asphalt concrete. The test specimens having an asphalt type with the higher penetration value had bigger thermal coefficients values compared with specimens with low penetration values. The reason for this phenomenon can be because of the different chemical compounds of the two types of asphalt.
- The effect of asphalt content on thermal coefficient was considerably significant and changes in the asphalt content caused drastic variations in the values of thermal coefficient. In this study, the optimum asphalt content resulted in the smallest thermal coefficient meaning that the flexible pavements made with that amount of binder are less prone to thermal cracking.
- The statistical analyses performed on different approaches for measuring the thermal fatigue life of asphalt concrete almost resulted in the same findings. For example, the ANOVA method that was applied for finding the significant mixture design variables revealed that the aggregate type and asphalt content have a dominating influence on the thermal fatigue performance of asphalt concrete in either of the applied approaches. However, the asphalt type did not show any significance in the results

obtained from different methods but for the approach that was used for measuring the number of cycles at 35% reduction in stiffness.

- The aggregate type was proved to be a significant factor in terms of affecting the thermal fatigue performance of asphalt concrete. Limestone outperformed basalt by resulting in a longer fatigue life in the test specimens that it was used. The reason for this behavior can be attributed to the physical characteristics of aggregates like surface texture and aggregate shape. As a result, using limestone in the mixtures improves the thermal fatigue performance of asphalt concrete.
- The effect of asphalt content on thermal fatigue performance of the asphalt concrete turned out to be extremely significant and changes in the asphalt content caused drastic variations in the thermal fatigue life of asphalt concrete. In this study, increasing the asphalt content resulted in a considerable improvement in the behavior of asphalt concrete in terms of resisting against thermal cracking. The reason for this phenomenon can be attributed to oxidation. Higher asphalt content means lower air void in the asphalt concrete, and, as a result, being less prone to oxidation. Oxidation causes aging in the flexible pavements and makes them susceptible to thermal cracking.
- The influence of asphalt type became significant just in the approach used for measuring the number of cycles at 35% reduction in stiffness. The binder with the lower penetration value of 54 outperformed the one with the penetration value of 74 in terms of sustaining more number of cycles when approaching to 35% reduction in stiffness.
- The results of ANOVA performed on the responses revealed that two design variables have the same effect on the thermal coefficient and the thermal fatigue cracking of asphalt concrete. The obtained results indicate that it is possible to make a correlation between the thermal coefficient value and the number of cycles representing the fatigue life of asphalt concrete. Limestone and the binder with the penetration value of 54 resulted in smaller thermal

coefficients and longer fatigue lives. If a specimen's thermal coefficient is small, it means that its thermal strain will be small as well. As a result, when thermal fatigue happens in a flexible pavement having a small value of thermal coefficient its fatigue life can be longer compared with the pavement made of an asphalt concrete with a high value of thermal coefficient.

- In this study, the range of temperature differential applied for measuring the thermal coefficient started from +15 and ended at -25. In this temperature range all of the thermal coefficients were easily calculated on the right-hand side of the glass transition temperature. As a result, for measuring the thermal coefficient pertaining to the temperatures above the glass transition there is no need to decrease the temperature to extremely low limits. In addition, that narrow range of applied temperature differential let the glass transition temperature be calculated for more than 80% of specimens.
- The paths that the reduction of stiffness followed for the specimens tested were similar to the paths attributed to the conventional traffic load-associated fatigue. In addition, the form of stiffness reduction paths all indicated that the strain field was unified in most of the tests during the runs.

6.3 Recommendations for future work

The following recommendations give some ideas about the future works that can be done on thermal fatigue cracking. It is hoped that if these recommendations are applied in the future researches, they can alleviate the problems related to thermal cracking.

- Modifying the asphalt concrete with SBS did not show any significant effect on the measured thermal coefficients or the thermal fatigue behavior of asphalt concrete. As a result, either the amount of modifier should be increased or its type must be changed for the future works.

- Since the specimens used in this study were fabricated for the measurement of thermal coefficient and thermal fatigue performance of asphalt concrete, it was better to select the asphalt type according to the performance grade.

REFERENCES

- Al-Qadi, I. L., Hassan, M. M., & Elseifi, M. A. (2005). Field and Theoretical Evaluation of Thermal Fatigue Cracking in Flexible Pavements. *Transportation Research Board*, 87-95.
- Anderson, O., K., & Epps, J. A. (1983). *Asphalt Concrete Factors Related to Pavement Cracking in West Texas*. AAPT.
- Arabzadeh, A., & Guler, M. (2014). Influence of Mixture Design Variables on Thermal Coefficient of Asphalt Concrete. *ACE*. Istanbul: Istanbul Technical University.
- Bahia, H. U., & Anderson, D. A. (1993). Glass Transition Behavior and physical hardening of Asphalt Binders. *Journal of the Association of Asphalt Paving Technologies*, 62-93, 93-129.
- Breen, J. J., & Stephens, J. E. (1967). The Glass Transition and Mechanical Properties of Asphalt. *Annual Conference of Canadian Technical Asphalt Association*.
- Bureau of Materials and Physical Research*. (2005). Retrieved from Illinois Department of Transportation: <http://www.dot.il.gov/materials/research/pdf/ptad4.pdf>, last accessed on 2/3/2014
- Carpenter, & H., S. (1983). *Thermal Cracking in Asphalt Pavements: an examination of models and input parameters*. USA CRREL.
- Carpenter, H., S., & Lytton, R. L. (1977). *Thermal Pavement Cracking in West Texas*. Texas Transportation Institute.
- Carpenter, S.H., Lytton, R. L., & Epps., J. A. (1974). *Environmental Factors Relevant to Pavement Cracking in West Texas*. Texas Transportation Institute.
- Colliou, A. M., & Powney, D. J. (1973). *The mechanical and thermal properties of materials*. London: Edward Arnold.
- Epps, A. L. (1999). AN APPROACH TO EXAMINE THERMAL FATIGUE IN ASPHALT CONCRETE. *Journal of the Association of Asphalt Paving Technologists*, 319-348.
- FHWA courses*. (1998).

Gerritsen, A. H., & Jongeneel, D. J. (1988). *FATIGUE PROPERTIES OF ASPHALT MIXES UNDER CONDITIONS OF VERY LOW LOADING FREQUENCIES*.

Haas, R., Meyer, R., Assaf, G., & Lee, H. (1987). A comprehensive study of cold climate Airport Pavement Cracking. *Journal of Association of Asphalt Paving Technologists.*, 56, 198-245.

Huang, Y. H. (2004). *PAVEMENT ANALYSIS AND DESIGN*. Pearson.

Jackson, M. N., & Vinson, T. S. (1996). Analysis of Thermal Fatigue Distress of Asphalt Concrete Pavements. *Journal of the Transportation Research Board*, 43-49.

Janoo, V., Bayer Jr, J., & Walsh, M. (1993). Thermal stress measurements in Asphalt Concrete. *CRREL REPORT*.

Keliewer, J. E., & Zeng, H. (1996). Aging and Low Temperature Cracking of Asphalt Concrete Mixtures. *Jurnal of Cold Regions Engineering*, 10, 134-148.

Lee, H. J. (1996). *Uniaxial Constitutive Modeling of Asphalt Concrete Using Viscoelasticity and Continuum damage theory*. Phd thesis.

Lundstrom, R., Bendetto, H. D., & Isacsson, U. (2004). Influence of Asphalt Mixture Stiffness on Fatigue Failure. *JOURNAL OF MATERIALS IN CIVIL ENGINEERING*, 516-525.

Miner, M. A. (1945). Cumulative Damage in Fatigue. *Journal of Applied Mechanics*.

Nam, K., & Bahia, H. U. (2009). Effect of modification on fracture failure and thermal-volumetric properties of asphalt binders. *Journal of materials in Civil Engineering*, 21(5), 198-209.

Qadir, A. (2010). *Investigation of Low Temperature Cracking in Asphalt Concrete Pavements*.

Qudais, S. A., & Shweily, H. A. (2007). Effect of aggregate properties on asphalt mixtures stripping and creep behavior. *Construction and Building Materials*, 21, 1886-1898.

Roberts, F., Kandhal, P. S., Brown, E. R., & Lee, D. Y. (1996). *Hot Mix Asphalt Materials, Mixture Design and construction*. Lanham, Maryland: Research and Education Foundation.

Shah, A. (2004). Influence of Binders & Mixture Properties on the Performace of Asphalt Concrete Pavements. *Phd Dissertetion*, 1-216.

Shahin, M. Y. (1977). Design system for minimizing asphalt concrete thermal cracking. *Fourth International Conference on the Structural Design of Asphalt Pavements*. . Ann Arbor.

Tan, Y. Q., Xu, H. N., Dong, Z. J., & Gong, W. Q. (2008). Effect of Aggregate Grading on Low temperature Cracking Resistance in Asphalt Mixtures Based on Mathematical Statistics. *Proceedings of Eighth International RILEM conference on cracking in pavements*, (pp. 387-394). Limoges.

Transportation, I. D. (2005). *POLYMER-MODIFIED HOT MIX ASPHALT*.

Vinson, T. S., Janoo, V. C., & Haas, R. G. (1989). Low Temperature and Thermal Fatigue Cracking. *Summary Report for A-003A of the strategic Highway Research Program (SHRP)*.

Wang, M., Wayoe, H. T., & Anderson, K. O. (1992). *Low temperature properties of asphalt cements and mixtures used in the C-SHRP Lamont Test Road un Alberta*. Alberta: University of Alberta.

Xu, Q., & Solaimanian, M. (2008). Measurement and evaluation of asphalt concrete thermal expansion and contraction. *Journal of Testing and Evaluation*, 140-149.

Zeng, M., & Sields, D. H. (1998). Nonlinear Thermal Expansion and Contraction of Asphalt Concrete. *Canadian Journal Of Civil Engineering*, 26-34.

APPENDIX A

THERMAL STRAIN PLOTS

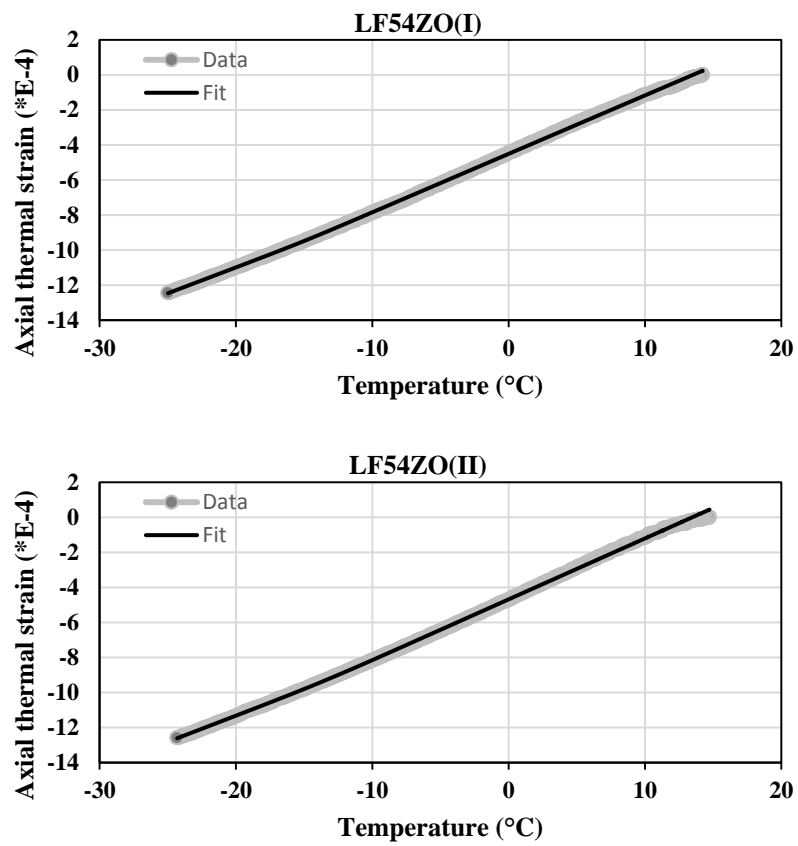


Figure A.1: Thermal strain plots for all the specimens.

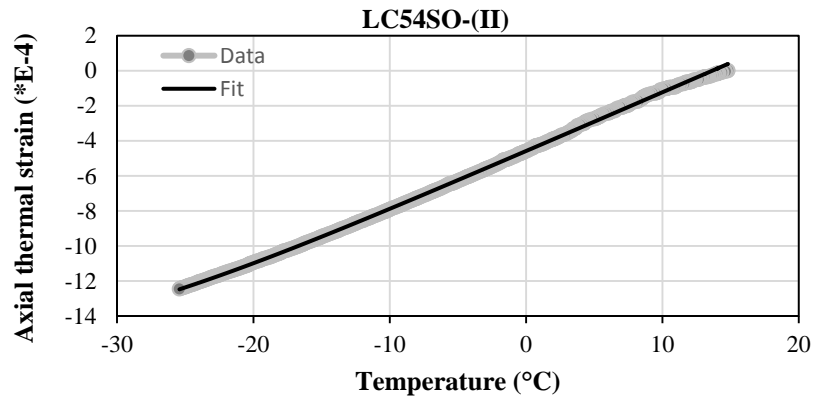
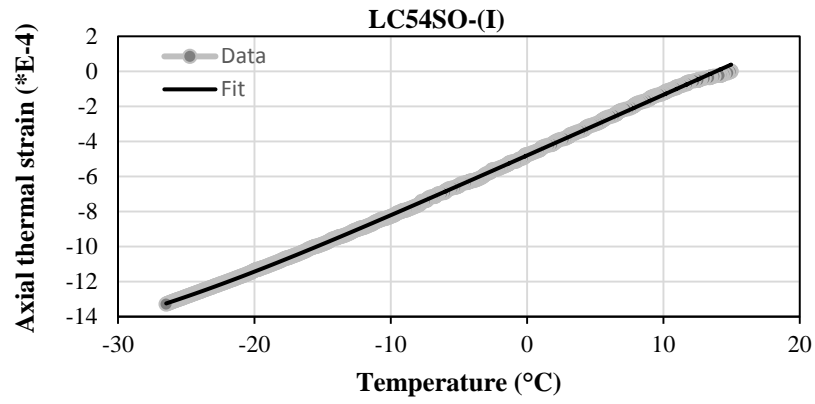
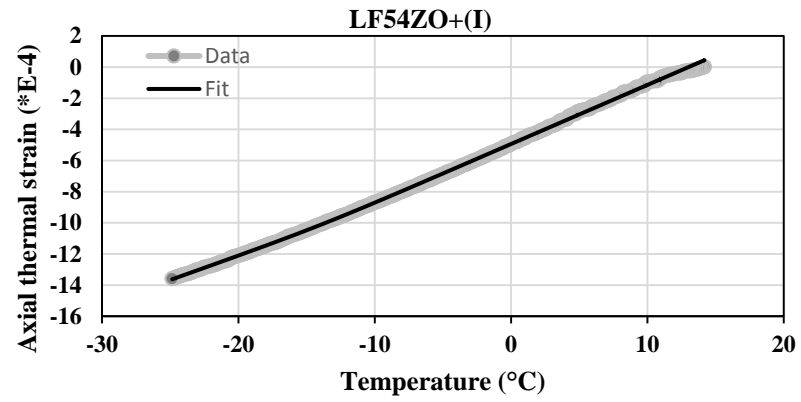


Figure A.1: (Continued)

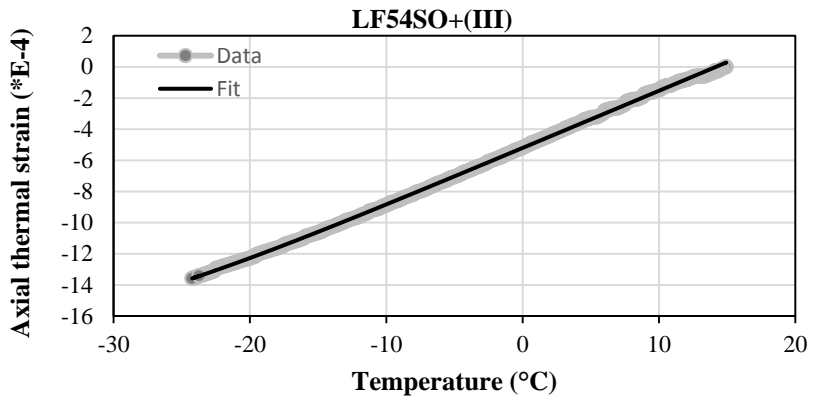
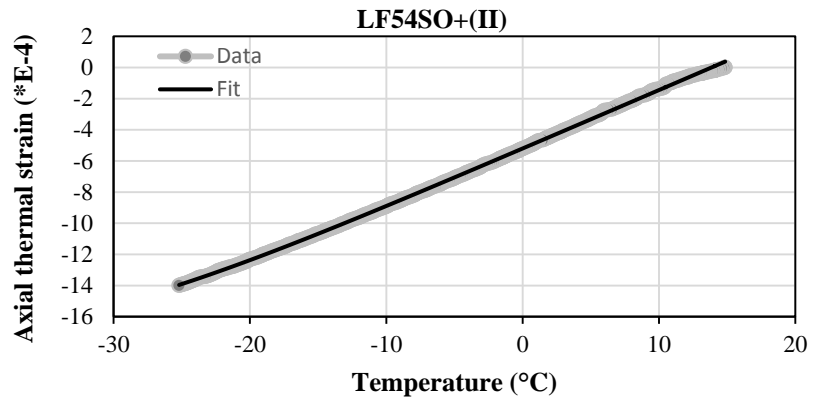
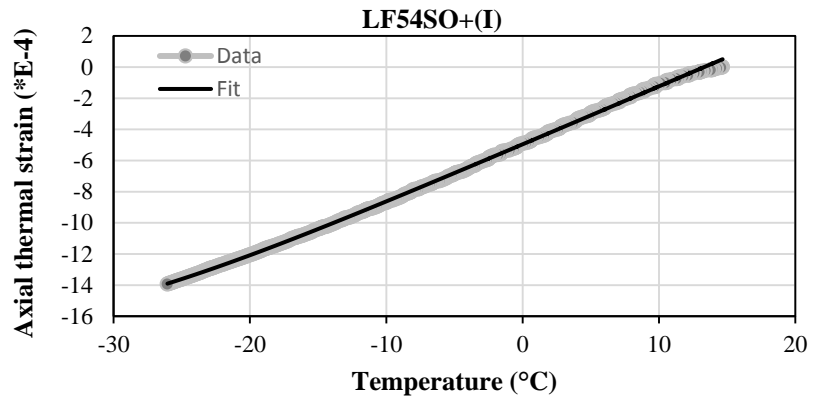


Figure A.1: (Continued)

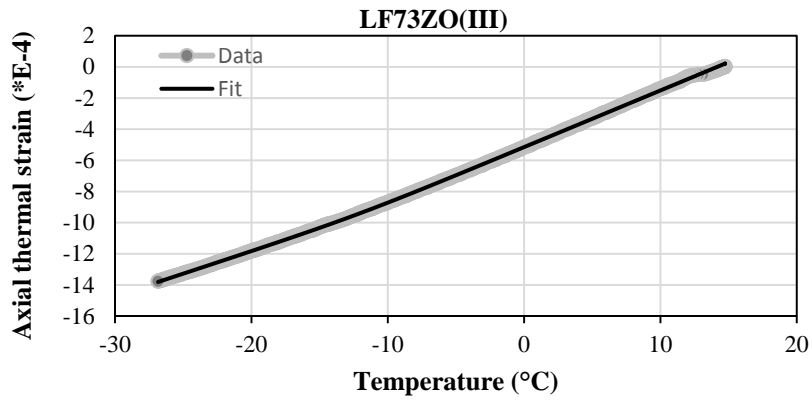
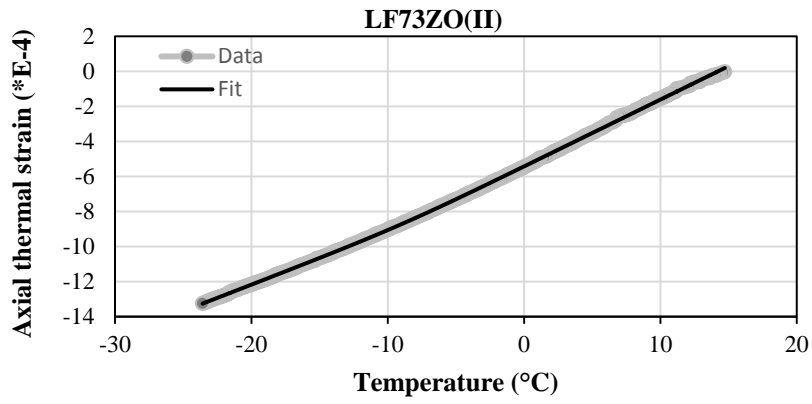
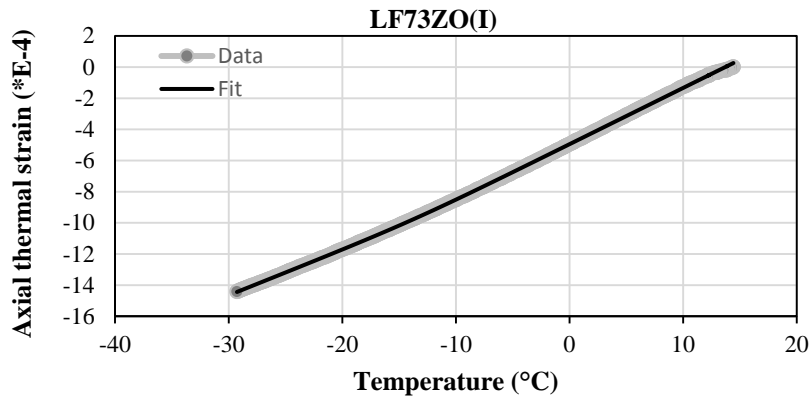


Figure A.1: (Continued)

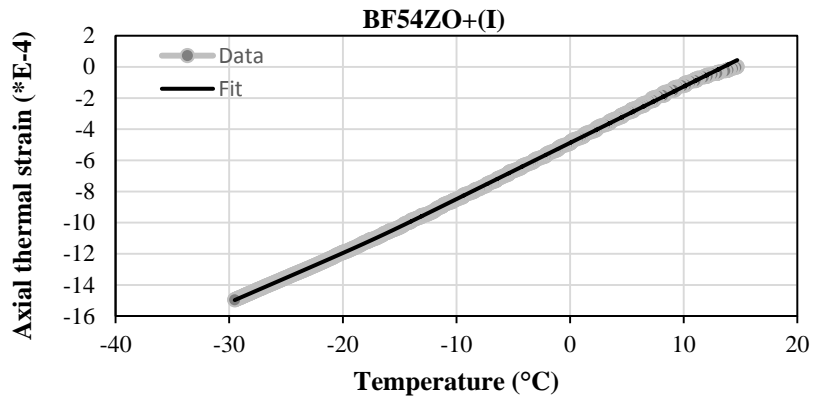
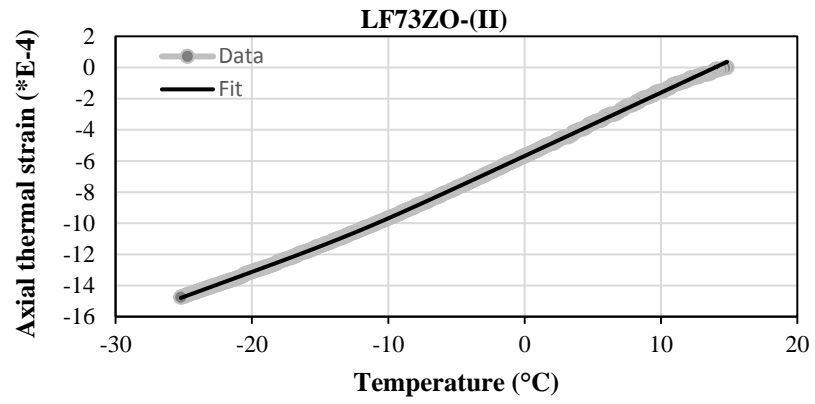
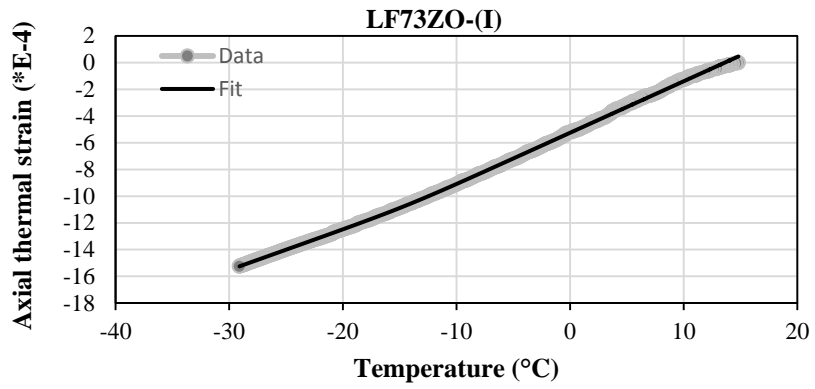


Figure A.1: (Continued)

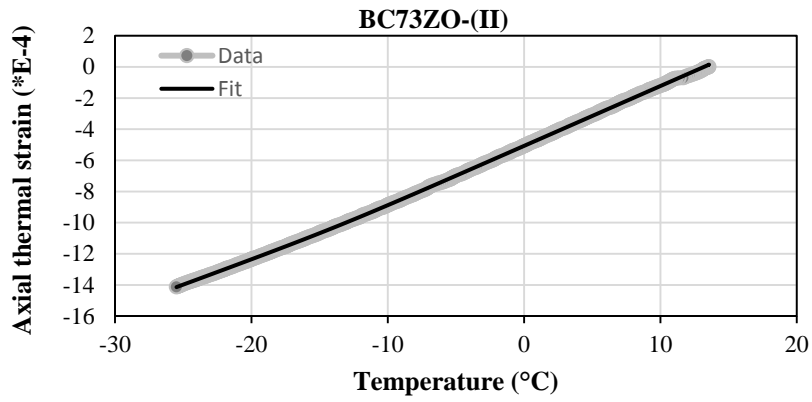
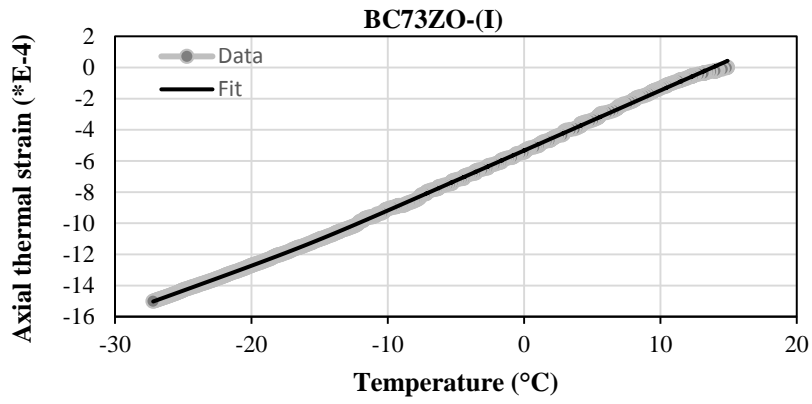
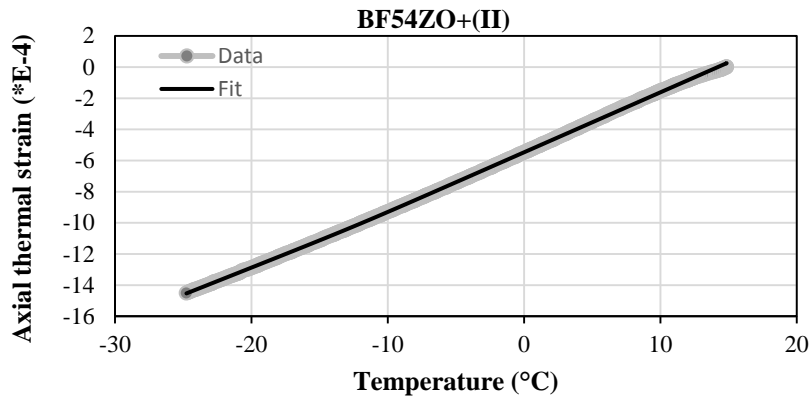


Figure A.1: (Continued)

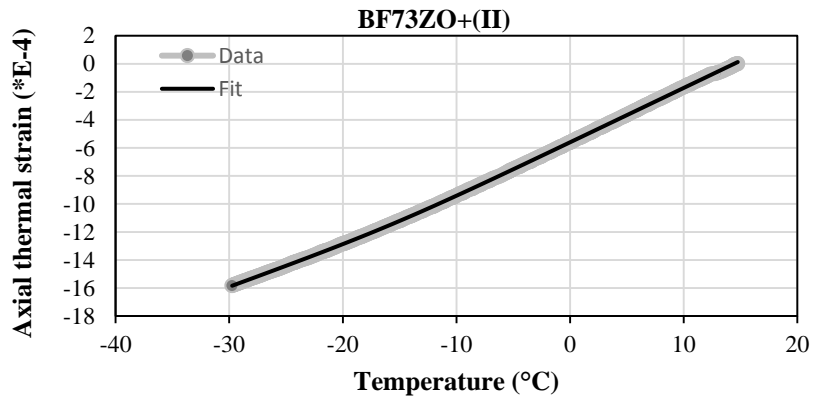
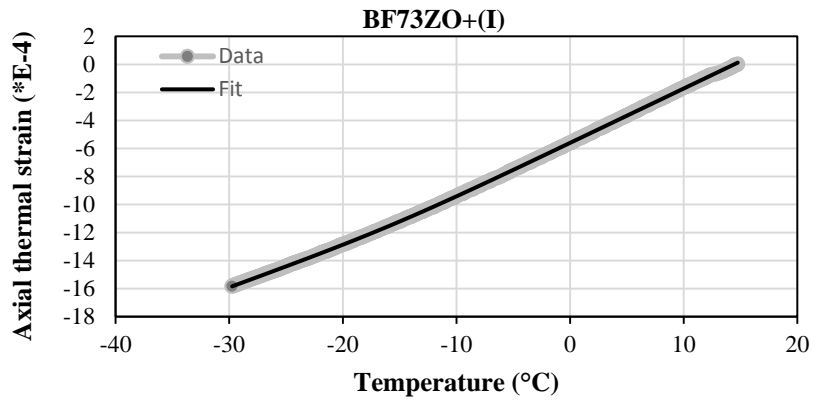
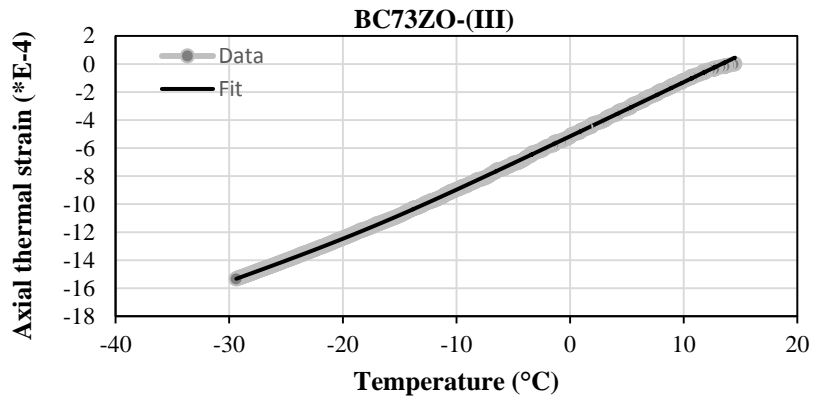


Figure A.1: (Continued)

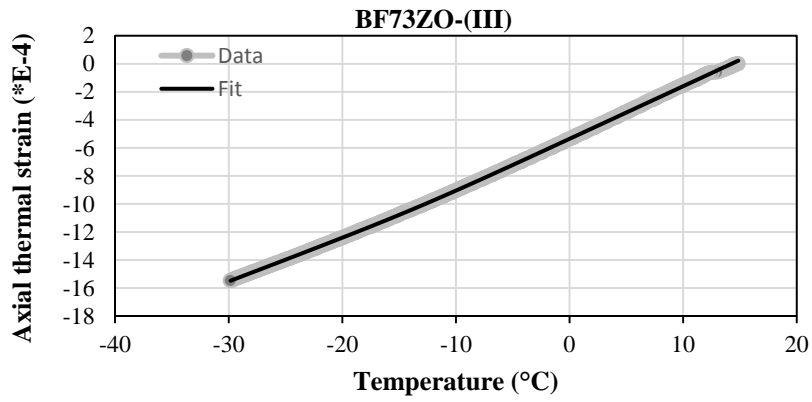
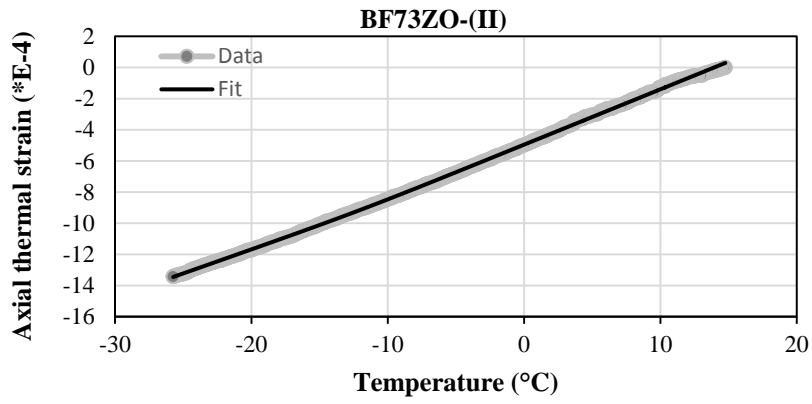
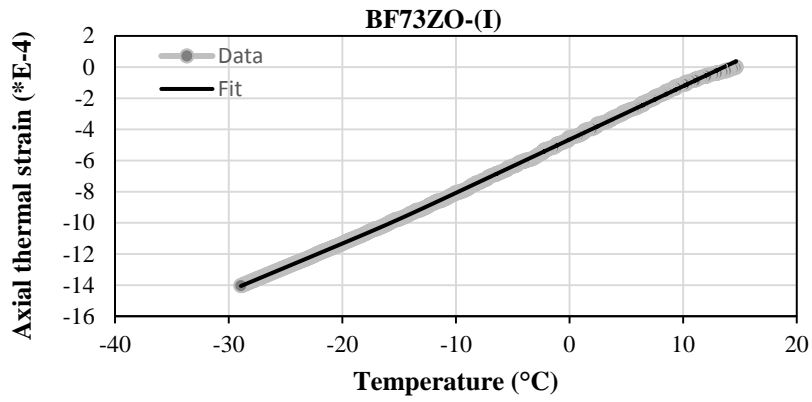


Figure A.1: (Continued)

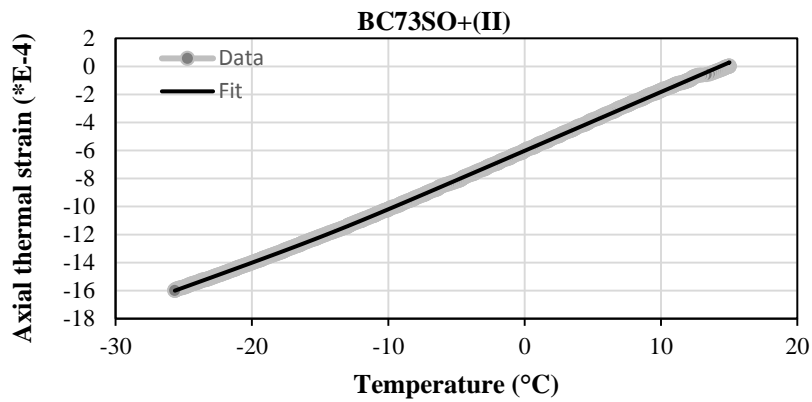
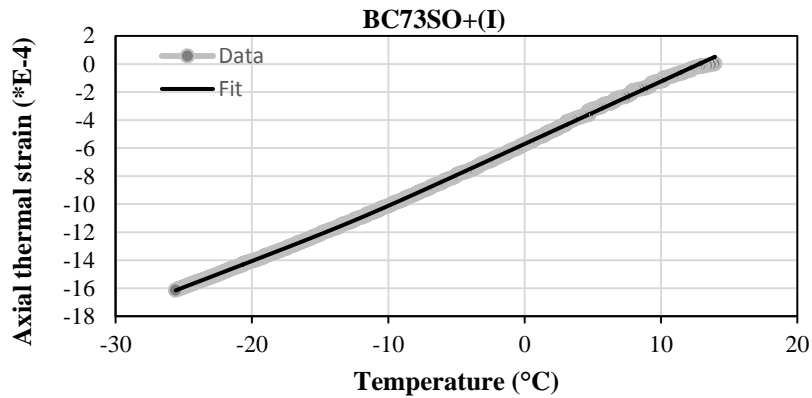


Figure A.1: (continued)

Symbols used:

Aggregate: L=limestone, B=basalt; Gradation: C=Coarse, F=Fine; Polymer modification: Z=no modification, S=SBS modification; Asphalt type: 54 and 73=penetration values (0.1mm); Asphalt content: O=optimum, O+=optimum + 0.5%, O- =optimum - 0.5%

APPENDIX B

STIFFNESS REDUCTION PLOTS

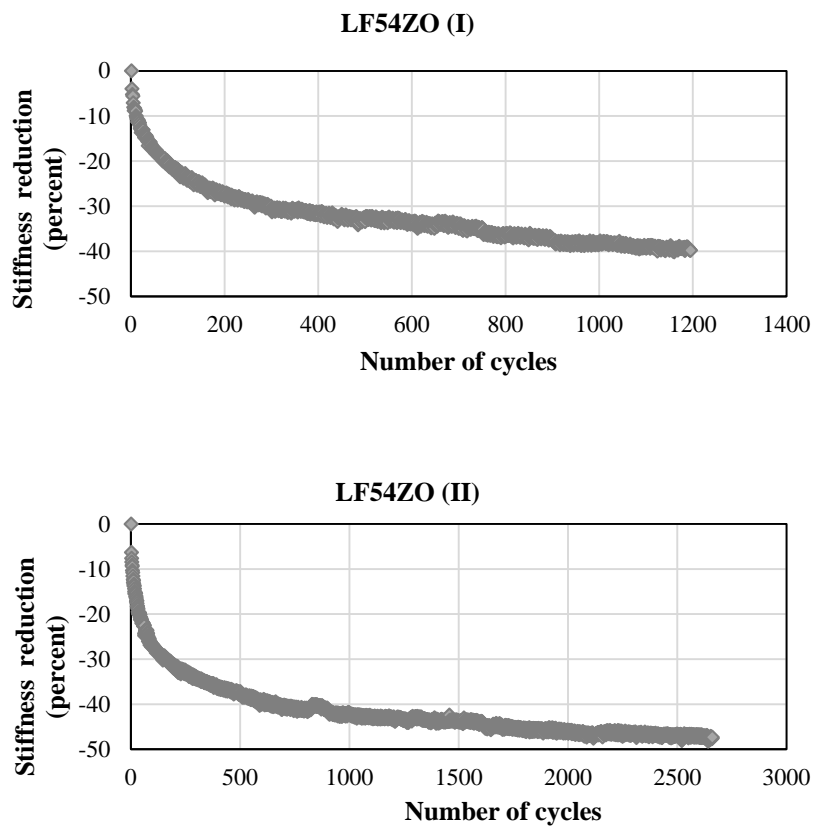


Figure B.1: Stiffness reduction plots for all the specimens.

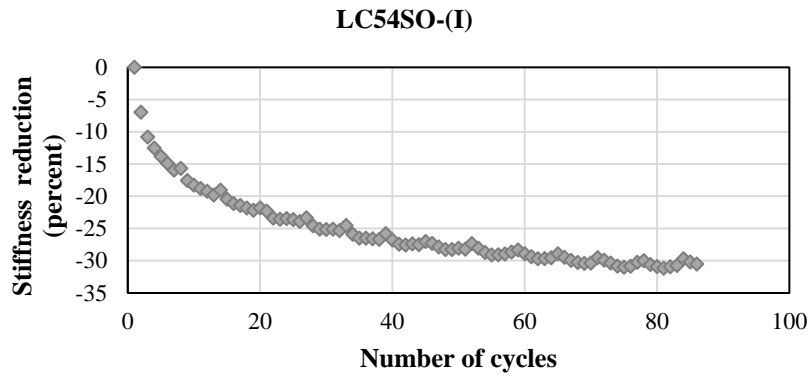
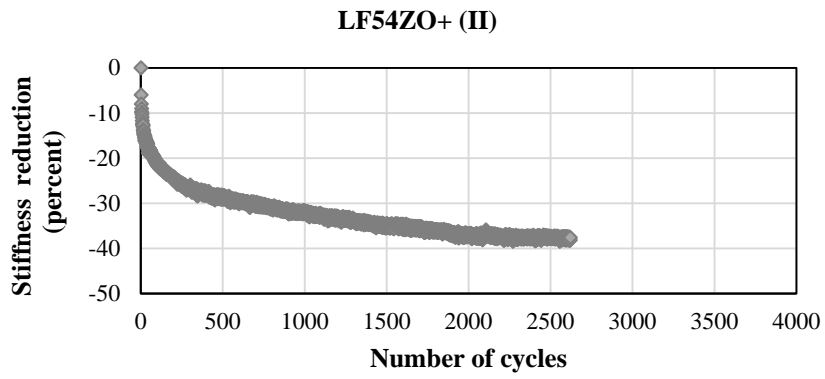
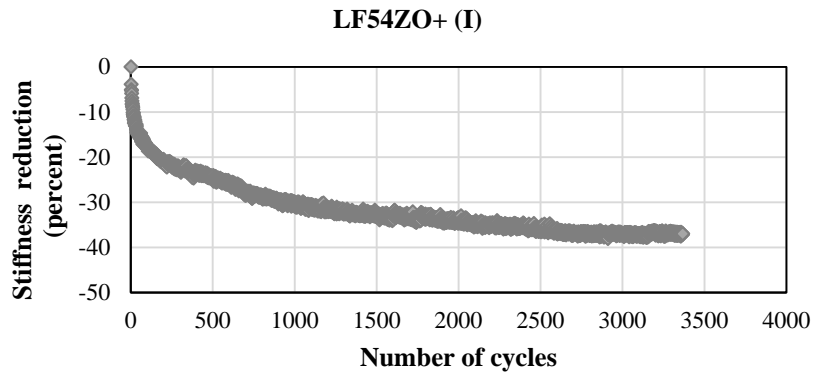
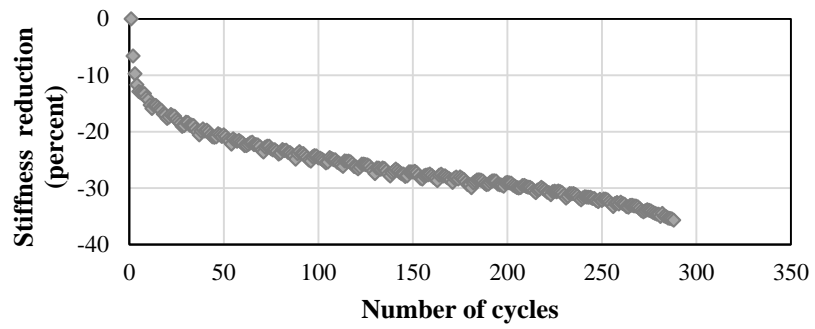
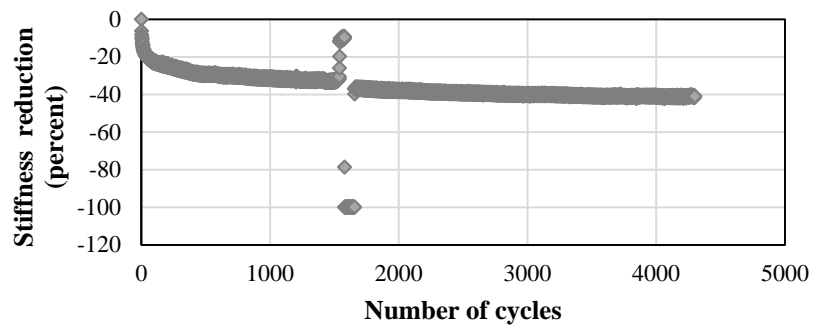


Figure B.1: (Continued)

LC54SO-(II)



LF54SO+(I)



LF54SO+(II)

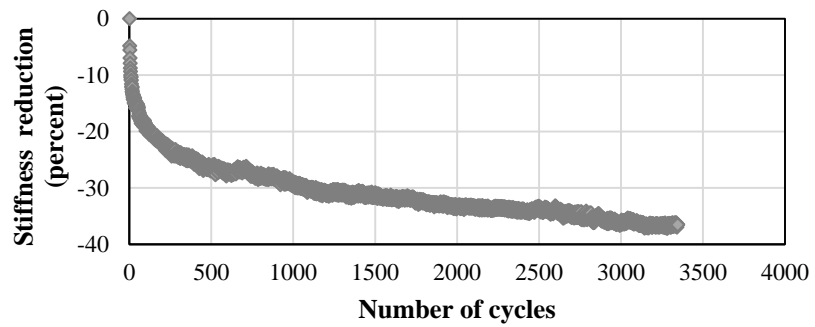
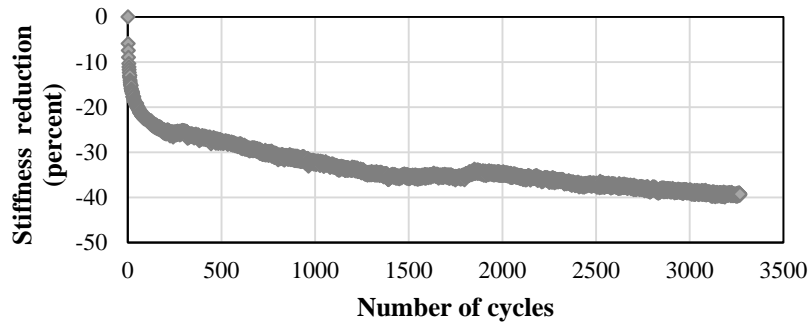
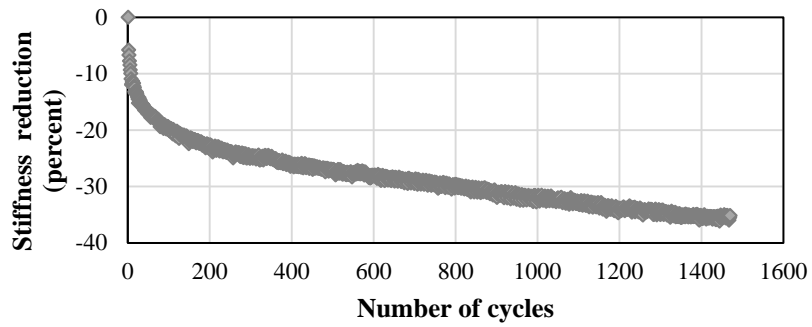


Figure B.1: (Continued)

LF54SO+(III)



LF73ZO(I)



LF73ZO(II)

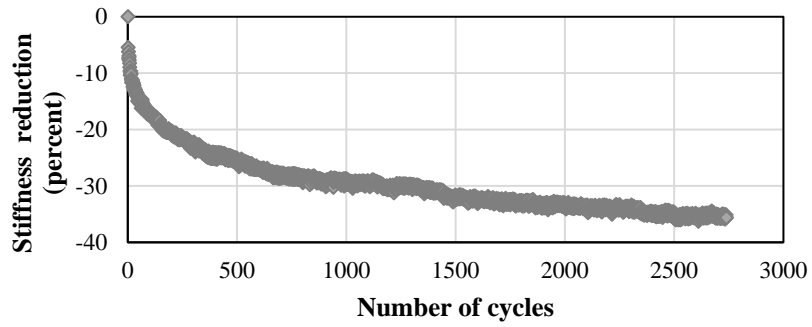
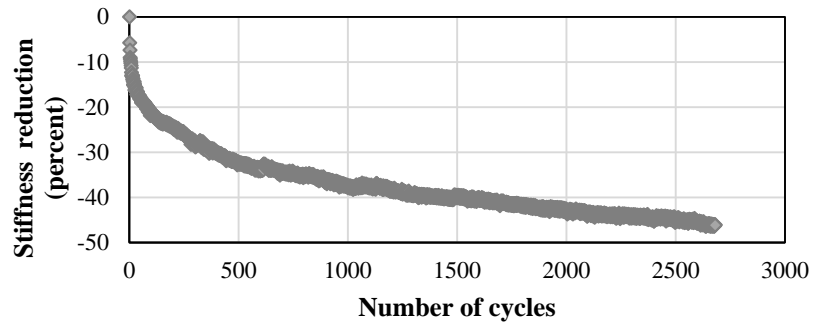
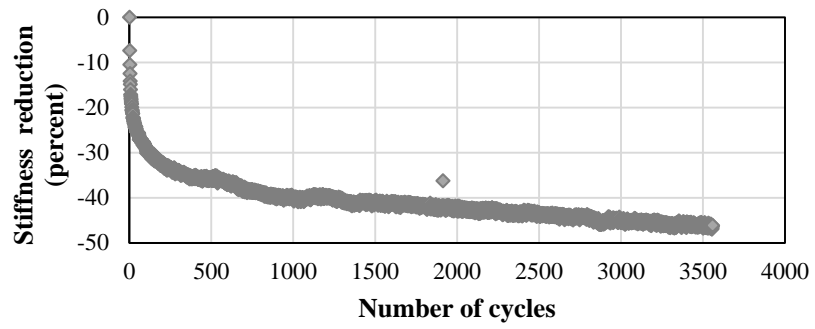


Figure B.1: (Continued)

LF73ZO(III)



LF73ZO-(I)



LF73ZO-(II)

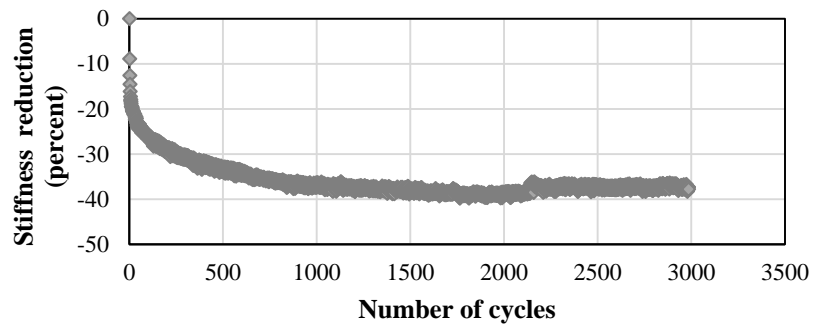


Figure B.1: (Continued)

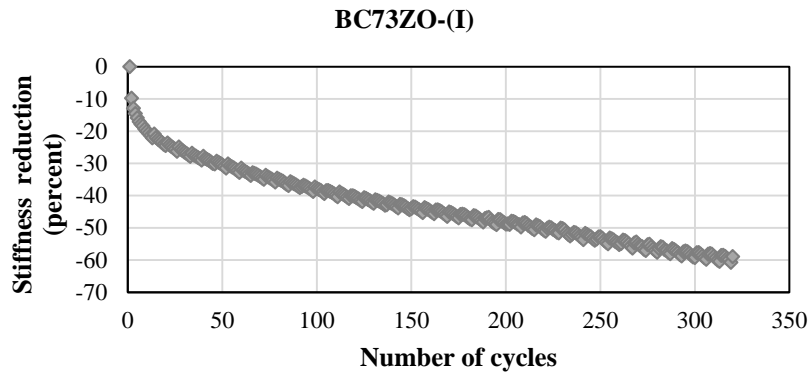
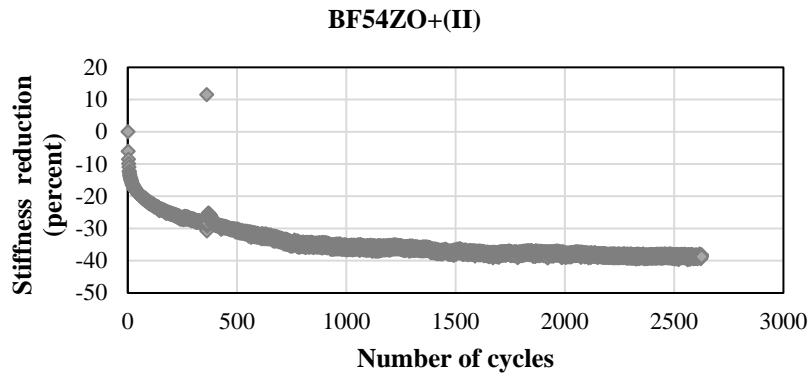
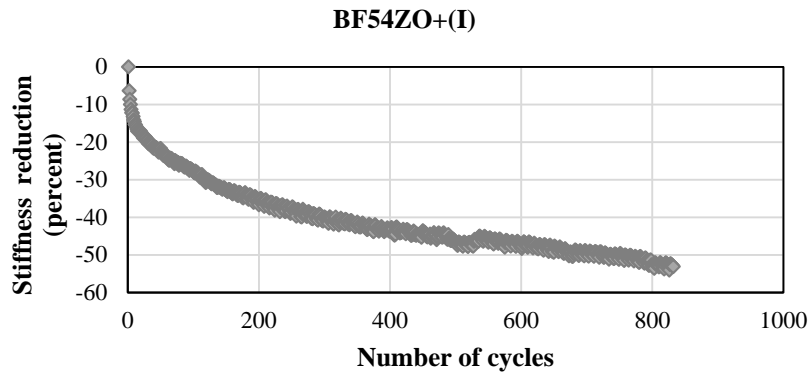
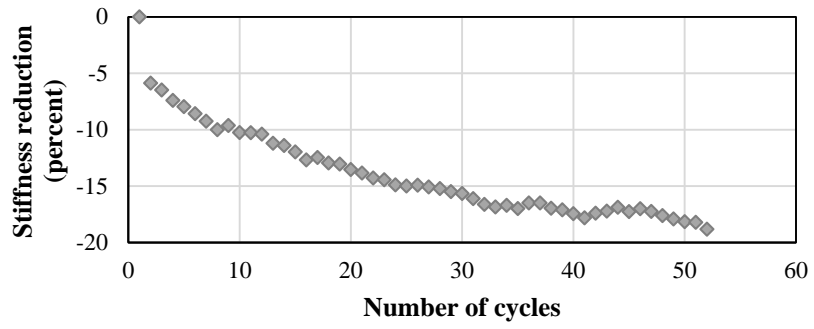
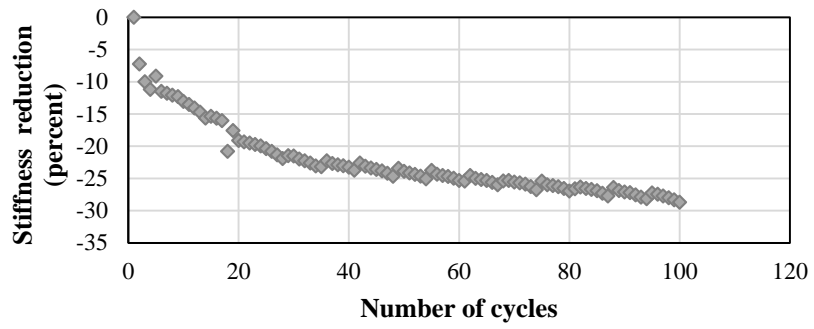


Figure B.1: (Continued)

BC73ZO-(II)



BC73ZO-(III)



BF73ZO+(I)

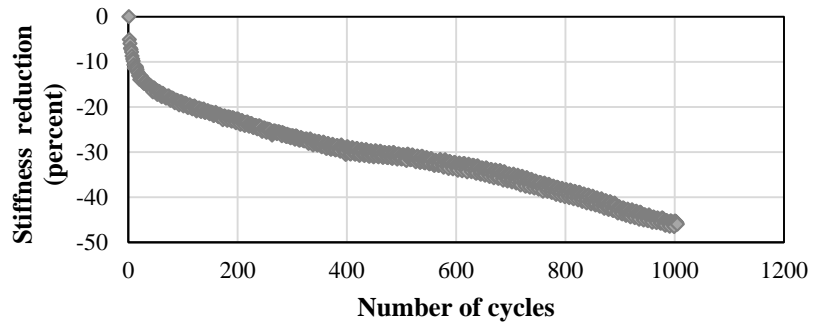
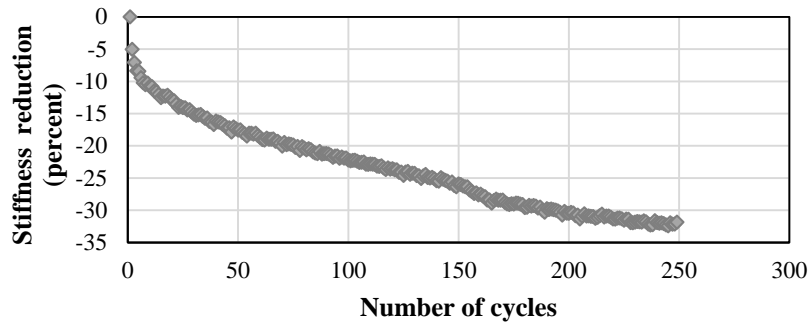
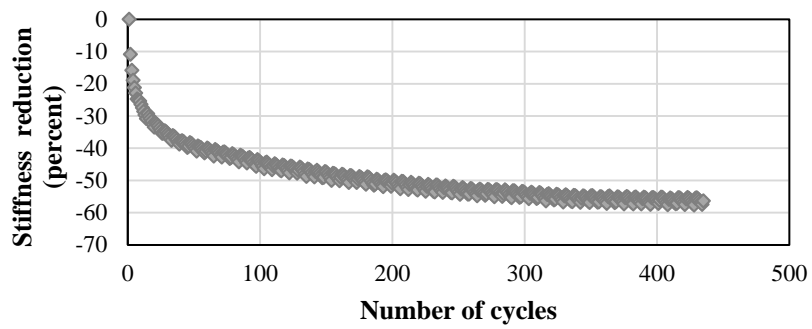


Figure B.1: (Continued)

BF73ZO+(II)



BF73ZO-(I)



BF73ZO-(II)

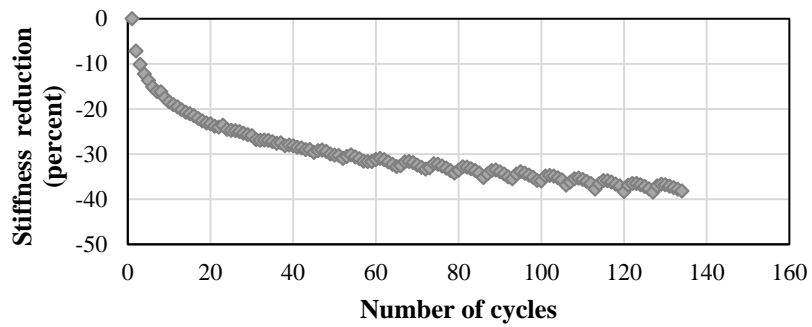
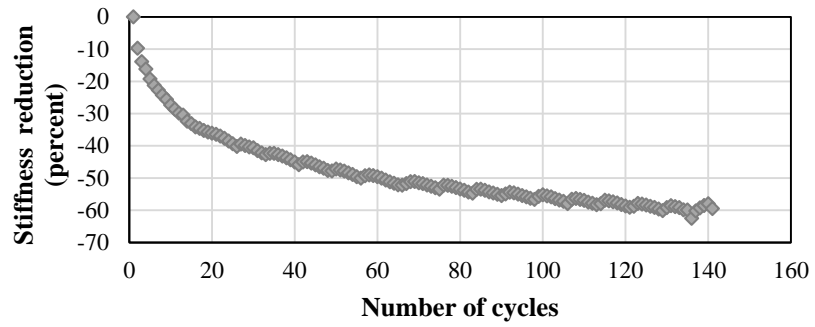
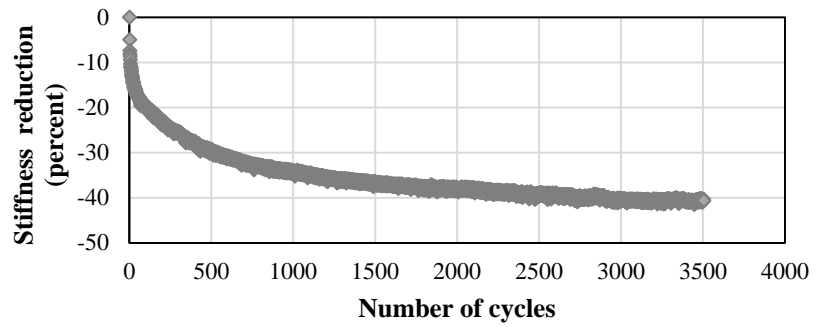


Figure B.1: (Continued)

BF73ZO-(III)



BC73SO+(I)



BC73SO+(II)

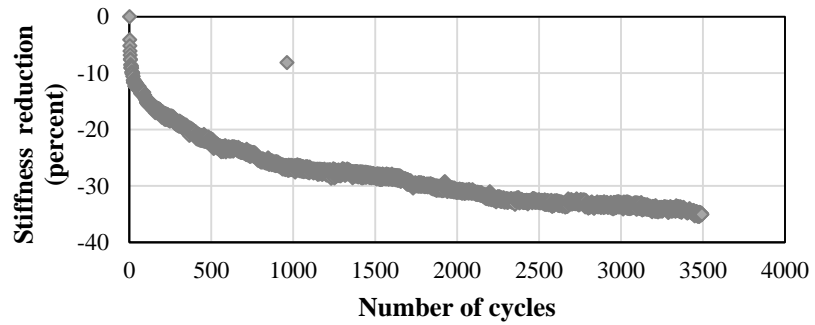


Figure B.1: (Continued)

Symbols used:

Aggregate: L=limestone, B=basalt; Gradation: C=coarse, F=fine; Polymer modification: Z=no modification, S=SBS modification; Asphalt type: 54 and 73=binder penetration values (0.1mm); Asphalt content: O=optimum, O+=optimum + 0.5%, O- =optimum- 0.5%

APPENDIX C

BEST LINEAR REGION PLOTS

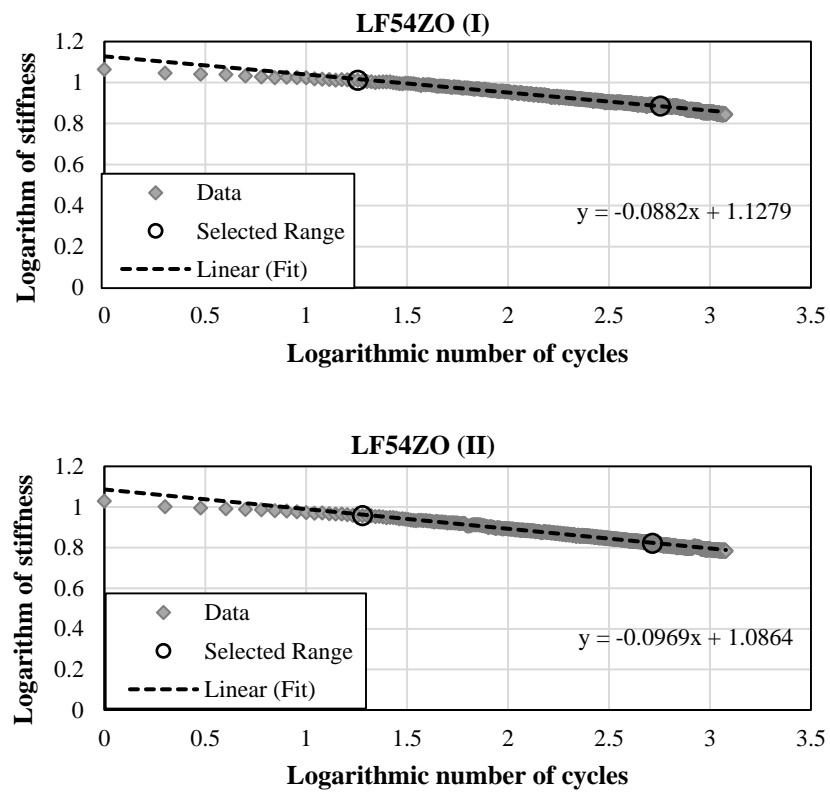


Figure C.1: The logarithmic data of stiffness vs. number of cycles for the specimens

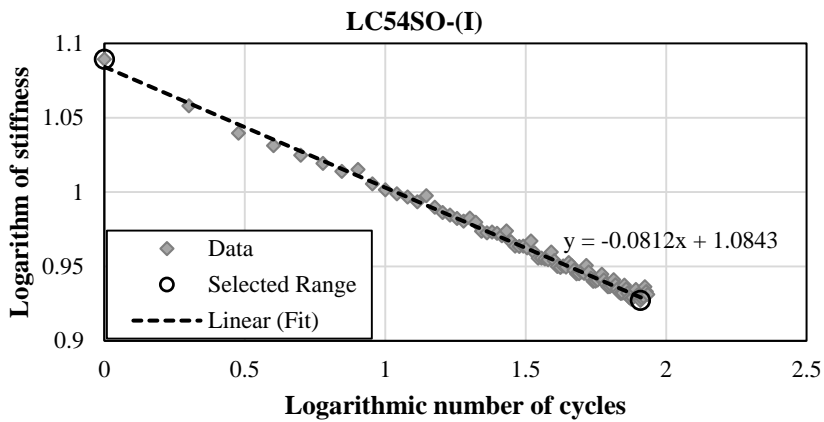
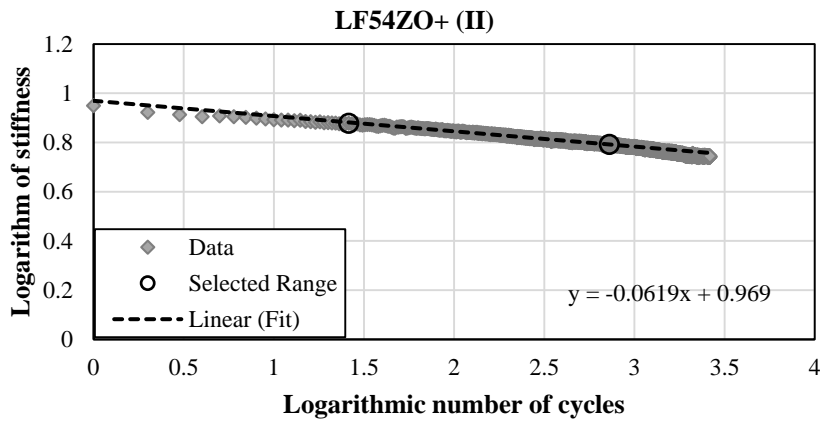
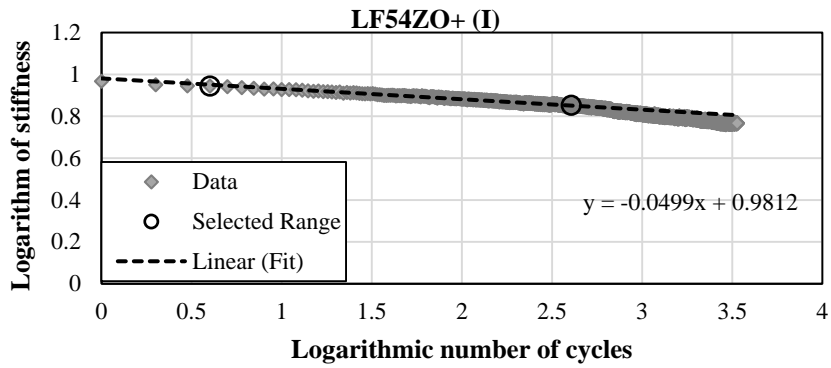


Figure C.1: (Continued)

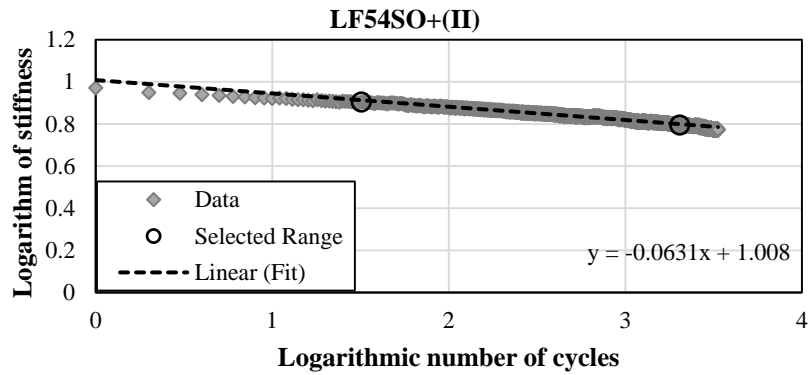
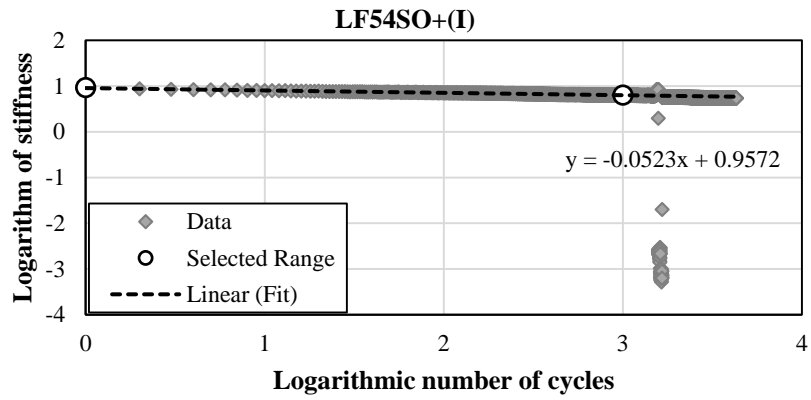
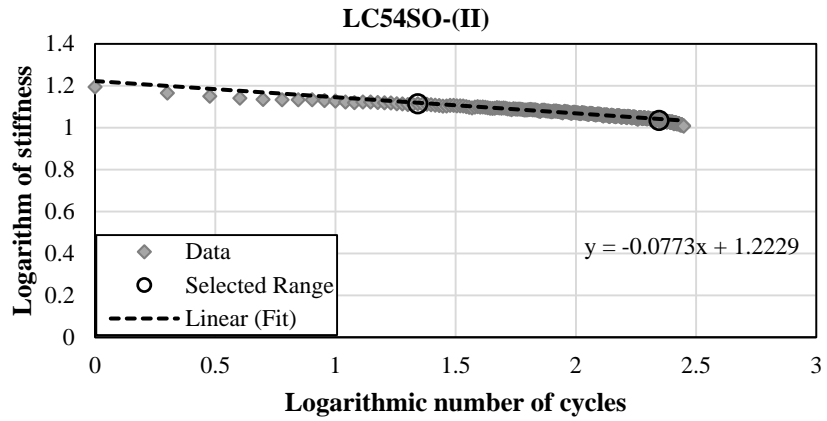


Figure C.1: (Continued)

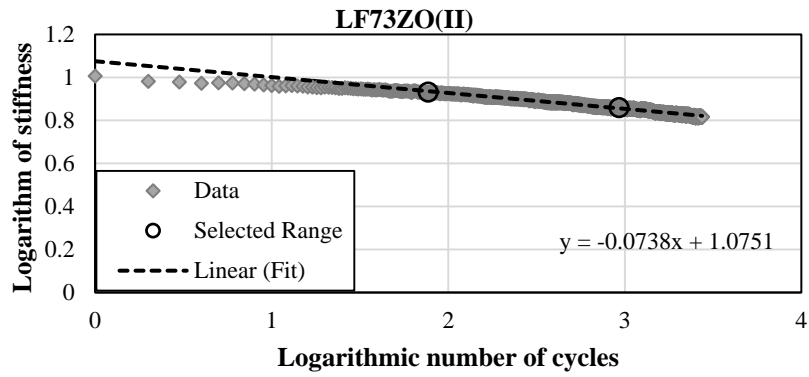
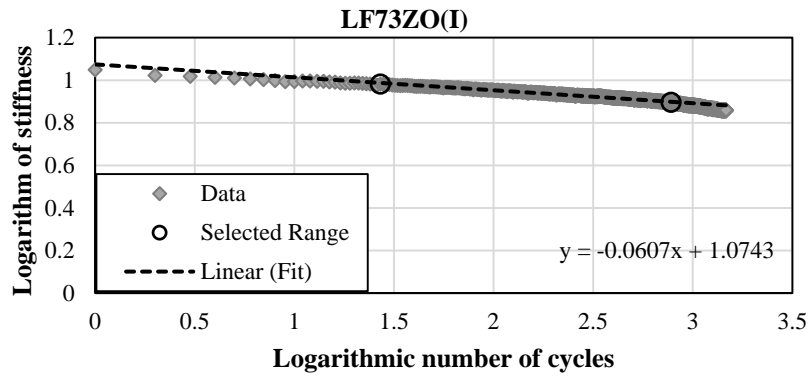
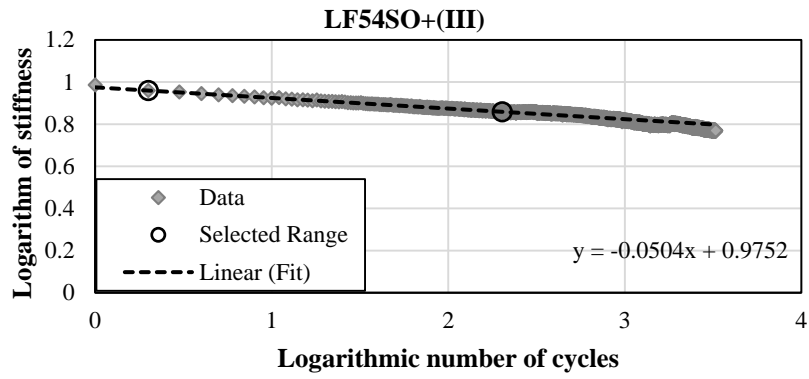


Figure C.1: (Continued)

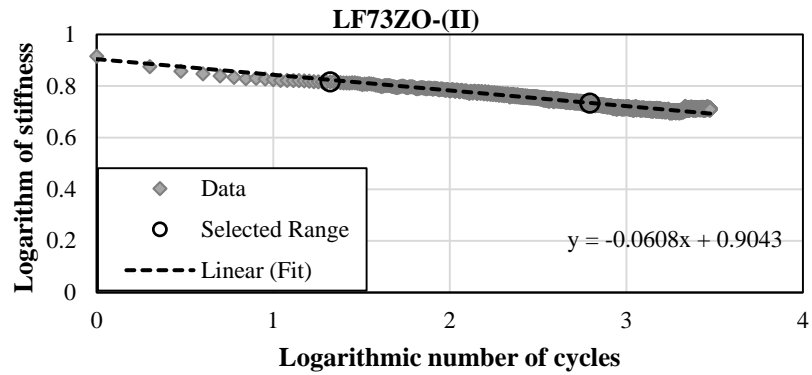
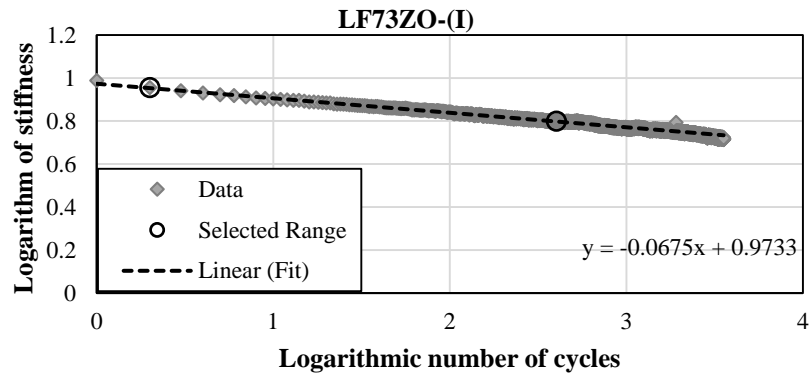
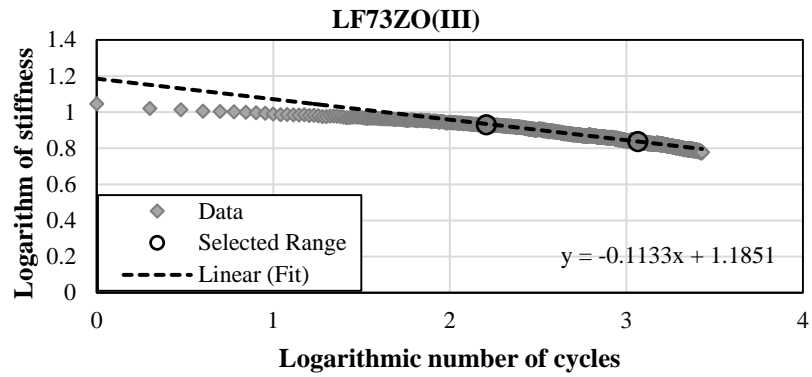
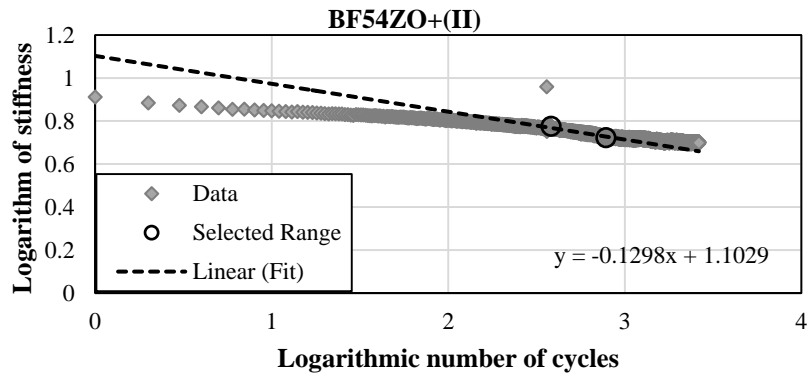
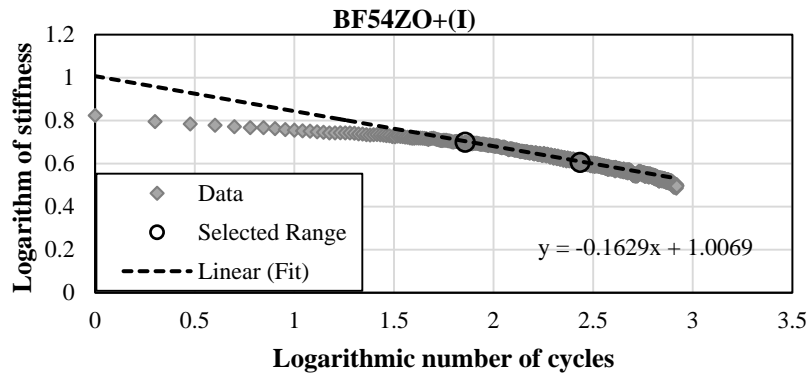


Figure C.1: (Continued)



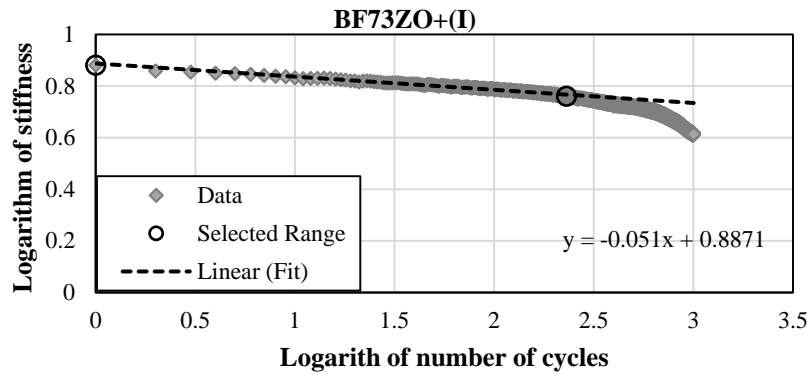
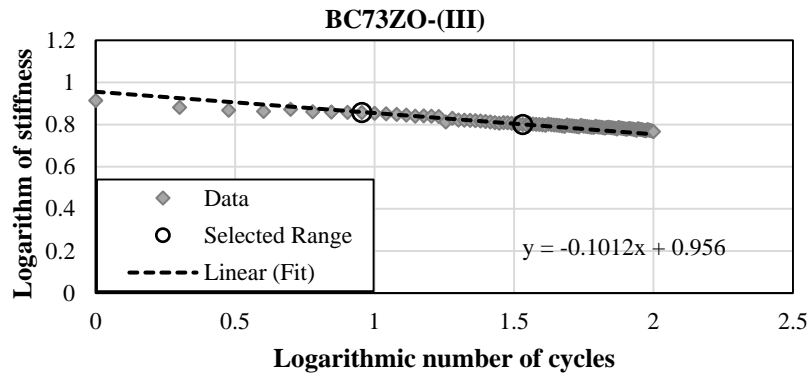
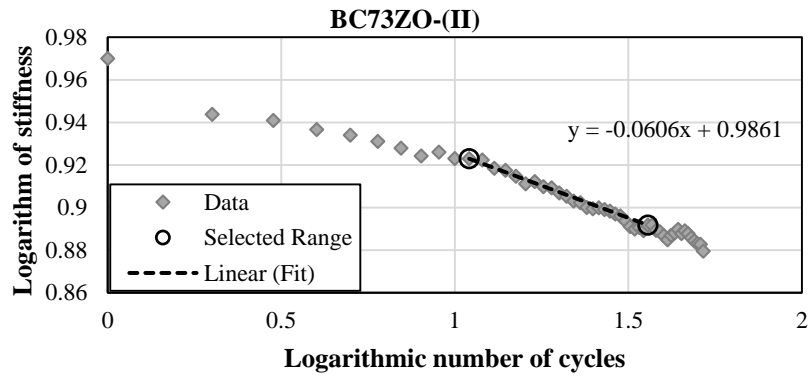


Figure C.1: (Continued)

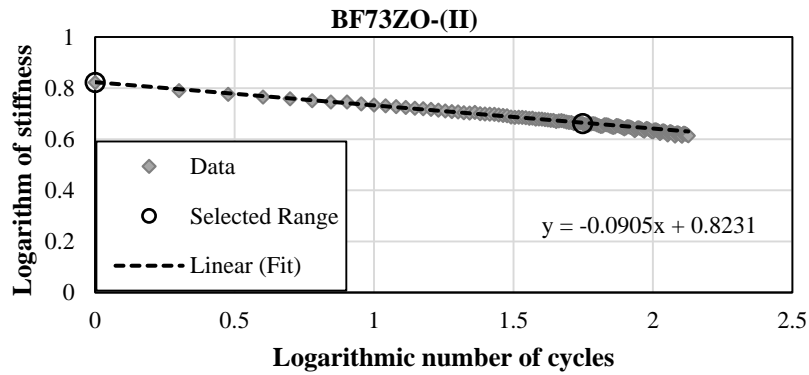
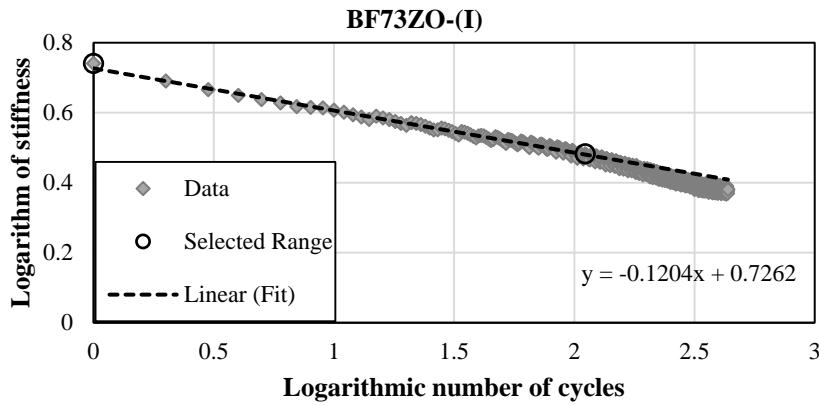
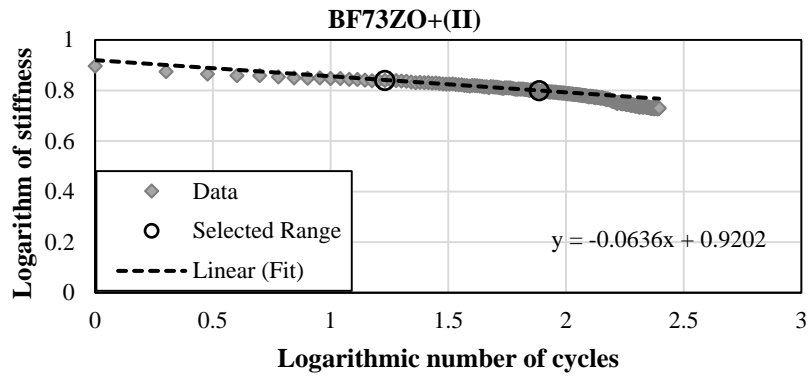


Figure C.1: (Continued)

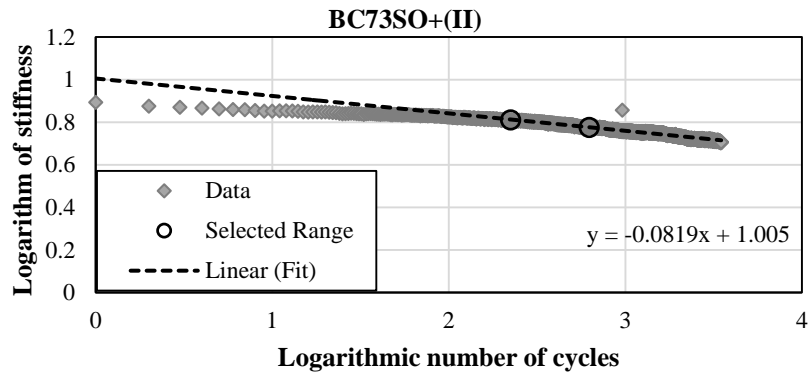
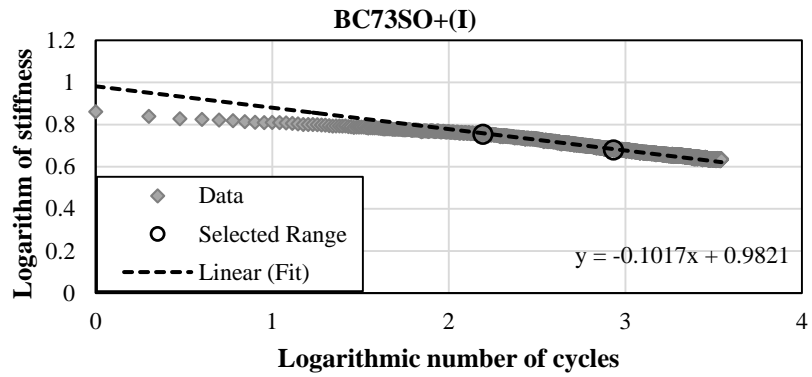
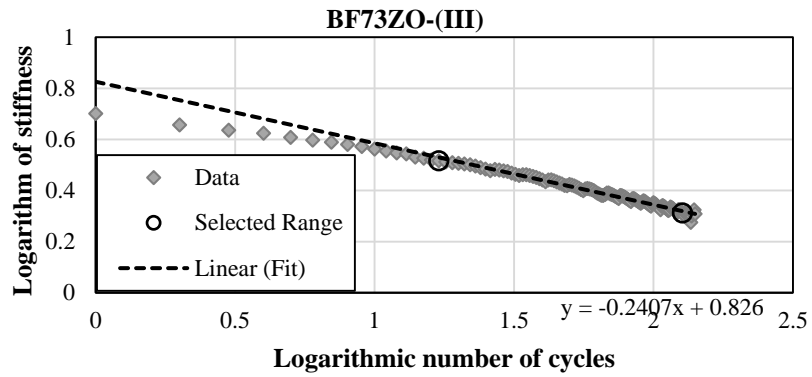


Figure C.1: (Continued)

Symbols used:

Aggregate: L=limestone, B=basalt; Gradation: C=coarse, F=fine; Polymer modification: Z=no modification, S=SBS modification; Asphalt type: 54 and 73=binder penetration values (0.1mm); Asphalt content: O=optimum, O+=optimum + 0.5%, O- =optimum – 0.5

APPENDIX D

POWER MODEL PLOTS

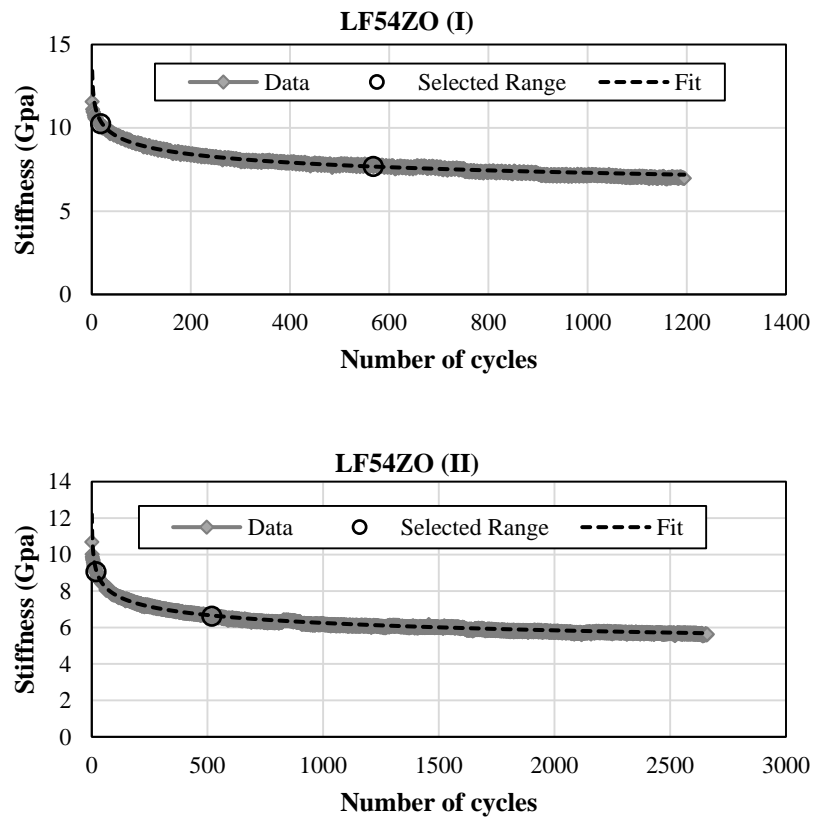


Figure D.1: The power model fitted to the data in the selected region for all the specimens.

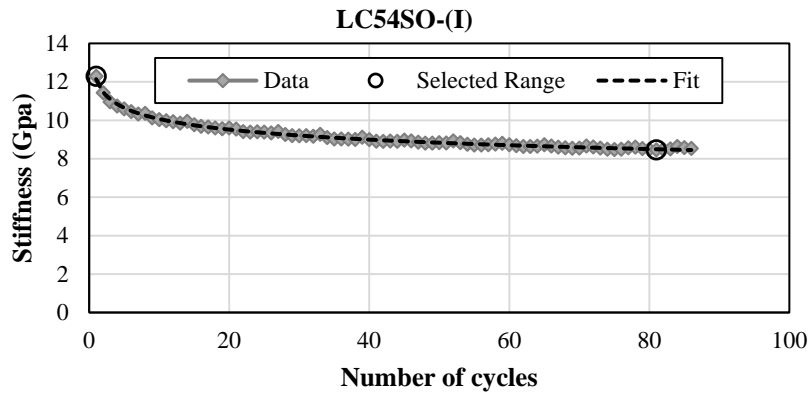
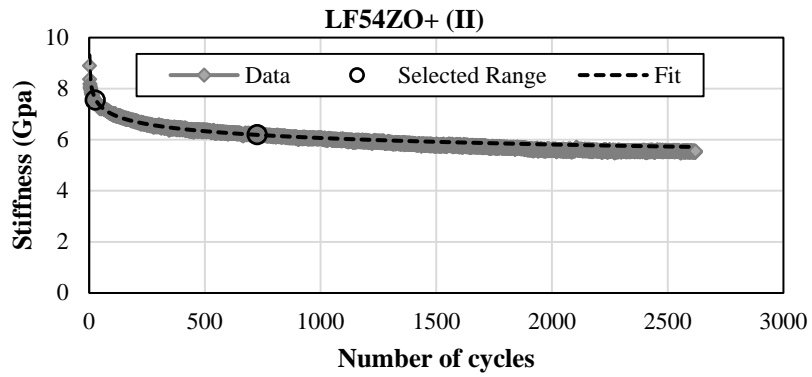
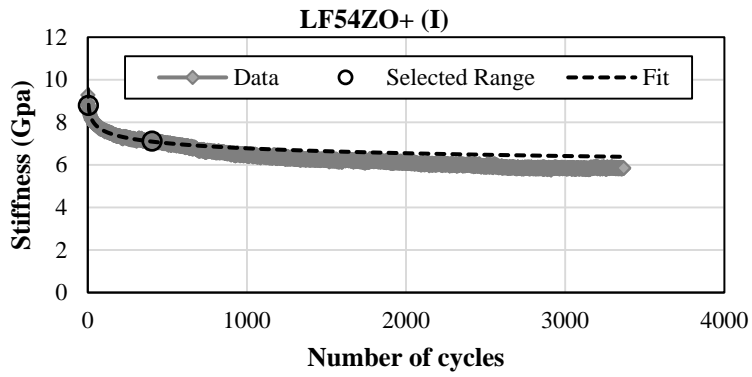


Figure D.1: (Continued)

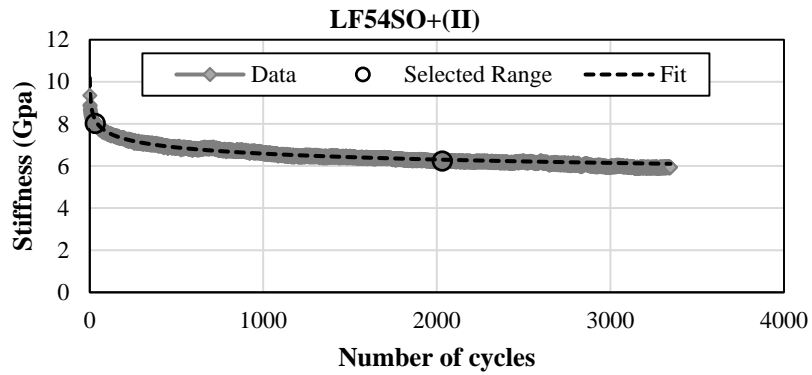
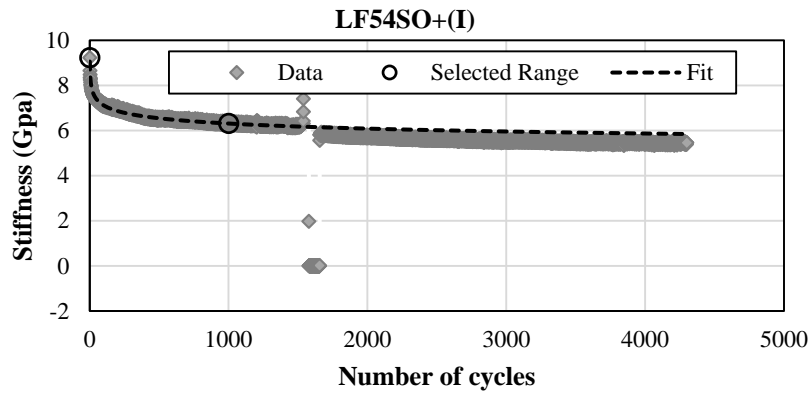
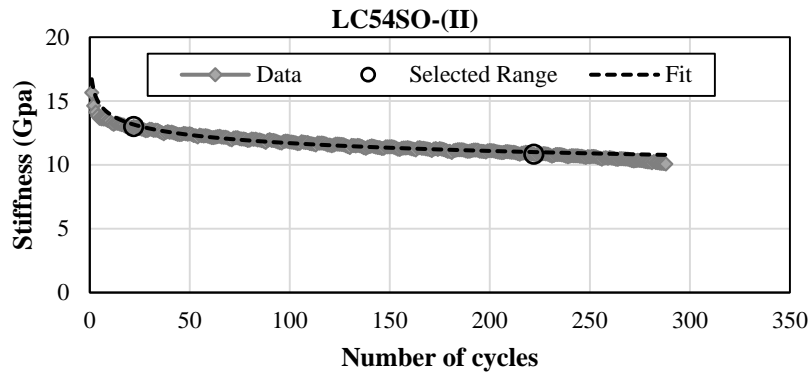


Figure D.1: (Continued)

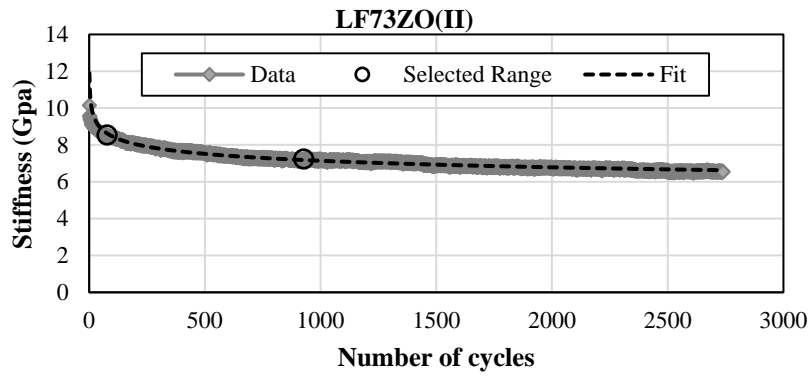
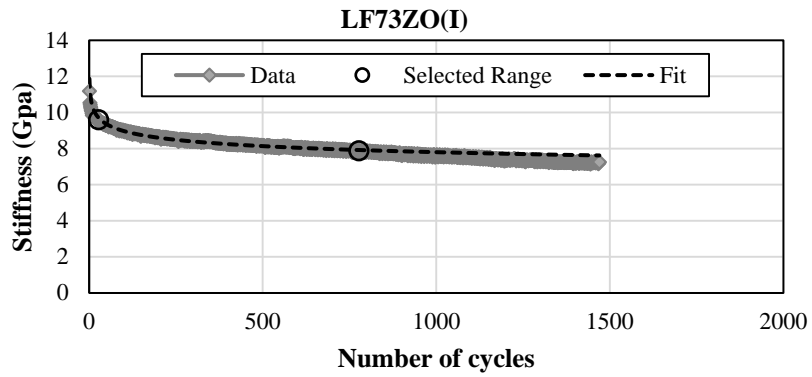
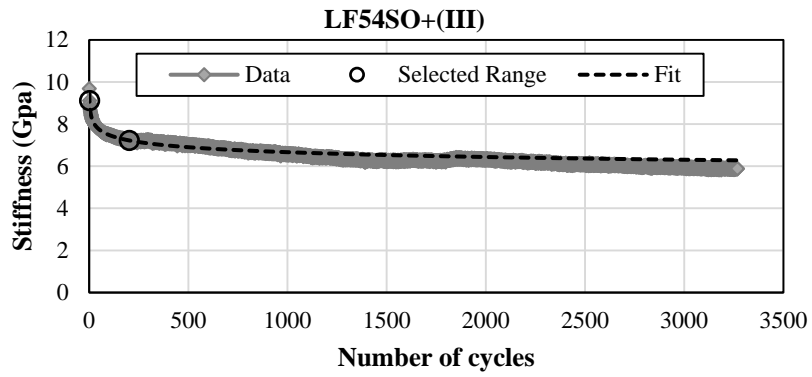


Figure D.1: (Continued)

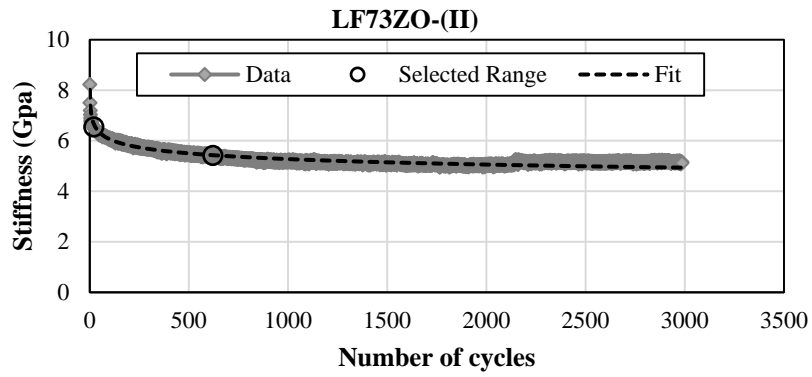
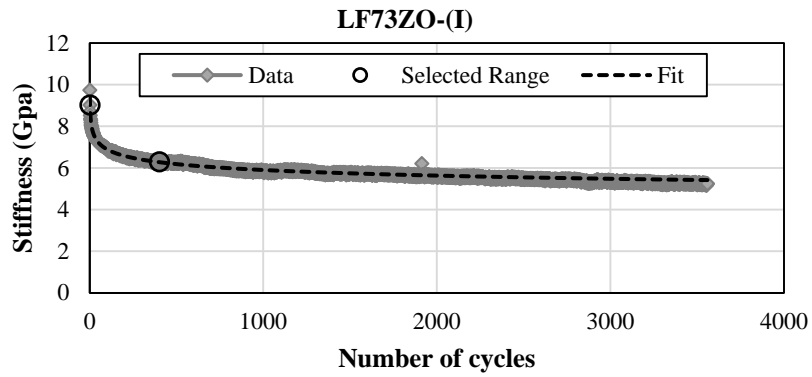
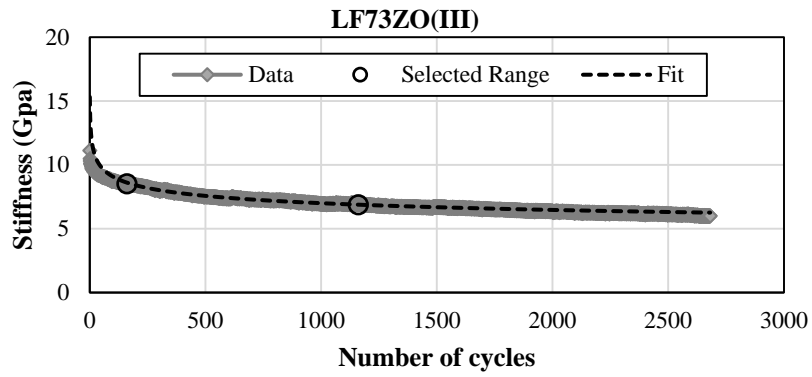


Figure D.1: (Continued)

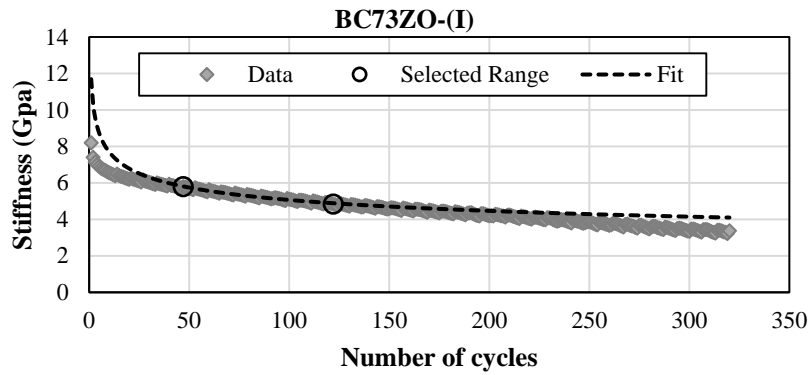
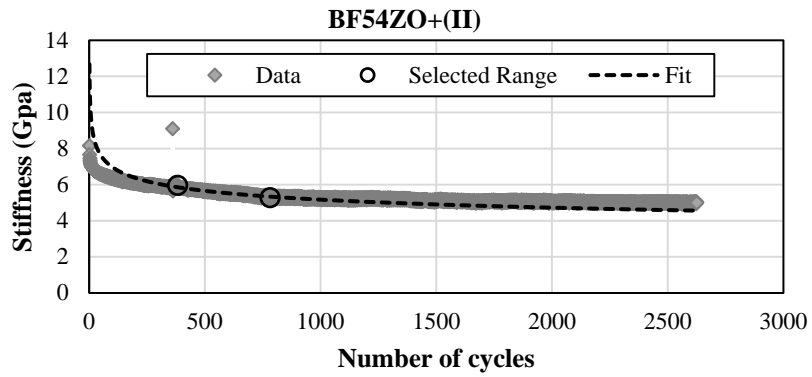
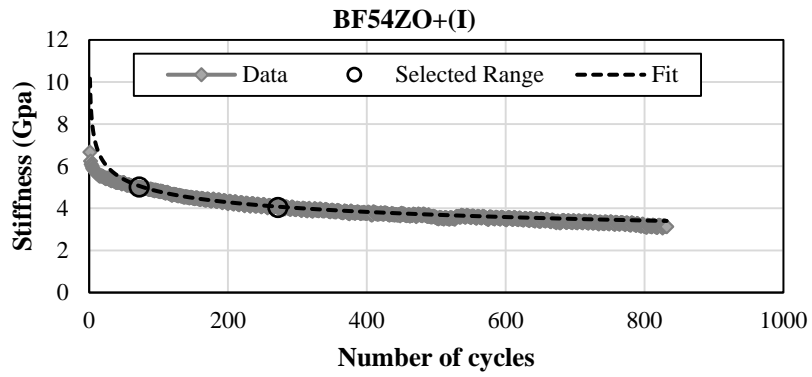


Figure D.1: (Continued)

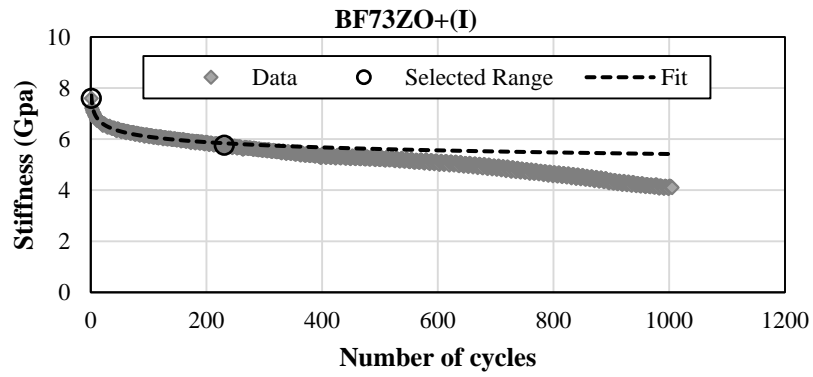
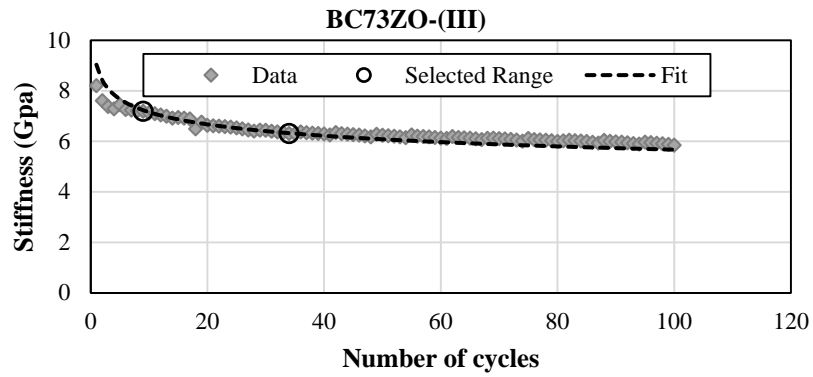
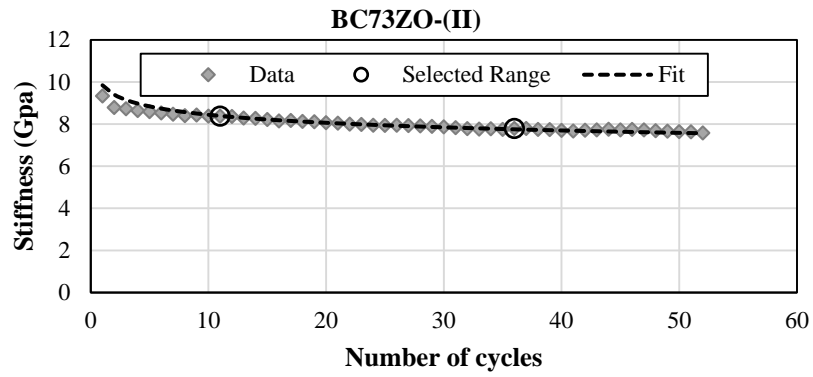


Figure D.1: (Continued)

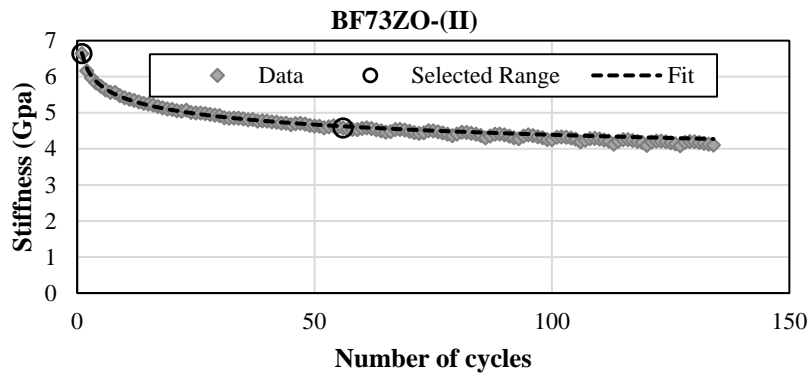
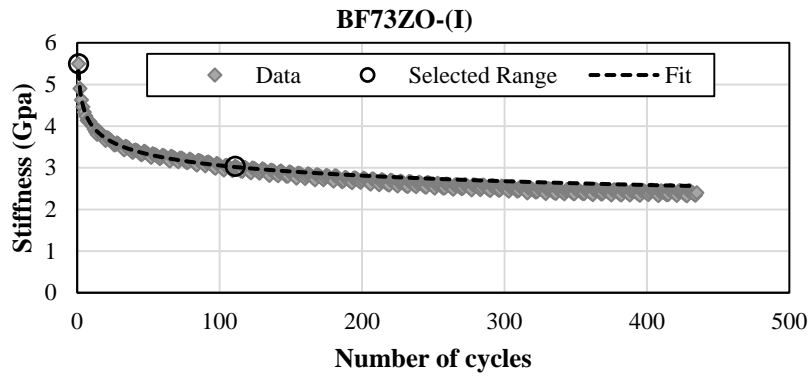
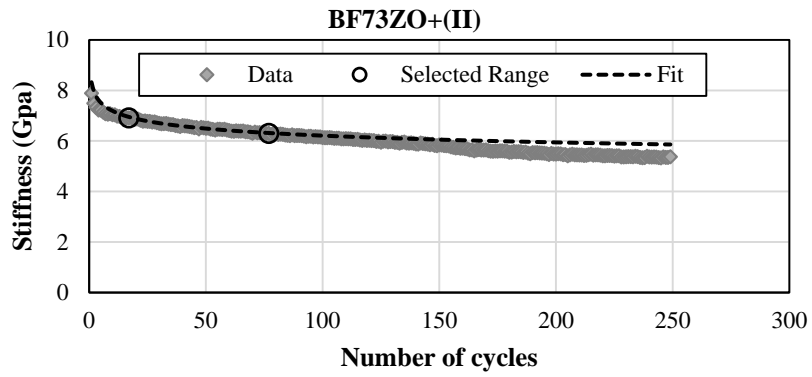


Figure D.1: (Continued)

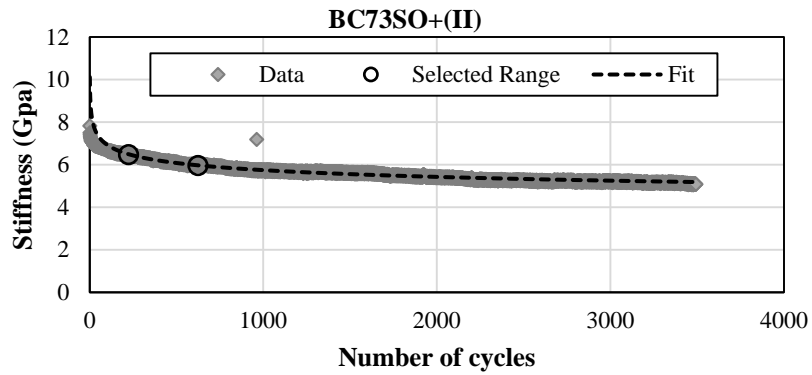
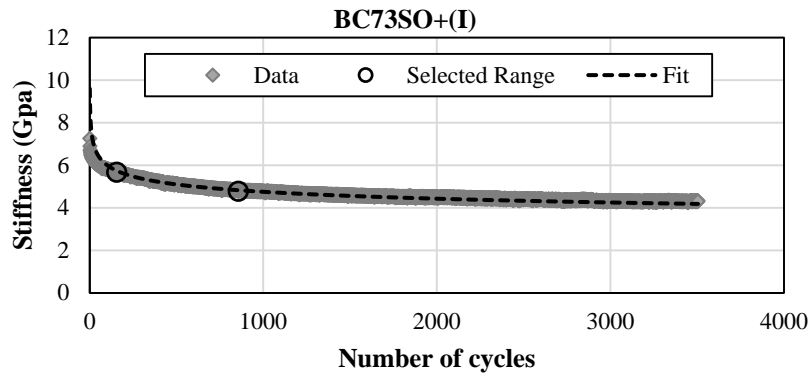
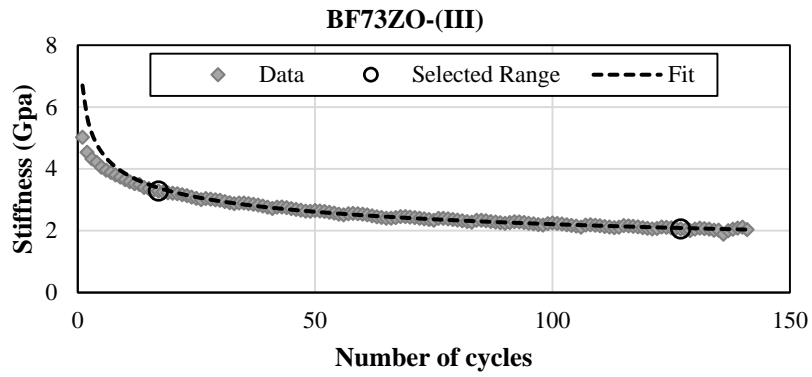


Figure D.1: (Continued)

Symbols used:

Aggregate: L=limestone, B=basalt; Gradation: C=coarse, F=fine; Polymer modification: Z=no modification, S=SBS modification; Asphalt type: 54 and 73=binder penetration values (0.1mm); Asphalt content: O=optimum, O+=optimum + 0.5%, O- =optimum - 0.5

APPENDIX E

MAXIMUM CALCULATED VALUES OF COEFFICIENT OF DETERMINATION FOR EACH SPECIMEN, FOR FINDING THE BEST LINEAR FIT IN LOG-LOG SCALE DATA

Table E.1: The maximum values of measured R²s

Specimen Type	Replicate Number	R ² Value
LF54ZO	I	0.992
LF54ZO	II	0.996
LF54ZO+	I	0.988
LF54ZO+	II	0.991
LC54SO-	I	0.993
LC54SO-	II	0.975
LF54SO+	I	0.978
LF54SO+	II	0.982
LF54SO+	III	0.996
LF73ZO	I	0.988
LF73ZO	II	0.985
LF73ZO	III	0.99
LF73ZO-	I	0.995
LF73ZO-	II	0.974
BF54ZO+	I	0.983
BF54ZO+	II	0.942
BC73ZO-	I	0.978
BC73ZO-	II	0.987

Table E.1: (Continued)

Specimen Type	Replicate Number	R ² Value
BF73ZO+	II	0.988
BF73ZO-	I	0.989
BF73ZO-	II	0.995
BF73ZO-	III	0.99
BC73SO+	I	0.992
BC73SO+	II	0.97
BC73ZO-	III	0.947
BF73ZO+	I	0.978

Symbols used:

Aggregate: L=limestone, B=basalt; Gradation: C=coarse, F=fine; Polymer modification: Z=no modification, S=SBS modification; Asphalt type: 54 and 73=binder penetration values (0.1mm); Asphalt content: O=optimum, O+=optimum + 0.5%, O- =optimum - 0.5

APPENDIX F

THE PLOTS SHOWING THE EFFECT OF DIFFERENT MIX DESIGN VARIABLE ON THE RESPONSES TAKEN FROM ALL 26 SPECIMEN

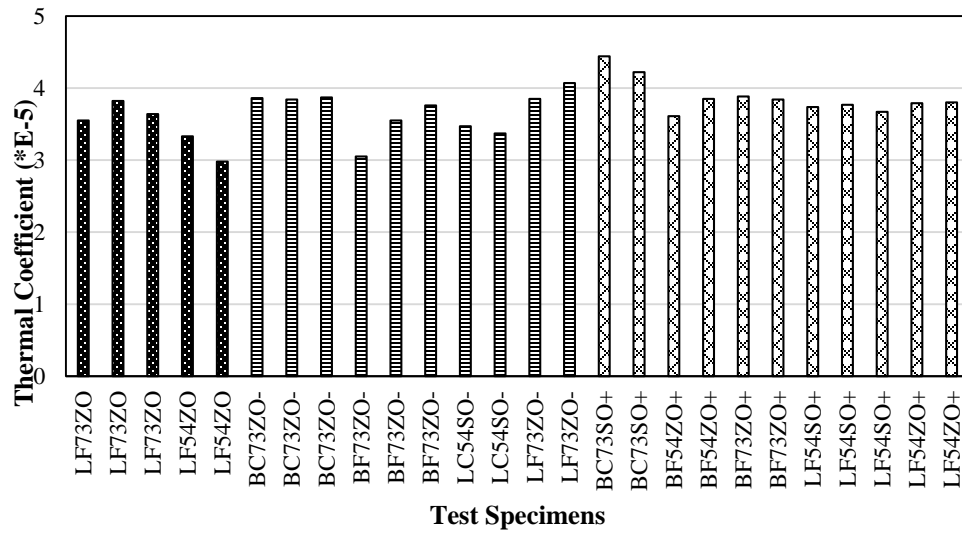


Figure F.1: The measured thermal coefficients for all the specimens grouped according to asphalt content.

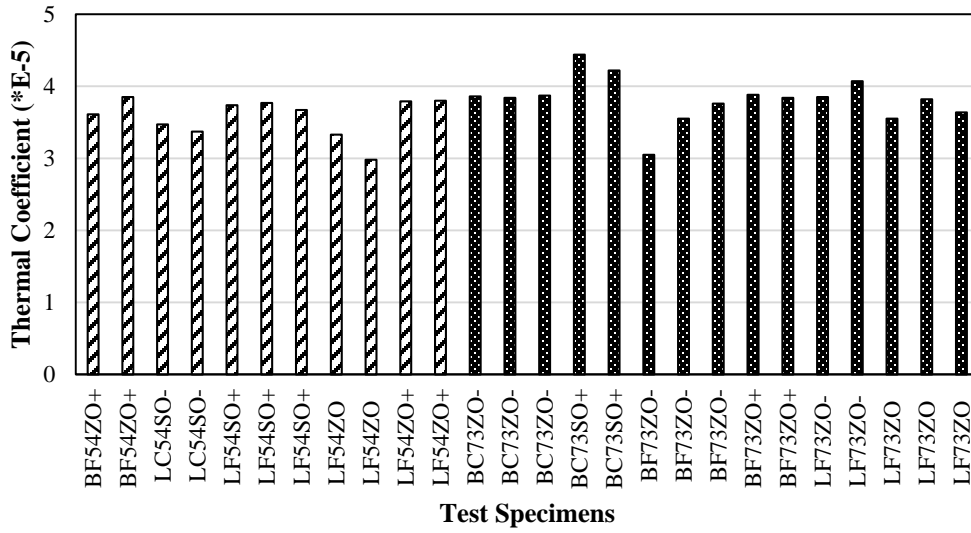


Figure F.2: The measured thermal coefficients for all the specimens grouped according to asphalt type.

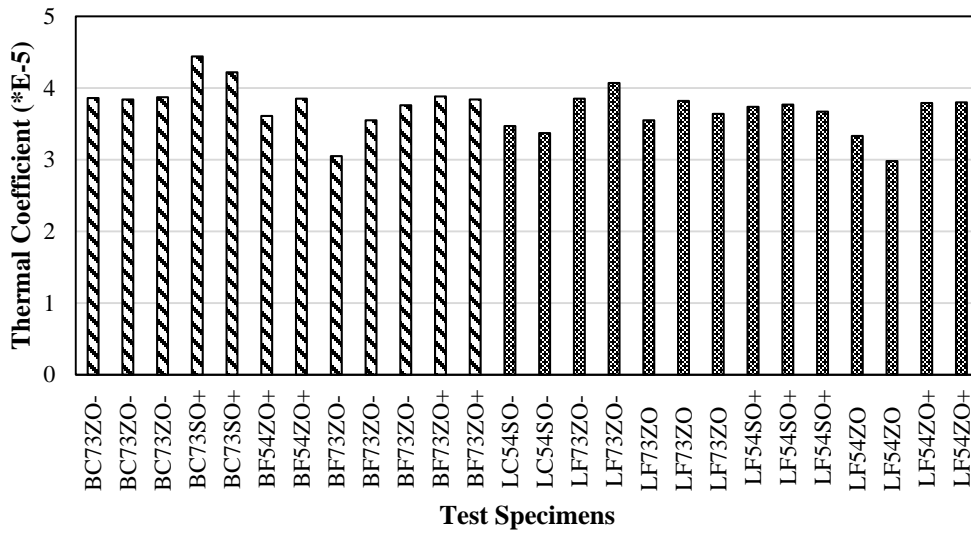


Figure F.3: The measured thermal coefficients for all the specimens grouped according to aggregate type

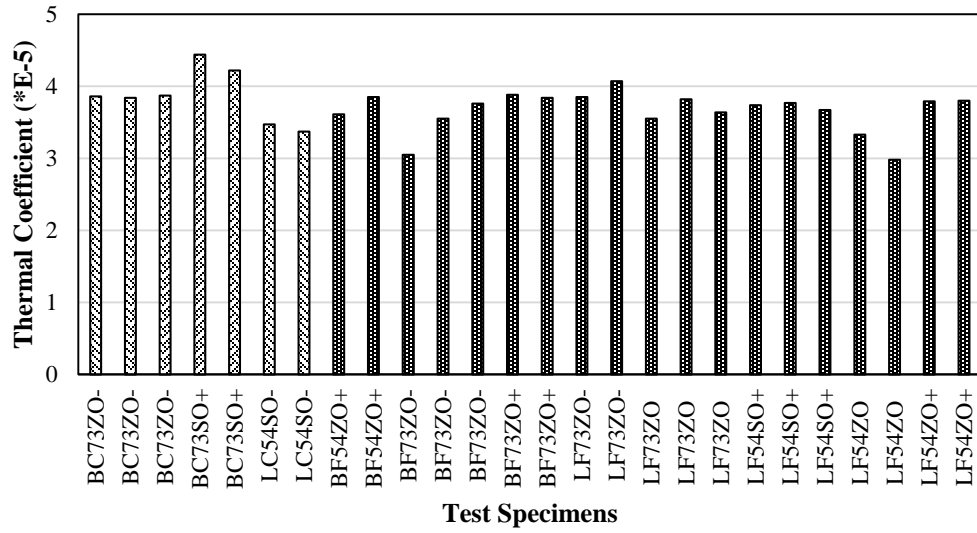


Figure F.4: The measured thermal coefficients for all the specimens grouped according to gradation

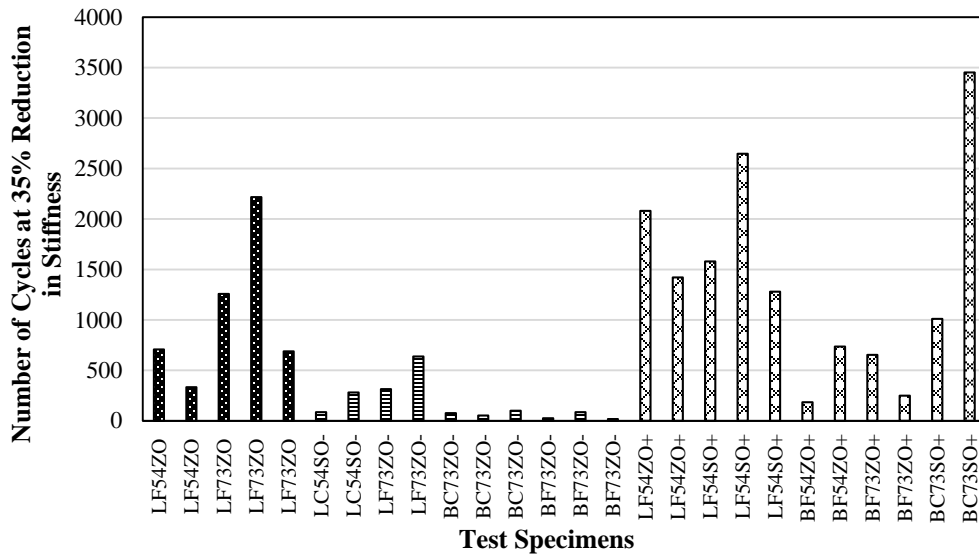


Figure F.5: The measured number of cycles at 35% reduction in stiffness for all the specimens grouped according to asphalt content.

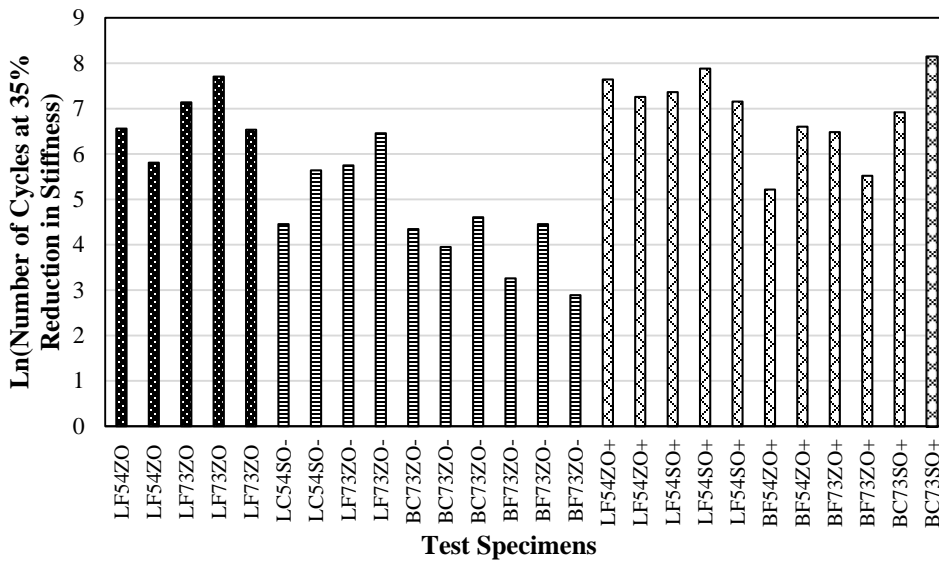


Figure F.6: The natural logarithm of measured number of cycles at 35% reduction in stiffness for all the specimens grouped according to asphalt content.

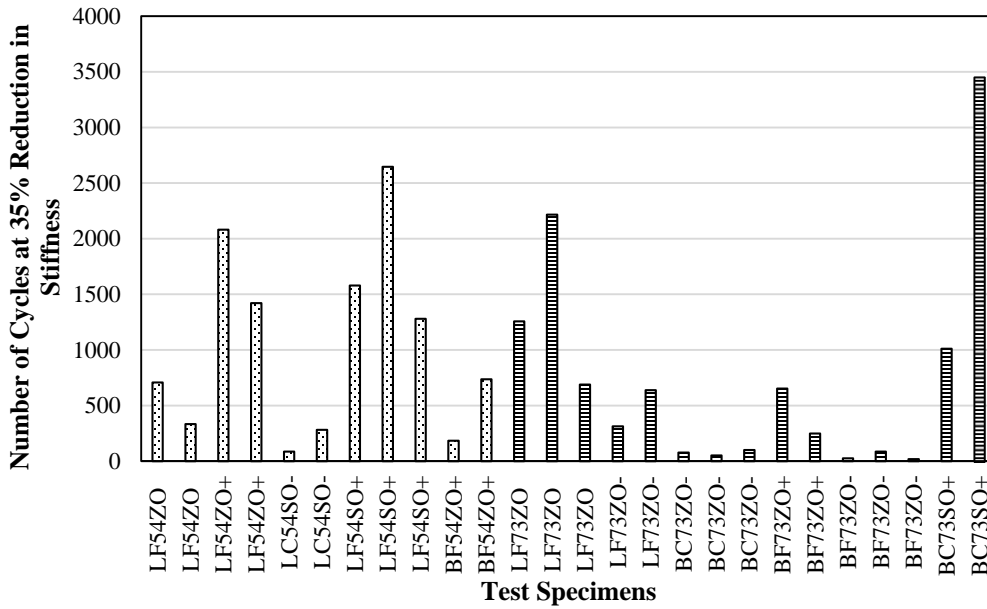


Figure F.7: The measured number of cycles at 35% reduction in stiffness for all the specimens grouped according to asphalt type.

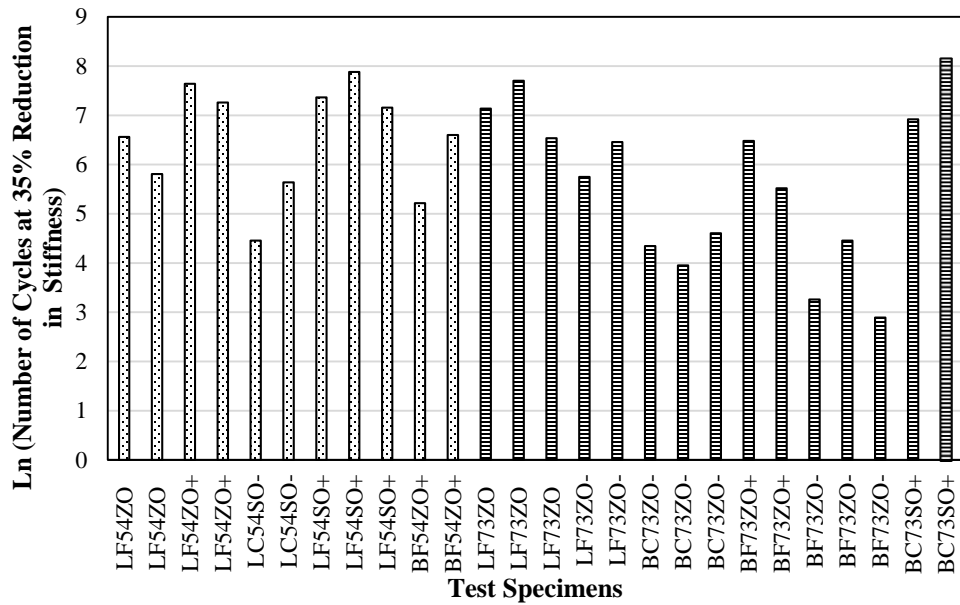


Figure F.8: The natural logarithm of measured number of cycles at 35% reduction in stiffness for all the specimens grouped according to asphalt type.

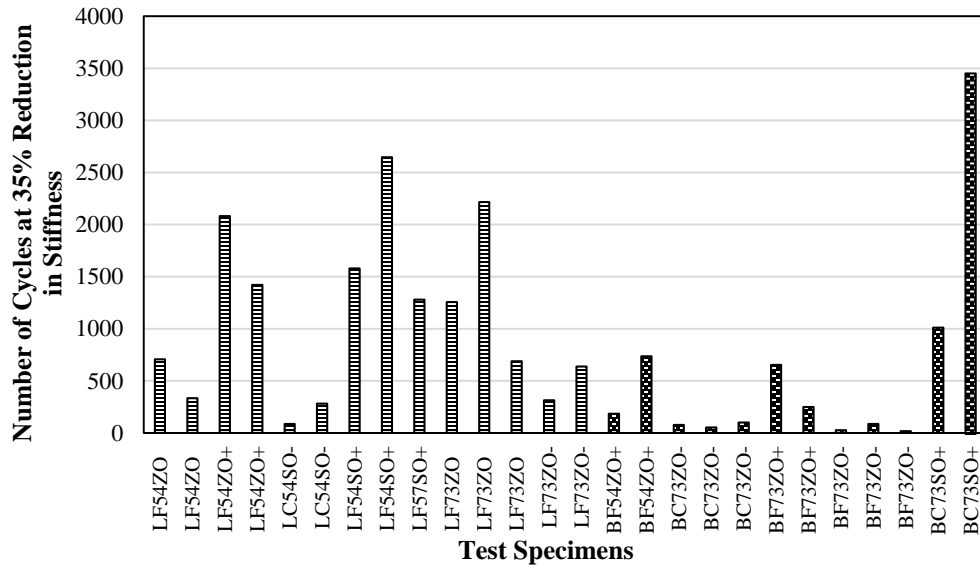


Figure F.9: The measured number of cycles at 35% reduction in stiffness for all the specimens grouped according to aggregate type.

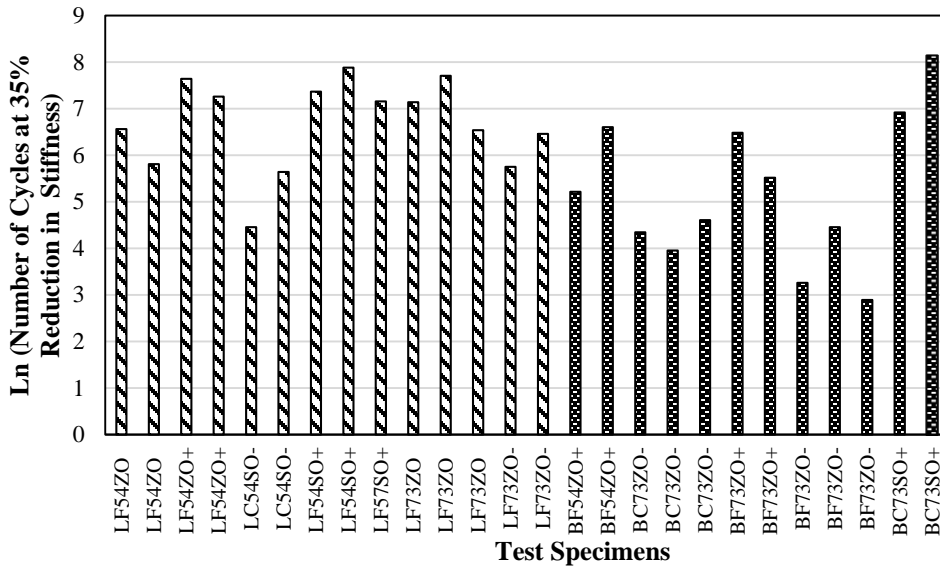


Figure F.10: The natural logarithm of measured number of cycles at 35% reduction in stiffness for all the specimens grouped according to aggregate type.

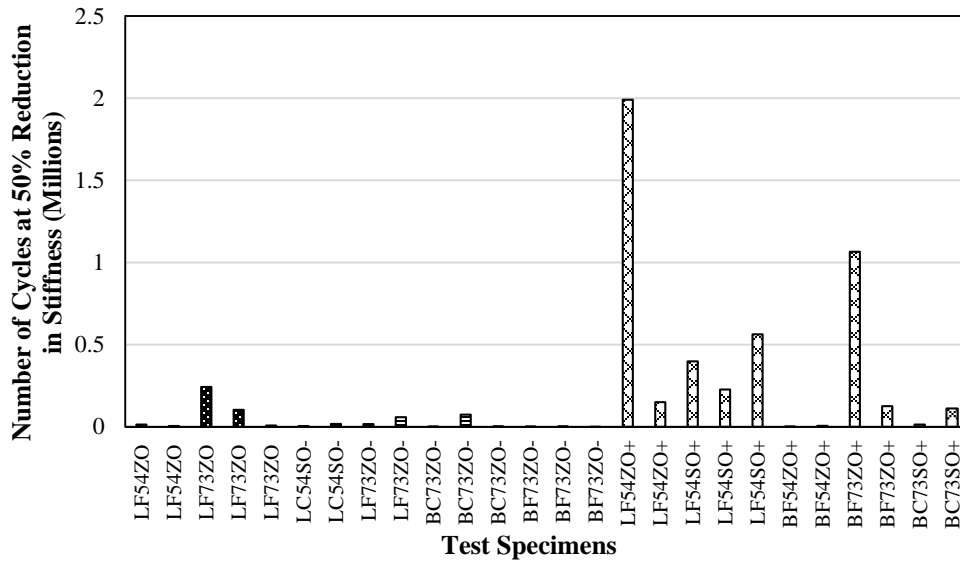


Figure F.11: The measured number of cycles at extrapolated 50% reduction in stiffness for all the specimens grouped according to asphalt content.

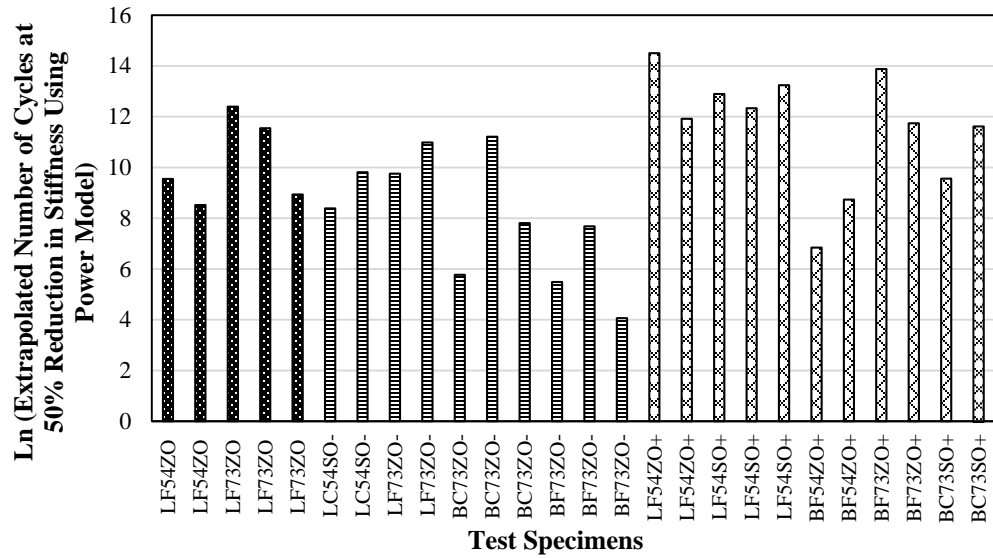


Figure F.12: The natural logarithm of extrapolated number of cycles at 50% reduction in stiffness for all the specimens grouped according to asphalt content.

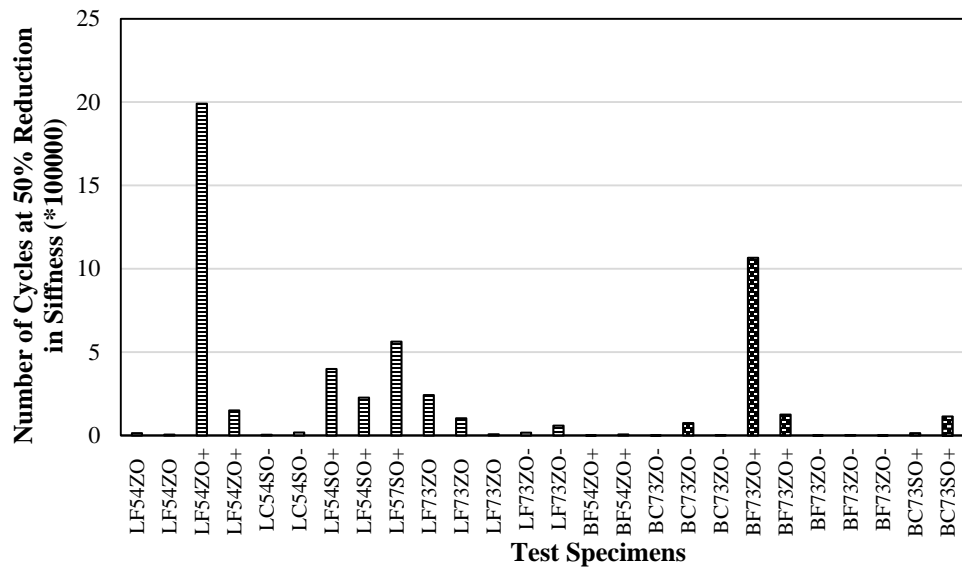


Figure F.13: The measured number of cycles at extrapolated 50% reduction in stiffness for all the specimens grouped according to aggregate type.

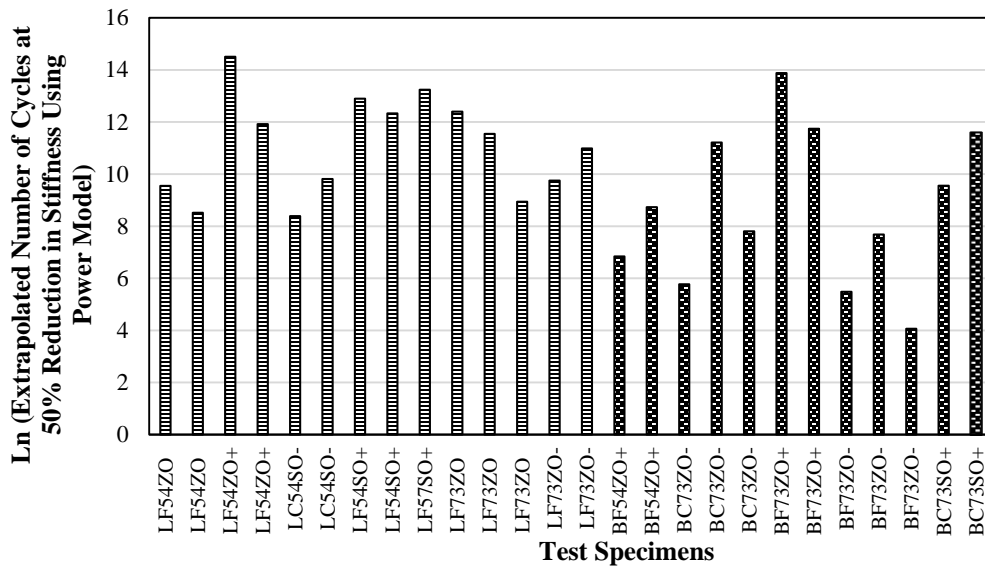


Figure F.14: The natural logarithm of extrapolated number of cycles at 50% reduction in stiffness for all the specimens grouped according to aggregate type.

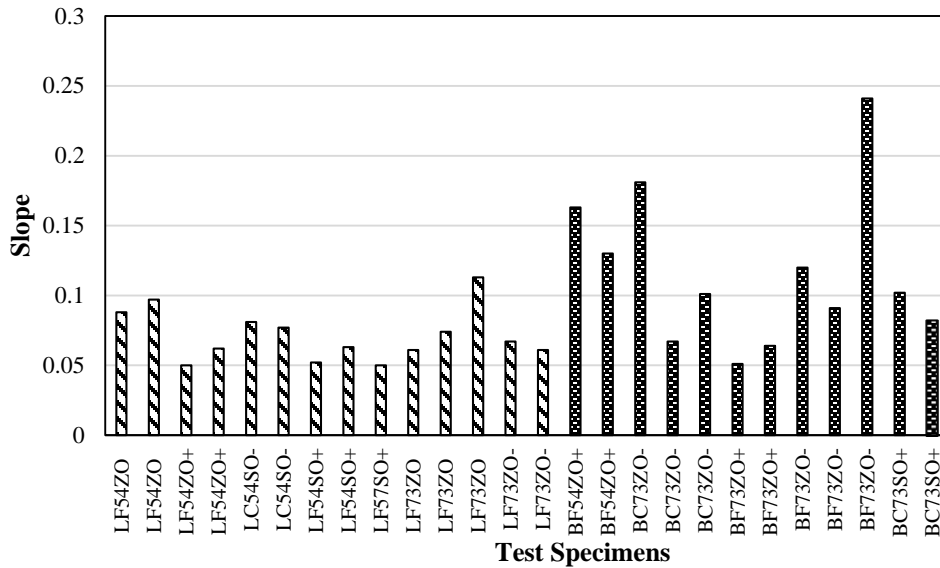


Figure F.15: The slopes measured for all the specimens grouped according to the aggregate type.

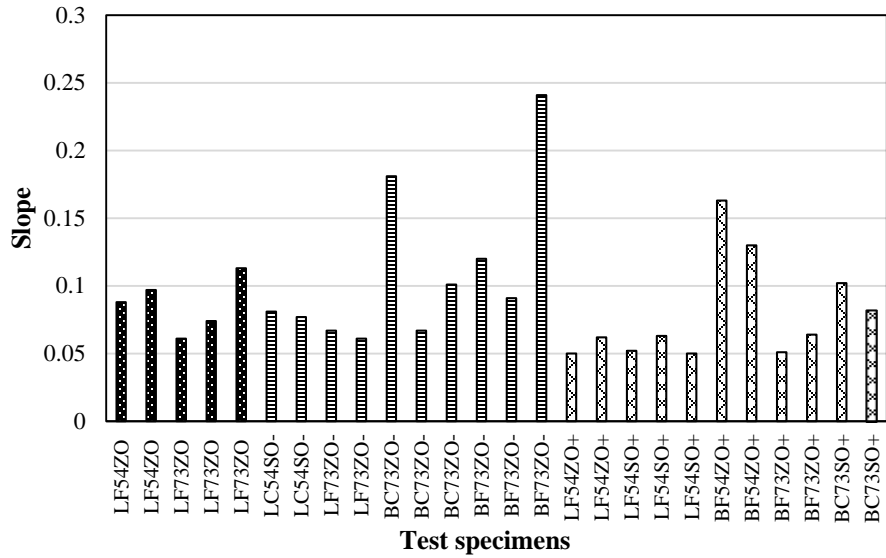


Figure F.16: The slopes measured for all the specimens grouped according to the asphalt content.

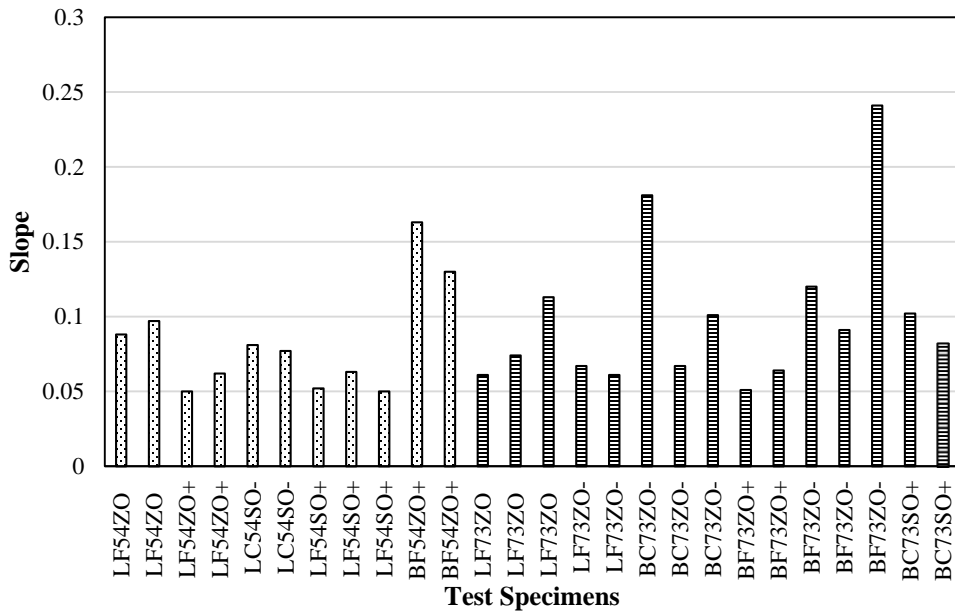


Figure F.17: The slopes measured for all the specimens grouped according to the asphalt type.

Symbols used:

Aggregate: L=limestone, B=basalt; Gradation: C=coarse, F=fine; Polymer modification: Z=no modification, S=SBS modification; Asphalt type: 54 and 73=binder penetration values (0.1mm); Asphalt content: O=optimum, O+=optimum + 0.5%, O- =optimum - 0.5

APPENDIX G

SOFTWARE MANUALS

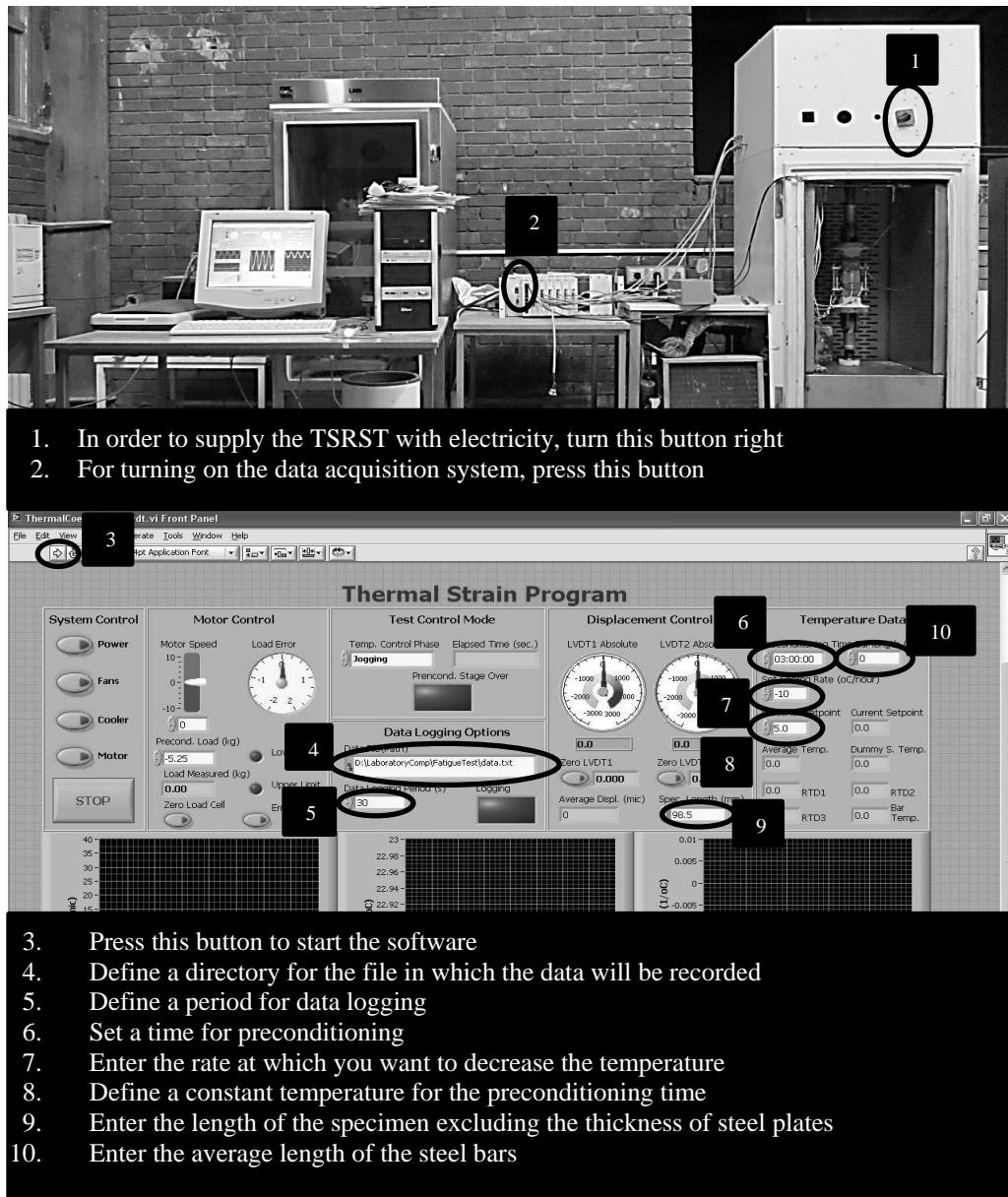
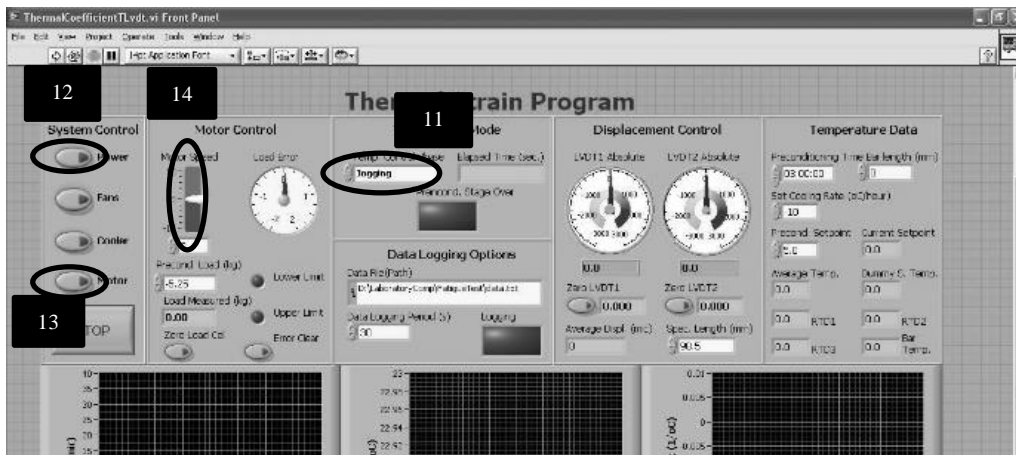
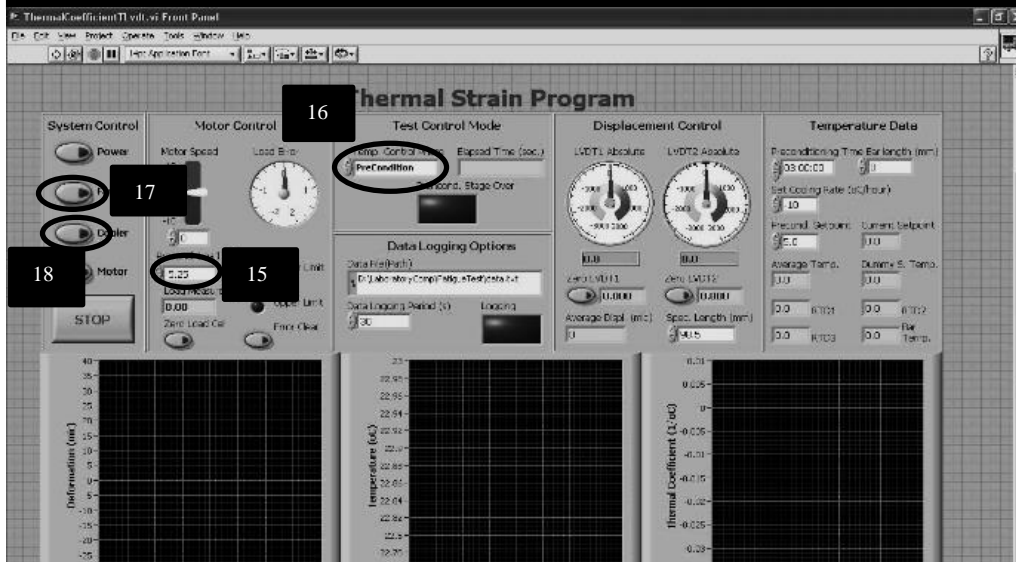


Figure G.1: Manual for the thermal strain test.



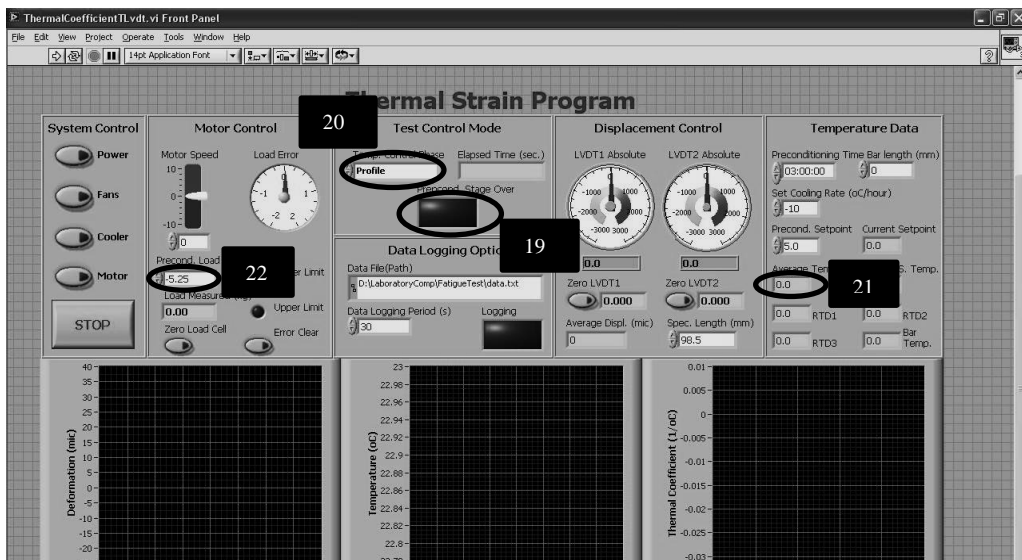
After accomplishing the 10th stage, you should hang the specimen stuck between the two steel plates to the actuator from the top, then:

- 11- Set the motor to the jogging mode
- 12- Press the power button. And wait for clicking sound
- 13- Press this button to turn on the motor
- 14- Slide this button to change the speed and the direction of motor rotation, so that you can adjust the distance between the two universal joints. Then, you can connect the bottom plate to the lower universal joint using a pin. In addition you must attach all of the sensors after the mounting stage



- 15- Enter a compressive load that is the half of the total weight of the specimen stuck between the two steel plates
- 16- Set the motor to preconditioning mode
- 17- Press this button to turn on the fan
- 18- Press this button to start the cooler

Figure G.1: (Continued)



- 19- You have to wait for the blinker to start blinking which means that the preconditioning time is over
- 20- Set the motor to profile mode
- 21- During the profile mode, keep an eye on the average temperature
- 22- Check the amount of preconditioning load during the tests

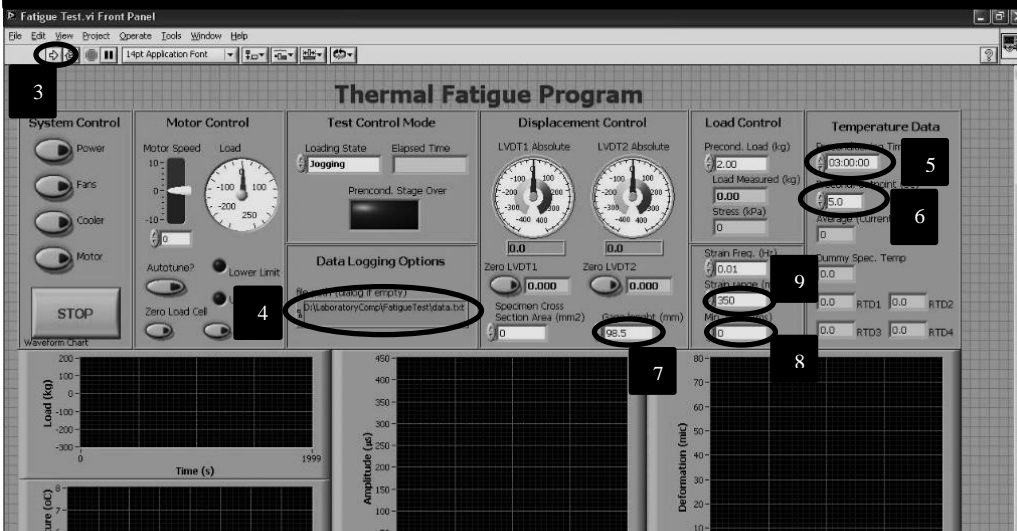


- 23. For stopping the test, set the motor to preconditioning mode
 - 24. Press this button to turn of the fan
 - 25. For turning on the cooler, press this button, this is the time for removing the specimen
 - 26. Press this button to turn off the motor
 - 27. Press this button to turn off the power
 - 28. For stopping the software, press this button
- Do not forget to turn of the TSRST machine and the data acquisition system

Figure G.1: (Continued)

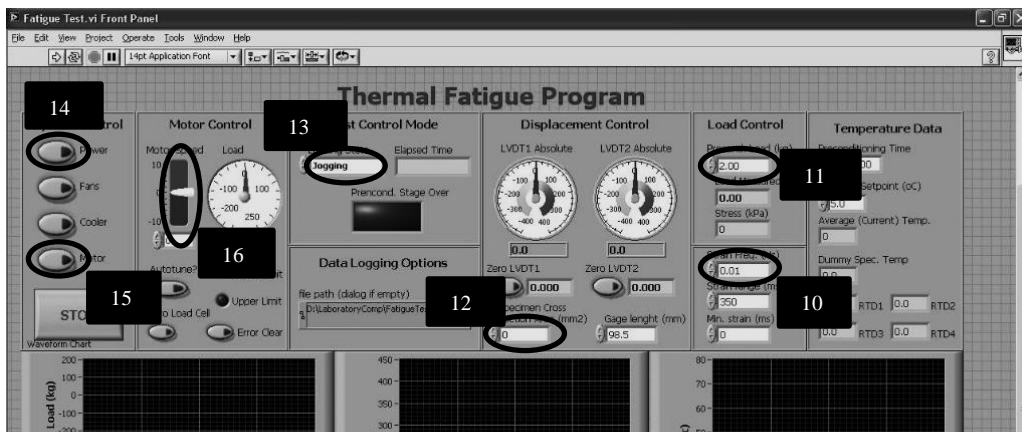


1. In order to supply the TSRST with electricity, turn this button right
2. For turning on the data acquisition system,

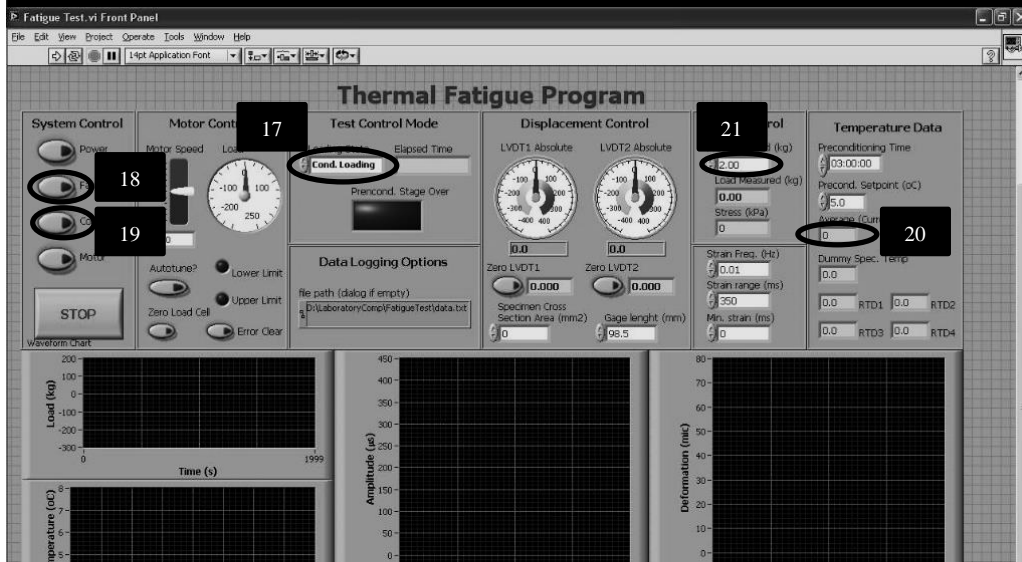


3. Press this button to start the software
4. Define a directory for the file in which the data will be recorded
5. Set a time for preconditioning
6. Define a constant temperature for the preconditioning time
7. Enter the gauge length at which you want to measure the strain
8. Enter the minimum strain from which you want to start applying the cyclic strains
9. Enter the range of cyclic strain that you are planning to apply

Figure G.2: Manual for the thermal fatigue test.

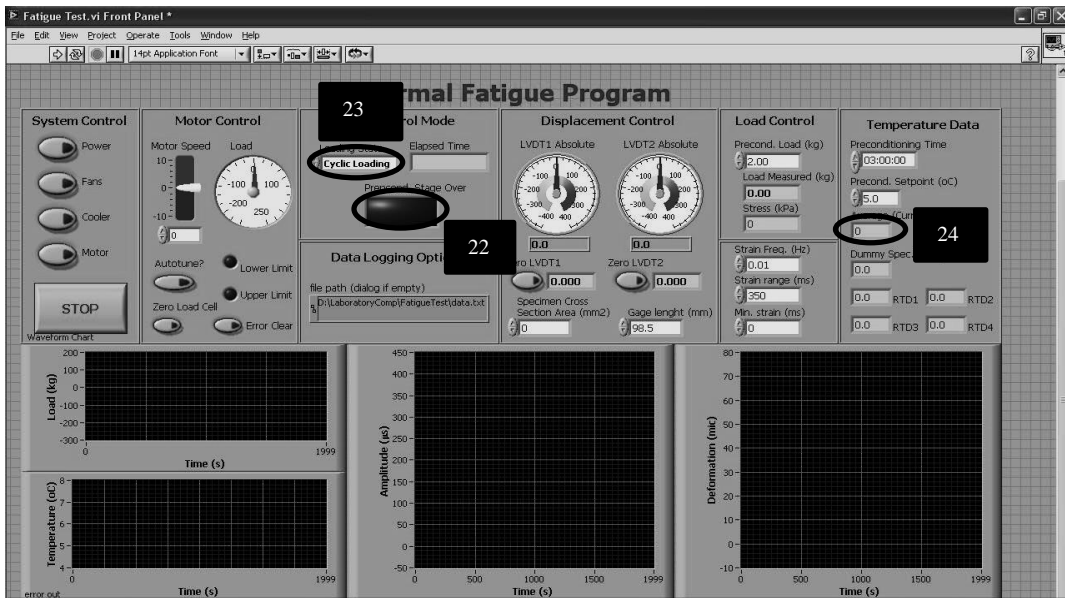


10. Enter the frequency at which you want to perform the test
11. Enter the amount of load to be applied on the specimen during the preconditioning state
12. Enter the cross section area of the specimen
13. Set the motor to jogging mode
14. Press this button and wait for a clicking sound
15. Press this button to turn the motor on
16. Hang the specimen's top plate to the upper universal joint. Then, using the sliding button adjust the motor speed and its direction of rotation so that you can connect the specimen's bottom plate to the lower universal joint using a pin. After the mount attach all of the sensors.

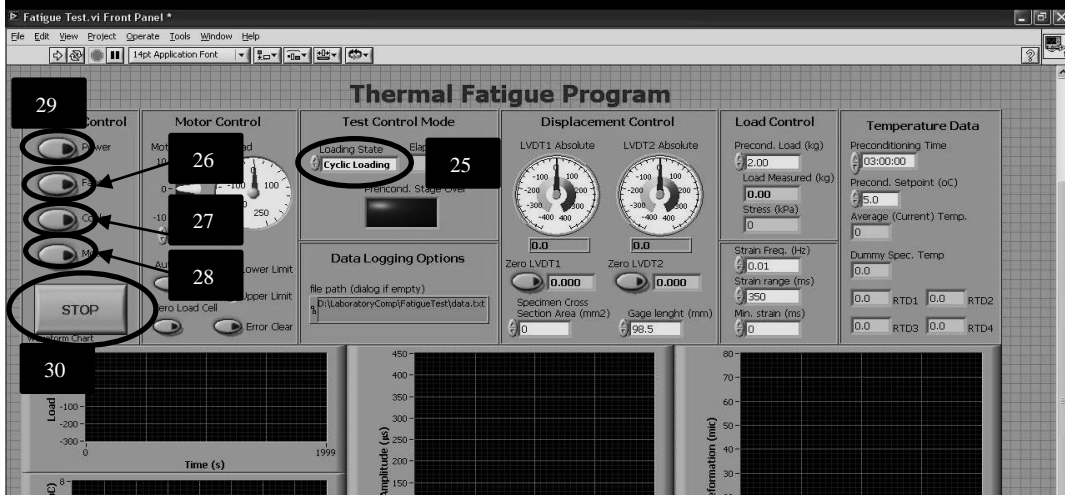


17. Set the motor to conditioning mode
18. Press this button to turn on the fan
19. Press this button to turn on the cooler
20. Keep an eye on the average temperature during the preconditioning mode
21. Check the preconditioning load, it should always be approximately near the half of the total weight of the specimen and the steel plates

Figure G.2: (Continued)



22. For applying the cyclic loads, this blinker must start blinking.
23. In order to start the cyclic loading, set the motor condition to cyclic loading
24. During the cyclic loading, pay attention to the average temperature it must be around and close to the set temperature.



25. For stopping the test, set the motor to preconditioning mode
 26. Press this button to turn of the fan
 27. For turning on the cooler, press this button, this is the time for removing the specimen
 28. Press this button to turn off the motor
 29. Press this button to turn off the power
 30. For stopping the software, press this button
- Do not forget to turn of the TSRST machine and the data acquisition system

Figure G.2: (Continued)